Carbon isotopes as monitoring tools for active volcanic systems

Fiona Danielle D'Arcy

Department of Earth and Planetary Sciences

McGill University, Montreal

December 2024

A thesis submitted to McGill University in partial fulfillment of the requirements of the degree of Doctor of Philosophy

Abstract

Volcanic eruptions can cause sudden devastation to communities, vegetation, and economies. As highlighted in the Sustainable Development Goals released by the United Nations, efforts to understand how and why certain volcanoes behave the way they do are needed to mitigate the risks associated with these natural disasters. In this thesis, I focus on how volcanic emissions and their effect on the surrounding environment can provide clues about volcanic activity. Specifically, I focus on carbon release from volcanoes using isotopes to advance our knowledge of precursory signals and expand our applications of isotopic tools. In chapters 1 and 2, I report a new methodology I developed for collecting stable carbon isotopes in volcanic gas plumes, which I tested at two contrasting volcano types. At Poás volcano, Costa Rica, I test a gas-sampling system onboard an Unoccupied Aerial System (UAS) in a fumarole field and central gas plume. Concurrent gas samples are taken from the ground using traditional methods, and all samples are processed by Cavity Ring-down Spectrometry (CRDS) to yield a chronology of stable carbon isotopes spanning 2017 to 2019. My findings validate that the UAS method can provide comparable results to traditional carbon dioxide sampling methods and provide evidence for a conceptual model encompassing both magmatic and hydrothermal processes in relation to phreatomagmatic sealing of the volcanic edifice. At Stromboli volcano, Italy, I expand the gas-sampling system to fit two alternate UAS and collect CO_2 samples from the summit. Samples are processed on two instruments, CRDS and Isotope Ratio Infrared Spectrometry (IRIS), yielding a contrasting set of carbon isotopes from both an inactive period (2018) and active period (2019). I argue that these results show that the onset of degassing of a carbon dioxide-rich magma may precede explosive events at Stromboli by weeks to months. To complement these two studies on volcanic plumes, I test the application of combined radiocarbon and stable carbon isotopes of

tree rings as an indicator of volcanic gas plume chemistry in chapter 3. This is applied at Etna volcano, Italy, where my combined ring width, stable carbon, and radiocarbon isotopic results constrain the limits and caveats of trees as biomonitors of volcanic plumes at low exposure levels. With these three case studies, my thesis demonstrates how carbon isotopes have many applications as monitoring tools, many of which are still to be discovered.

Résumé

Les éruptions volcaniques peuvent provoquer une dévastation soudaine des communautés, de la végétation et des économies. Comme le soulignent les objectifs de développement durable publiés par les Nations Unies, il faut s'efforcer de comprendre comment et pourquoi certains volcans se comportent comme ils le font afin d'atténuer les risques associés à ces catastrophes naturelles. Dans cette thèse, je me concentre sur la façon dont les émissions volcaniques et leurs effets sur l'environnement peuvent fournir des indices sur l'activité volcanique. Plus précisément, je me concentre sur les émissions de carbone des volcans en utilisant des isotopes pour faire progresser notre connaissance des signaux précurseurs et étendre nos applications des outils isotopiques. Dans les chapitres 1 et 2, je présente une nouvelle méthodologie que j'ai mise au point pour recueillir des isotopes stables du carbone dans les panaches de gaz volcaniques, et que j'ai testée sur deux types de volcans différents. Au volcan Poás, au Costa Rica, je teste un système d'échantillonnage de gaz à bord d'un système aérien inoccupé (UAS) dans un champ de fumerolles et un panache de gaz central. Des échantillons de gaz sont prélevés simultanément au sol à l'aide de méthodes traditionnelles, et tous les échantillons sont traités par spectrométrie à cavité « ring-down » (CRDS) pour obtenir une chronologie des isotopes stables du carbone de 2017 à 2019. Mes résultats confirment que la méthode UAS peut fournir des résultats comparables aux méthodes traditionnelles d'échantillonnage du dioxyde de carbone et fournissent des preuves pour un modèle conceptuel englobant à la fois les processus magmatiques et hydrothermaux en relation avec le scellement phréatomagmatique de l'édifice volcanique. Au volcan Stromboli, en Italie, j'agrandis le système d'échantillonnage des gaz pour l'adapter à deux UAS alternatifs et collecter des échantillons de CO_2 depuis le sommet. Les échantillons sont traités par deux instruments, le CRDS et la spectrométrie infrarouge à rapport

isotopique (IRIS), ce qui permet d'obtenir un ensemble contrasté d'isotopes du carbone provenant à la fois d'une période inactive (2018) et d'une période active (2019). Je soutiens que ces résultats montrent que le début du dégazage d'un magma riche en dioxyde de carbone peut précéder les événements explosifs à Stromboli de quelques semaines à quelques mois. En complément de ces deux études sur les panaches volcaniques, je teste l'application de la combinaison du radiocarbone et des isotopes stables du carbone des cernes d'arbres comme indicateur de la chimie des panaches de gaz volcaniques dans le chapitre 3. Ceci est appliqué au volcan Etna, en Italie, où mes résultats combinés sur la largeur des cernes, le carbone stable et les isotopes du radiocarbone décrivent les limites et l'utilité des arbres en tant que biomoniteurs des panaches volcaniques à de faibles niveaux d'exposition. Avec ces trois études de cas, ma thèse démontre que les isotopes du carbone ont de nombreuses applications en tant qu'outils de surveillance, dont beaucoup restent encore à découvrir.

Table of Contents

We have much to learn by studying nature and taking the time to tease out its secrets

- David Suzuki

Acknowledgments

I would first like to thank my supervisor, John Stix, for his guidance throughout my PhD journey. Thank you for encouraging me to continue, for rising early on those crucial early morning hikes and flights to volcanic summits before the clouds rolled in, and for sharing your science wisdom. Thanks also to Dora and Cleo for hosting me in Montreal during the final stages of lab work.

My time at McGill has been enriched by the many people who have helped me along my doctoral journey. To the heart of Earth and Planetary Sciences: Angela, Kristy, and Anne. Though you have moved on, your support was invaluable to so many graduate students and their projects, including this one. I can't forget Clara Waelkens, Mathilde Jutras, and Marko Prasek, whose friendship, encouragement, and incredible doctoral theses inspired me. I would especially like to thank the Graphos team at McGill, especially Alexandra, Marième, and Yvonne, for introducing me to self-care and healthy writing habits. Thank you to many others at McGill, including the members of the volcanology group for keeping the magma chamber alive, my committee members and the faculty and staff in EPS. Special thanks to Inga, Esther, and Flavio for all the pomodoros and pep talks in the final months.

I must thank Etienne Boucher for many thoughtful discussions on trees, data, and skiing, as well as Sepideh, Camille, Emilie and the whole dendrochronology group for sharing their space. Thanks to the Geotop administrators, members, and students whose programming has provided excellent networking, language, social, and financial support throughout my degree.

I am grateful for my co-authors in Italy and Costa Rica for their unwavering encouragement, for hosting us in their beautiful countries, and for their tolerance of my broken Spanish and Italian.

I wish to thank my parents for raising me to be curious about nature and for supporting me from afar. Thanks to the friends and family who have encouraged me along this journey.

For my partner Robert, my cat Taavi, and my daughters Eileen and Natalie: you keep me grounded and my world revolves around you. Thank you for being along for the adventure.

Contribution to original knowledge

This thesis highlights my contributions to the field of volcanic gas monitoring through the preparation of three manuscripts based on original research. When we started designing the first UAS gas-sampler for chapters 1 and 2 in 2018, we were among the first in the world to conceptualize this technique and likely the first to attempt to capture volcanic plume gases in this way. When we published chapter 1, our paper became one of the keystone papers for the method of monitoring stable carbon isotopes in volcanic plumes by UAS. Our key findings were that simultaneous UAS and traditional sampling are comparable so long as spatial differences and statistical robustness are taken into account, and that temporal changes in carbon isotopes can reveal minute changes in magmatic-hydrothermal systems. Chapter 2 is another application of this methodology, which has demonstrated how this technique can be used on vastly different volcanic systems, whether open-vent or hydrothermal. Our key findings in chapter 2 are that carbon isotope anomalies may precede paroxysmal activity in cases where degassing regimes transition from closed to open. The other main take-away is that carbon isotopes in volcanic plumes are a valuable addition to routine gas monitoring of carbon to sulfur ratios since they further constrain degassing models and timing of reservoir changes. Chapter 3 is an entirely different technique in volcano monitoring which is one of the first to attempt to combine stable carbon and radiocarbon analysis in tree rings to track magmatic CO_2. We show that in order to definitively link elevated CO_2 and SO_2 from a volcanic plume with tree ring isotopic geochemistry, a controlled analysis of climatic and atmospheric conditions is likely needed to isolate the volcanic signal. Our results will aid future studies which aim to refine and further explore the feasibility of this type of biomonitoring technique.

Throughout the development of these manuscripts, I was able to make significant contributions to the field of volcanic gas geochemistry. In addition to the manuscripts presented in this thesis, my doctoral work garnered me invitations to co-author a review chapter on UAS in volcanology (James et al., 2020), a summary chapter of gas monitoring in the Treatise of Geochemistry (Stix et al., 2024), and an advances in volcano monitoring chapter in the Encyclopedia of Volcanoes 3rd edition (Poland et al., 2025). I also wrote a science news piece using journalistic writing for The Conversation Canada and a blog post for the Geotop Research Centre in Earth System Dynamics. This thesis comprises a substantial contribution to original knowledge and dissemination of volcano science to academics, students, and the general public.

Contribution of Authors

The body of this manuscript-based thesis consists of three journal articles intended for publication in scientific journals. I am the first author of all three journal articles. I was responsible for the project planning, fieldwork, sample analysis, data collection, and writing for all three chapters.

The first chapter, entitled "New Insights into carbon isotope systematics at Poás volcano, Costa Rica" was originally published in the Journal of Volcanology and Geothermal Research in 2022. I am the first author, and it was co-authored by J. Maarten De Moor, John Stix, Alfredo Alan, Robert Bogue, Ernesto Corrales, Jorge Andres Diaz, Emily Mick, Jessica Salas-Navarro, and Romain Lauzeral. I was the project lead for design of the UAS gas-sampler, fieldwork and data analysis, as well as drafting all figures and the original manuscript. JS and MdM conceived the project and were vital in the project administration, field planning, logistics, data visualization, interpretations and editing of the manuscript. AA, EC, and JAD provided advice, expertise, and equipment for modifying the UAS gas-sampler along with invaluable field support. RB, EM, JSM, and RL contributed to flight preparation, sample collection, and analyses in the field. All authors reviewed and approved the final version of the manuscript.

The second chapter, entitled "Large isotopic shift in volcanic plume CO_2 prior to a basaltic paroxysmal explosion" was published in Geophysical Research Letters in 2024. I am the first author, and it was co-authored by Alessandro Aiuppa, Fausto Grassa, Andrea Luca Rizzo, and John Stix. I was the project lead for design of the UAS gas-sampler, fieldwork and data analysis, as well as drafting all figures and the original manuscript. JS and AA conceived the project and

provided supervision and logistical oversight. FG provided access to instrumentation and safe storage of our instrumentation after the field campaign. JS, AA, FG and ALR provided guidance in the field and contributed to discussions on calibration, data analysis, interpretations, and revisions to the manuscript. AA provided modelling parameters and equations for the CO_2 degassing model.

The third chapter, entitled “Stable and radiogenic carbon isotopes in tree rings as a record of degassing at Etna volcano, Italy” is in preparation for submission the Journal of Geophysical Research: Biogeosciences. I am the first author and it was co-authored by Robert Bogue, Etienne Boucher, Sergio Calabrese, Peter Douglas, and John Stix. I conceived the project and was the project lead for planning the field campaign, laboratory and data analysis, as well as drafting all figures and the original manuscript. RB and SC assisted in fieldwork and sample collection. EB provided expertise on sample treatment, dendrochronology, and statistical analysis. JS provided supervisory support and guidance on early drafts. All authors contributed to discussions and interpretations of the research project.

List of Figures

Chapter 1

Chapter 2

Chapter 3

Appendix 1

Appendix 2

List of Tables

Chapter 3

Appendix A

Appendix B

Introduction and literature review

General introduction

The impact of volcanoes on our lives is far-reaching. On the one hand, volcanic features are beautiful, natural wonders often protected in national park areas. They bring heat and valuable elements close to the surface, providing energy for geothermal power generation, natural resource extraction, and fertile soils for agricultural purposes. On the other hand, volcanic eruptions can result in lives lost, infrastructure destroyed, and disruptions to local communities including water and air quality deterioration. In 2023, there were 69 volcanic eruptions, 47 in continuous eruptions (Global Volcanism Program, 2024). The ash plume produced in the 2010 eruption of Eyjafjallajökull volcano, Iceland, led to $1.7 billion USD in losses from flight carriers alone (Sigurdsson, 2015). The 2018 eruption of Mayon volcano, Philippines, displaced 66000 people and cost $3.5 million in damage to local agriculture (De Guzman, 2023). Volcanic surveillance is important in mitigating the hazards of eruptions, providing advance warning on the timing, location, and type of hazards expected to occur. Surveillance measures range from geophysical monitoring using seismic arrays, tiltmeters, GPS, and satellite-based radar, to geochemical monitoring which centres on various techniques of evaluating volatiles in magma and their surface manifestations, volcanic gases.

Volatiles that are dissolved in magma are exsolved as gas as pressure decreases with magma ascent. The way this gas behaves, along with magma volume, temperature, viscosity, crystal content, and external factors, will govern eruption intensity (Sigurdsson, 2015). Gas behavior can also affect the stability of a magma chamber and trigger eruptions (Wilson and Head, 1981). Volcanic gases are generally composed of water vapour (75-98%), carbon dioxide (0.3-13%),

sulfur dioxide (0.3-3%), hydrogen sulfide (0.02-2%), and trace amounts of other species including halides, helium, carbon monoxide, carbonyl sulfide, and carbon disulfide (Giggenbach, 1996; Kern et al., 2022). Carbon dioxide, being the second most abundant gas in volcanic emissions, is extremely important in volcanology. Carbon in the deeper layers of the earth comprise up to 99% of terrestrial carbon (Werner et al., 2019), with dissolved CO_2 contents generally up to 500 ppm in silicic magmas (Shinohara, 2008) and reported in excess of 5000ppm for some basaltic magmas (e.g. Helo et al., 2011). Not only is carbon abundant, its low solubility also renders it a potent driver of eruption dynamics and an early indicator of unrest to come. At the same time, the deep carbon brought to earth's surface during volcanic eruptions is one component balancing out the geologic carbon cycle (Burton et al., 2013). Sediments and dead matter from terrestrial and oceanic environments are brought into the mantle during subduction processes before being expelled during metamorphism and volcanism.

Carbon cycling at volcanoes has been studied extensively for decades, and yet there is still much that is unknown (Burton et al., 2013; Werner et al., 2019; Kern et al., 2022). The amount of carbon released from subaerial volcanoes over time, called the carbon flux, is not well constrained, with estimates ranging from 540 Mt CO_2/yr (Burton et al., 2013) to between 220 and 300 Tg CO_2/yr (Werner et al., 2019). For example, in 2018 it was discovered that the subglacial volcano in Iceland, Katla, emits up to 4% of global emissions from volcanoes which aren't in eruption at the time (Ilyinskaya et al., 2018). This is only one of five volcanoes in Iceland whose CO_2 flux has been measured at all, and in many other countries around the world there is a dearth of carbon flux data. Another reason why global extrapolations may not be well-constrained is because a proportion of magmatic CO_2 emissions come from passive outgassing, that is to say non-eruptive emissions from fumaroles, vents, and hidden sources such as diffuse

degassing through soil, volcanic lakes, and tectonic features. Finally, while CO_2 is the dominant species of carbon found in these surface environments, a total carbon flux would ideally include the other carbon species present in volcanic emissions. CH_4 flux has been measured and compared to CO_2 flux (D'Alessandro et al., 2006), and global estimates put CH_4, CO, and OCS fluxes orders of magnitude lower than that of CO_2 (Burton et al., 2013). Volcanic deposits also can form colonization sites for CO and CH_4-seeking bacteria which draw in atmospheric gases in these locations with little competition (Hernández et al., 2020). In this thesis, the interaction of volcanic emissions with the atmosphere, biosphere, and hydrosphere will be central in each chapter, with the major difference being the mechanisms and techniques applied.

A useful tool to examine carbon cycling at volcanoes are measurements of the isotopes of carbon. Carbon exists in nature in three forms: two stable isotopes, ^{12}C and ^{13}C, and an unstable radiogenic isotope, ^{14}C. The most common isotope of carbon is by far ^{12}C, at just over 98.89 percent of all carbon on earth, followed by ^{13}C at 1.11 percent (Aubaud, 2022). ^{14}C, also known as heavy carbon or radiocarbon, has a half-life of 5730 years and is produced almost exclusively in the atmosphere as cosmic radiation converts ^{14}N to ^{14}C. The only exception is anthropogenic production of ^{14}C through nuclear bomb testing prevalent in the 1960s. All three isotopes of carbon undergo stable isotope fractionation and are found in varying ratios to one another depending on their provenance. The lighter isotopes, ^{12}C and ^{13}C, are measured as a ratio, while the rarity of ^{14}C allows it to be excluded without affecting the ratio. This ratio of ^{13}C /^{12}C has been standardized to express the ratio with reference to an international standard, the Pee Dee Belemnite (Urey et al., 1951), now a reference ratio known as the Vienna Pee Dee Belemnite scale (VPBD) and is usually reported in delta notation, $\delta^{13}C$ (Fleisher et al., 2021). The units reported are per mil, ‰. The source signatures of $\delta^{13}C$ cover specific ranges for marine

carbonates, terrestrial plants, fossil fuels, and magmatic regimes (Coplen et al., 2006; Fleisher et al., 2021), with a value of -6.5 ‰ for mid-ocean ridge basalts (MORB) (Mattey et al., 1989).

In this thesis, I explore two applications of carbon isotopes as monitoring tools at volcanoes. In chapters 1 and 2, I develop UAS-mounted gas-sampling devices which were deployed at two different volcanoes to refine the spatial and temporal variability of stable carbon isotopes in relation to eruptions. These two studies retrace the path of carbon from plume gas measurements at the summit to their deep origins in a magmatic system. In chapter 3, I explore a second application of carbon isotopes, this time in a multidisciplinary study at the crossover of volcanology and dendrochronology. This study uses radiogenic isotopes in tree rings to identify carbon of magmatic origin, while stable isotopes pinpoint any occurrences of sustained plume gases reaching down on the flanks of the volcano. Poás volcano in the Central American volcanic arc of Costa Rica and Stromboli volcano in the Aeolian arc, Italy, were chosen as the study sites for chapters 1 and 2, and Etna volcano on the island of Sicily, Italy, was chosen for chapter 3. These two applications of carbon isotopes work backwards to trace carbon from surface to source, with the first application focusing on capturing the "fresh" isotopes as soon as they are emitted at the summit vents, while the second application looks at "stale" isotopes as in fossil volatiles or their evidence preserved in trees at some distance from the summit emissions.

While the three manuscripts presented in the body of this thesis, chapters 1 through 3, contain substantial literature review in their introductory paragraphs, these are complemented by an additional literature review in this introduction. I then provide a comprehensive discussion tying all three chapters together and using the results in their entirety to examine how I have advanced our knowledge of the behaviour of carbon at volcanoes. This discussion summarizes the lessons

learned, limitations, and ways forward in using these techniques for volcano monitoring before closing the thesis with a section on main conclusions.

Methodology, rationale, and objectives for chapters 1 and 2

Methods of measuring CO_2 gas at volcanoes vary widely depending on what exactly is being measured and for what purpose. Gas ratios are the molar ratio of one gas relative to another, and are a useful tool for detecting changes in magma supply (Allard et al., 1991; Shinohara, 2005; Aiuppa et al., 2005, 2007) . This is because each of the main gases exsolves from magma at different times relative to one another according to their respective solubility laws (Giggenbach, 1996). The gas phase first exsolving from a magma will initially be CO_2-rich due to its comparatively low solubility, while H_2O is progressively exsolved in greater quantities as the magma rises (Holloway, 1976). Commonly measured ratios incorporating CO_2 include CO_2/SO_2, H_2O/CO_2, CO_2/H_2S, and CO_2/CH_4. Firstly, CO_2/SO_2, sometimes expressed as C/S_{total} when both CO_2/SO_2 and CO_2/H_2S are included, is useful for detecting the presence of a new influx of magma (Aiuppa et al., 2007, 2021; Shinohara et al., 2008; de Moor et al., 2016) . CO_2/CH_4 is governed by oxidation state, similar to SO_2/H_2S, and is useful for assessing inputs of magmatic and hydrothermal fluids (Chiodini, 2009; Salas-Navarro et al., 2022). CO_2/H_2S is especially helpful in volcanic systems with little to no SO_2 gas, e.g., La Soufrière in Guadeloupe (Moune et al., 2022). Owing to the latest advances in compact sensors, these measurements are now routinely made with a MultiGAS instrument (Shinohara, 2005; Aiuppa et al., 2005) which is placed at a crater rim or passed through the plume by ground or air transport. Carbon fluxes are another helpful tool to recognize and quantify new batches of magma injected beneath a volcano. These can be calculated by either combining the SO_2 flux with measurements of CO_2/SO_2

(Burton et al., 2013; Werner et al., 2019; Kern et al., 2022) or by using airborne measurements of CO_2 concentration fields with wind speeds (Ilyinskaya et al., 2018).

Methods of measuring stable carbon isotopes in volcanic environments begins with the question of how to sample the gases. Unlike gas ratios and fluxes, isotopic analyses usually require discrete samples which can be transported to an instrument setup in a stable environment for the analysis. These instruments include isotope-ratio mass spectrometers (IRMS), or Isotope Ratio Infrared Spectrometry (IRIS) and Cavity-ring-down spectrometry (CRDS). Due to the remote locality of many volcanoes including summits and islands with poor road access to gas vents, few studies exist in which the heavy, delicate instrumentation required for $\delta^{13}C$ analyses have been used in the field in near real time. (Rizzo et al., (2014) made measurements of the plume of Etna volcano, Italy, using an IRIS installed in a ground vehicle. Fischer and Lopez (2016) deployed a CRDS aboard a helicopter for measurements made at Redoubt volcano, Alaska. While these studies were successful in their respective contexts, deploying these instruments in-situ is not feasible in all situations due to topography, weather, time constraints, and budget.

With the advent of Unoccupied Aerial Vehicles (UAS) in volcanology, many types of measurements have been transformed (James et al., 2020). In gas geochemistry, various instrumentation has been made compact and lightweight for use onboard UAS, including measuring gas ratios with MultiGAS (Liu et al., 2018; Stix et al., 2018), collecting aerosol samples with filter and sorbent pack samplers (Mandon et al., 2018; Mason et al., 2021) and combinations of both (Edwards et al., 2024). The equipment for CO_2 flux measurements has also been made portable for UAS (Liu et al., 2018, 2020; Stix et al., 2018; McCormick Kilbride et al., 2023).

Chapter 1 examines C isotopes in gases at Poás and chapter 2 at Stromboli volcano, Italy. These are ideal localities because Stromboli is exemplified by magmatic processes, while Poás exhibits strong interactions between a shallow magmatic system and a shallow hydrothermal system. Volcanic CO_2 is composed of magmatic carbon whose $\delta^{13}C$ can be modified by a variety of processes, including crustal assimilation (Troll et al., 2012), degassing as magma rises to the surface (Lucic et al., 2014), or interaction with a hydrothermal system (Venturi et al., 2017), if present. My hypothesis for chapter 1 proposes that $\delta^{13}C$ at Poás is governed by both the degassing of batches of magma and by the hydrothermal system, which will be reflected in the $\delta^{13}C$ of the volcanic gas. I propose that, by collecting gases from the main plume by UAS and comparing these with samples collected from the fumaroles with direct sampling, differences in $\delta^{13}C$ will reflect varying contributions, both spatially and temporally from each of these two main processes occurring at Poás. Stromboli is a simpler volcano which does not possess a hydrothermal system, allowing me to focus on purely magmatic processes controlling the volcanic CO_2. My second hypothesis proposes that there are subtle $\delta^{13}C$ variations in the weeks to months prior to large explosive bursts at Stromboli as a result of gas being alternately supplied by the deeper or the shallower magma system and subsequently being degassed.

Methodology, rationale, and objectives for chapter 3

Methods on gauging plant physiology in response to elevated levels of volcanic gases are still being explored, yet it is well-known that such gases can be detrimental to the health of people, animals, and vegetation. For example, the 2014-2015 Holuhraun eruption in Iceland produced a sustained volcanic plume whose SO_2 reacted in the lower atmosphere to produce SO_4 levels that often surpassed background levels over 250km away in the capital city of Reykjavik (Ilyinskaya et al., 2017). Decades-long degassing of low-altitude gas plumes causes SO_2 damage to

vegetation from acid deposition, as observed at volcanoes with nearly continuous degassing such as Masaya volcano, Nicaragua (Delmelle et al., 2002) and Turrialba volcano, Costa Rica (Tortini et al., 2017). Diffuse CO_2 emissions likewise have created large dead zones in forested areas (Cook et al., 2001; Lewicki et al., 2014). Biomonitoring in volcanology could also be helpful in assessing plume impacts on vegetation to gauge future unrest. Trace metals from volcanic plume emissions have been studied as biomonitors of plume dispersal and composition in moss (Calabrese et al., 2010; Bonanno et al., 2012; Arndt et al., 2017), lichen (Perez Catán et al., 2020), and foliage (Watt et al., 2007; Bellomo et al., 2007). The frequency of stomata, the pores through which trees exchange gases with the atmosphere, vary in the needles of a species of conifer relative to fluctuations in atmospheric CO_2 concentration (Lin et al., 2001), allowing for a detailed reconstruction of past CO_2 over the past millennia (Kouwenberg et al., 2005). These biomonitoring techniques are useful for either very recent pollution events (i.e., active specimen collection over the course of the study) or for historical events (i.e., samples obtained from stratified sediment layers), but these conditions cannot always be met.

Trees provide a continuous archive of environmental conditions from the present all the way to centuries past. Depending on the species and climate, trees produce annual wood which is preserved in visible rings segregated by latewood (darker wood) and earlywood (lighter wood), making them the ultimate choice for biomonitoring techniques. Dendrochronology is the study of these tree rings, based upon the principle that earlywood represents fast cell-growth in the cambium, the outer layer of the tree, during the spring and summer while latewood represents slower cell-growth in the late summer and fall (Fritts, 1976). These growth relationships can be used to cross date, i.e. to compare ring size across multiple trees and sites to match up patterns in their growth. Anomalies can indicate climate events such as floods, fires, and volcanic eruptions

(LaMarche and Hirschboeck, 1984; Watmough, 1997). Dendrochemistry is the study of chemical variations in tree rings (Guyette et al., 1992; Watmough, 1997) which has been applied to assess tree exposure to volcanic gas, aerosol, and ash deposition using a variety of trace elements (Hall et al., 1990; Pearson et al., 2005, 2009; Watt et al., 2007; Sheppard et al., 2008, 2010; Rodríguez Martín et al., 2013; Hevia et al., 2018; Teran-Hinojosa et al., 2019; Alfaro-Sánchez et al., 2020). These dendrochemical methods use Inductively-Coupled Plasma Mass Spectrometry or Orbital Emission Spectroscopy (ICP-MS or ICP-OES), Laser-Induced Breakdown Spectroscopy (LIBS) or micro xray fluorescence (uXRF). However, radial translocation of elements across ring boundaries can complicate the use of trace elements in dendrochemistry (Wagner et al., 2012). Hence the field has expanded to encompass other elements, specifically isotopes, in recent years.

Carbon isotopes in tree rings are excellent proxies to use for environmental reconstruction. Wood is around 50% carbon, and the mechanisms by which it is incorporated from the atmosphere into leaf sugars and tree growth are well-constrained. Stable carbon undergoes a known fractionation, or isotopic shift, at each step of its integration into tree growth (McCarroll and Loader, 2004), so it is a good proxy for environmental and climatic changes (Saurer et al., 2004; Treydte et al., 2009; Johnstone et al., 2013; Belmecheri and Lavergne, 2020). The uptake of radiocarbon into trees has been studied extensively, whether the source of the radiocarbon is nuclear bomb testing (Grootes et al., 1989; Ancapichún et al., 2021), the burning of fossil fuels (Vásquez et al., 2022), or solar activity (Brehm et al., 2021). Additionally, radiocarbon is a useful tracer of magmatic (Cook et al., 2001; Evans et al., 2010; Lewicki et al., 2014) and hydrothermal (Van Gardingen et al., 1995; Saurer et al., 2003) CO_2 in trees. Analyzing both $\delta^{13}C$ and ^{14}C usually starts with removing resins (the soluble compounds in the tree) as they are transported across rings and have

been found to possess a lower $\delta^{13}C$ signal than wood (Rissanen et al., 2021). Taking it one step further, lignin is also often removed from whole wood to target pure cellulose because of a further difference in $\delta^{13}C$ signal between the two components (Weigt et al., 2015).

While the standard for analyzing $\delta^{13}C$ in tree rings is usually by cutting and combusting individual rings in an Elemental Analyzer coupled with an isotope ratio mass spectrometer (EA-IRMS), recent advances have allowed for intra-annual $\delta^{13}C$ analysis in thin sections by laser ablation (LA-IRMS) (Skomarkova et al., 2006; Saurer et al., 2023). With the exception of exploratory studies in benchtop CRDS analysis (Fleisher et al., 2017), C^{14} analysis methods remain limited to destructive techniques where samples are combusted in an Elemental Analyzer to produce pure carbon gas before graphitization and analysis on an accelerator mass spectrometer (Crann et al., 2017). For studies combining ^{13}C and ^{14}C analysis, therefore, tree rings are dissected manually and a portion saved for each analysis type (Saurer et al., 2003; Seiler et al., 2021), which is the method I chose to use in chapter 3 of this thesis.

In chapter 3, I examine C isotopes in trees at Etna volcano, Italy. Etna is the ideal location because of its forested slopes as well as its high gas output which has been studied measured extensively for the last several decades. My first hypothesis is that the ^{14}C method can be used to identify magmatic plume CO_2 uptake in tree rings and to differentiate it from that of soil degassing. My second hypothesis is that once this volcanic CO_2 is quantified using radiocarbon of tree rings, and if the $\delta^{13}C$ value of the volcanic plume CO_2 is known, I can interpret the $\delta^{13}C$ of the tree rings to infer periods of SO_2 degassing.

Preface to chapter 1

In the introduction chapter, I discussed the versatility of carbon isotopes as tools in studying modern volcanism. One of the questions I seek to answer in the following chapter is whether these isotopes can be sampled safely at volcanic summits by remote means. The second question is what they can tell us when we piece them together into a high resolution timeseries spanning several phases of activity at a volcanic centre. In the introduction chapter, I also mention UAS-mounted gas-sampling devices which were deployed at two different volcanoes. Chapter 1 represents an exciting first case study of the application of the Compact Aerial Receiver-Initiated Gas-Sampling Operation (CARGO). We derive a carbon signature of the volcanic source of Poás volcano in April 2019 using samples collected with CARGO 2.0 and 3.0. We use these along with carbon signatures spanning 2001-2009 (previous studies) and 2017-2019 (this work) to derive a conceptual model. Chapter 1 was published in the Journal of Volcanology and Geothermal Research in 2022 and authored by Fiona D'Arcy, J. Maarten De Moor, John Stix, Alfredo Alan, Robert Bogue, Ernesto Corrales, Jorge Andres Diaz, Emily Mick, Jessica Salas-Navarro, and Romain Lauzeral.

Citation:

D'Arcy, F., de Moor, J. M., Stix, J., Alan, A., Bogue, R., Corrales, E., Diaz, J. A., Mick, E., Salas-Navarro, J., & Lauzeral, R. (2022). New insights into carbon isotope systematics at Poás volcano, Costa Rica. Journal of Volcanology and Geothermal Research, 431. https://doi.org/10.1016/j.jvolgeores.2022.107639

Chapter 1

New insights into carbon isotope systematics at Poás volcano, Costa Rica

Fiona D'Arcy[1,6*], J. Maarten de Moor[2,3], John Stix[1,6], Alfredo Alan[4], Robert Bogue[1,6], Ernesto Corrales[4], Jorge Andres Diaz[4,5], Emily Mick[1], Jéssica Salas-Navarro[1], Romain Lauzeral[1]

[1] McGill University, Montreal, Canada

[2] OVSICORI, Universidad Nacional, Heredia, Costa Rica

[3] University of New Mexico, Albuquerque, NM, USA

[4] GasLAB, CICANUM, Universidad de Costa Rica, San José, Costa Rica

[5] INFICON Inc. Syracuse, NY, USA

*Corresponding author: fiona.darcy@mail.mcgill.ca

Abstract

In April 2017, an intense phreatomagmatic eruptive phase took place at Poás volcano in Costa Rica. This was the most significant eruptive activity at the volcano since the 1950's. Unlike previous eruptions, gas ratios were closely monitored during this event with the use of both ground-based MultiGAS and uncrewed aerial system (UAS) real-time monitoring, providing valuable insight into the nature of the eruption. This well-studied eruption presents a unique opportunity to examine hydrothermal and magmatic processes occurring at Poás during periods of unrest versus quiescent periods. Here, we present stable carbon isotopic results of volcanic CO_2 at Poás spanning the pre-eruptive as well as eruptive and post-eruptive phases in 2017 through 2019. Samples were collected by a combination of direct sampling (analyzed by Isotope Ratio Mass Spectrometry [IRMS] or Cavity Ring Down Spectroscopy [CRDS]), as well as UAS and ground-based plume sampling (analyzed by CRDS). Direct samples range from -6.17 to -3.73 ‰ during 2017 to 2019. Using the Keeling approach, we calculate $\delta^{13}C$ magmatic source values of -3.97 ± 1.94 ‰ and -3.64 ± 0.48 ‰ using UAS sampling and ground-based sampling,

respectively, for April 2019. We propose that these values for $\delta^{13}C$ are being governed by a combination of magmatic and hydrothermal fluctuations related to sealing and unsealing of the upper magma carapace. This process results in comparatively heavy values when the system is being buffered by fluid-gas interaction as the hydrothermal system seals and expands, while lightest values are predominant during unsealed phases where degassed magma supplies the volatiles along with phreatic or phreatomagmatic activity. The significance of this work is two-fold: it demonstrates the use of a rapid volcanic gas sampling strategy applicable for monitoring at other volcanoes prone to phreatomagmatic and/or phreatic eruptions, and it provides a new conceptual model to interpret the phreatic/phreatomagmatic eruptive activity at Poás over the last 20 years.

Keywords: Carbon isotopes, Volcanic gases, UAS gas sampling, Poás volcano, Geochemistry, Drones

Introduction

Carbon isotopes are becoming a standard tool for assessing hydrothermal and magmatic processes through analysis of thermal waters (Venturi et al., 2017), calcite precipitates (Chiodini et al., 2015), soil gas (e.g. (Hanson et al., 2018), fumaroles (Troll et al., 2012), fluid inclusions (Boudoire et al., 2018), and mantle minerals (Rizzo et al., 2018; Sandoval-Velasquez et al., 2021). Volcanic plumes are a valuable means of volcanic carbon isotopic monitoring at active volcanoes. Plumes represent a mixture of gases from a source or multiple sources along with background air at some distance from the vent, which means that with the right equipment, they can be safely and rapidly accessed during times of unrest. While dilute volcanic plumes have been sampled for subsequent isotopic analysis of carbon dioxide by helicopter (Fischer and Lopez, 2016) and from the ground (Chiodini et al., 2011; Rizzo et al., 2014, 2015; Malowany et

al., 2017; Schipper et al., 2017), attempts to apply UASs (Uncrewed Aerial Systems) to this end are limited (Liu et al., 2020; Shingubara et al., 2021; Tsunogai et al., 2022). Nevertheless, UAS have proven to be vital to volcanological monitoring for topographic surveys, hazard mapping, instrument deployment, and gas measurements (James et al., 2020). In this work, we combine direct sampling of fumaroles with indirect volcanic plume sampling both from the ground and by UAS at Poás volcano, Costa Rica, to characterize the stable carbon isotopic variations in the volcanic CO_2. We draw comparisons between the two methods and use our extensive suite of samples to provide new insight into the processes governing the magmatic-hydrothermal interactions at Poás.

Poás volcano is one of Central America's most dynamic volcanoes. It is characterized by cycles of phreatic and phreatomagmatic activity centered around a dome and crater which has hosted an intermittent crater lake (Laguna Caliente) closely monitored since 1980 (Rowe et al., 1992; Martínez et al., 2000; Rouwet et al., 2017). Changes in crater lake level have been associated with shallow intrusions in 1981 beneath the dome, and in both 1985-1990 and 1998-2004 beneath the lake-filled pit crater (Rymer et al., 1998, 2005). Currently, CO_2, SO_2, and H_2S are the main gases used to monitor the activity of Poás by MultiGAS and other methods (e.g. Fischer et al., 2015; de Moor et al., 2016; de Moor et al., 2019; Vaselli et al., 2019). Large changes in SO_2/CO_2 are interpreted to be driven by variations in SO_2 flux due to interactions between S-rich magmatic gas and acid hydrothermal fluids (de Moor et al., 2019). This process is common in other volcanic systems which host crater lakes, such as Ruapehu (Christenson et al., 2010) and Rincón de la Vieja (Battaglia et al., 2019). In these sulfur-rich environments, small variations in CO_2 flux are less useful as a monitoring tool because they are eclipsed by larger variations in sulfur and have large associated errors. On the other hand, carbon isotopic compositions of gas

emissions are unaffected by fluctuations in sulfur, so they are sensitive to small changes in CO_2 sources or fractionation processes, making them a useful monitoring tool in these systems.

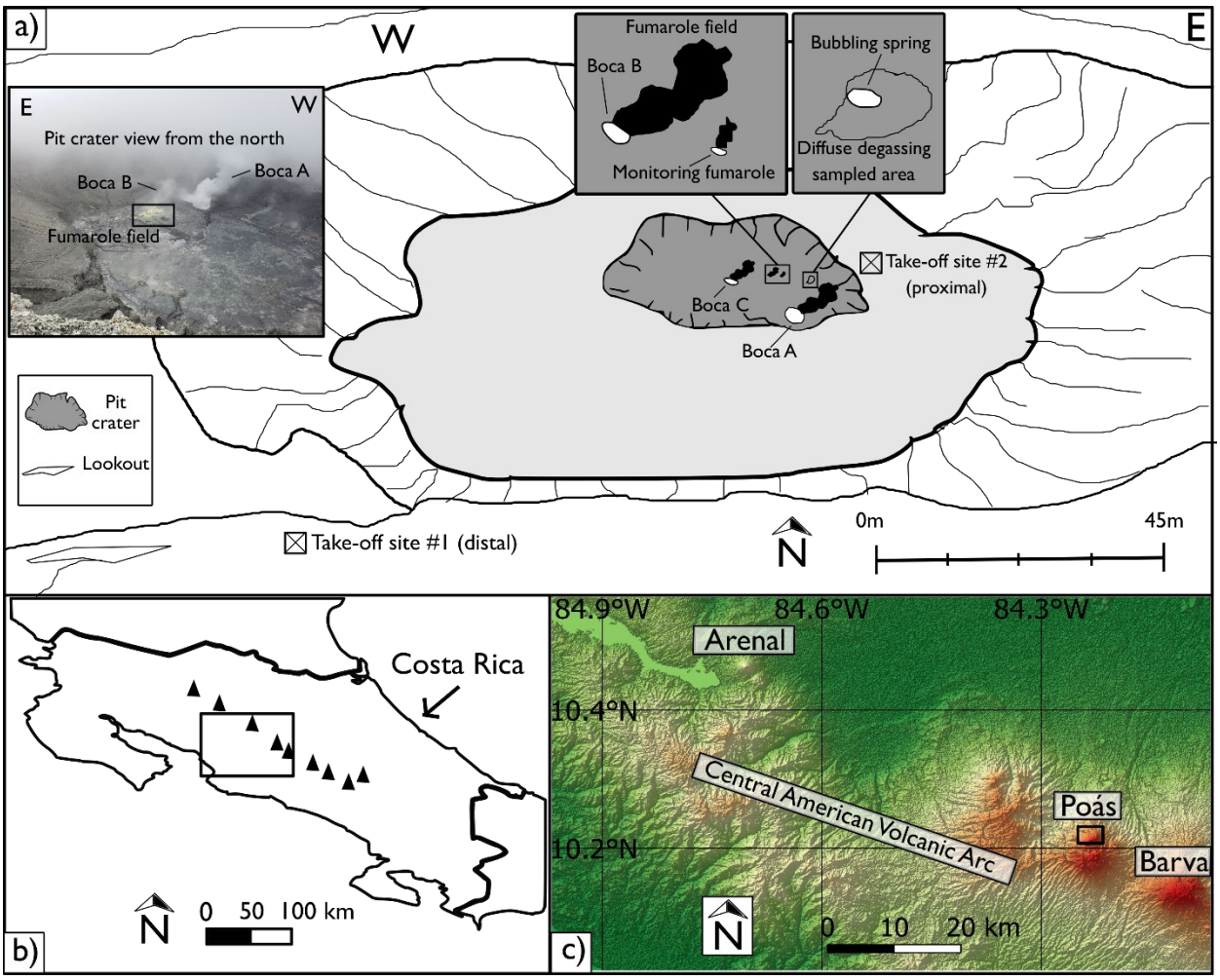

Figure 1: (a) Map showing the location of takeoff site #1 and #2, Boca A, Boca B, Boca C, the monitoring fumarole, bubbling spring, and diffuse degassing area. (b) General location of Poás volcano in Costa Rica. (c) Location of Poás volcano with respect to the Central American Volcanic Arc (CAVA) as an inset of the box outlined in (b). DEM data for (c) was generated using Advanced Spaceborne Thermal Emission and Reflection Radiometer (ASTER) Global 341 Digital Elevation Model (GDEM) data, a product of METI and NASA.

The April 2017 phreatic and phreatomagmatic activity at Poás resulted in the drying out and disappearance of the Laguna Caliente and destruction of most of the adjacent pyroclastic dome structure (Vaselli et al., 2019). This was the most significant eruptive activity since the 1950's,

and juvenile magmatic material of andesitic composition (~57.4 wt. % SiO_2; de Moor et al., 2019) was expelled during these eruptions. During the present study, Poás crater contained a large vent ("Boca A" produced by the 2017 eruption and destruction of the dome) emitting a near constant, highly convective gas plume. Hosted within the bed of the previous crater lake were two smaller flooded vents occupied by vigorously bubbling S-rich pools (Boca C) and an adjacent fumarole field (Boca B; Figure 1). The dynamic environment of the crater of Poás poses a challenge to long-term monitoring of gases, as different sites have appeared and disappeared over the years, preventing robust comparison among different studies (Vaselli et al., 2019). In order to compare spatial variations, we collected $\delta^{13}C$ results from samples taken across five sites in the active crater area within a 5-day time period in 2019, ranging from the ambient plume to diffuse degassing from the bed of the previous crater lake. Measurements of $\delta^{13}C$ from fumaroles at Poás were reported from 2000 to 2004 (Vaselli et al., 2019) and from 2001 to 2008 (Hilton et al., 2010); here we report a new time series of measurements spanning January 2017 to April 2019. We use the isotopic data reported here for 2017 to 2019, in conjunction with gas ratios reported elsewhere, to build a new conceptual model involving hydrothermal buffering and degassed shallow magma which we apply to activity at Poás spanning the last 20 years.

Material and methods

Direct samples were obtained from February 2017 through February 2019 with Giggenbach bottles (Giggenbach, 1975). Fumaroles were sampled with a titanium tube, and bubbles emanating from the crater lake and subsequent isolated pools were collected using an inverted funnel. Gases were bubbled through a 4N NaOH solution in a glass Giggenbach bottle and returned to the lab at OVSICORI, where this solution was extracted and oxidized. Aliquots of 0.5 ml of the oxidized solution were then introduced into 12 ml exetainer vials. These samples were

then acidified using 30% orthophosphoric acid by an automated autosampler and resulting CO_2 gas was analyzed by Cavity Ring-Down Spectrometry. All other samples were collected in 2019 from 25 to 30 April using UAS plume sampling, ground-based plume sampling, and direct sampling and subsequently analyzed by Cavity Ring-Down Spectrometry.

UAS plume sampling

We collected UAS samples on two days, a distal sampling campaign on 25 April 2019 and a proximal campaign on 30 April. The distal UAS sampling assembly (Figure 2A) was used on 25 April during five sampling flights of the plume taken 20 to 100 m above the pit crater. Take-off and landing took place from take-off site #1 at the lookout or "Mirador" where tourists gather (Figure 1). The assembly consisted of a quadcopter (TurboAce Matrix-i) and flight time of ~10 minutes with payload comprising the gas sampling configuration attached on top of the UAS body and secured with bungee cords, while gas sample bags were attached directly below the drone. The payload (700 grams) consisted of a pump (micropump®, model d3k, 2.5L/minute) connected to an electronic switch (Turnigy 10A/30V) which utilized an empty standard port on the UAS receiver. An SO_2 sensor (Citicell 0-200 ppm range) was included with a voltage sensor (Futaba SBS-01V) connected to the SBUS2 port of the receiver and one of the inlet tubes of the pump. A portable USB-powered charger supplied power to the pump while a 9 volt battery powered the SO_2 sensor. The four sampling bags (Altef, 800 ml) were connected in series via the outlet tube of the pump and contained in a mesh bag connected by a carabiner and 0.1 m rope under the drone. The pump switch and SO_2 sensor were mapped to channels on the remote controller for the drone, allowing the pilot to use two-way telemetry to read the voltage of the SO_2 sensor and turn the pump on and off for sampling.

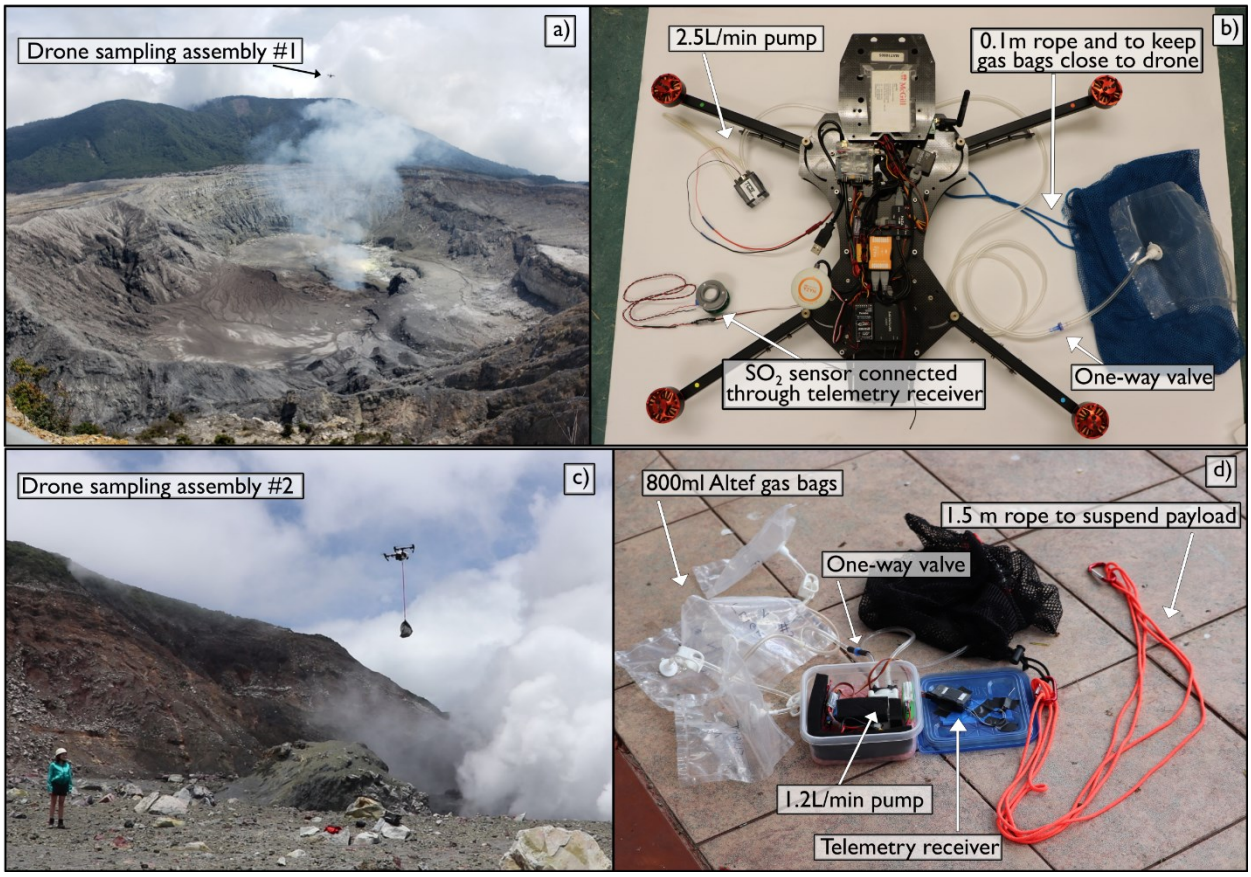

Figure 2: Sampling assembly by UAS used at Poás in April 2019. a) Distal assembly used for sampling the volcanic plume on 25 April b) Distal assembly components and specifications. c) Proximal assembly used for sampling at Poás crater on 30 April 2019. d) Proximal assembly components and specifications.

The proximal UAS sampling assembly (Figure 2B) was used on 30 April during three sampling flights of the plume 10-20 meters above the fumarole field. Take-off and landing occurred from take-off site #2 located within the crater, adjacent to the previous site of the crater lake (Figure 1). The assembly consisted of a quadcopter (DJI Inspire 1, flight time of ~6 minutes with payload) with the gas sampling configuration as a separate unit suspended 1.5 metres below the UAV. The payload (360 grams) consisted of a pump (1.2 L/minute) connected to an electronic switch (Turnigy 10A/30V) and a stand-alone receiver (Futaba R70087B) along with a battery pack. The four sampling gas bags (Altef, 800 ml) were connected in series from the outlet tube of the pump and contained in a mesh bag along with the gas sampling unit. The UAS was

maneuvered with one remote controller by the pilot, while the gas sampling unit was controlled by a second person using a secondary remote controller to switch the pump on and off. The convective nature of Boca A and Boca B prevented UAS sampling from those plumes at this proximal location.

Ground-based plume sampling

On 26 and 30 April, near-source ambient plume samples were taken in the fumarole field by placing the inlet tube on top of boulders in the fumarolic plume and using a pump to purge 5 meters of tubing before filling sample bags (Figure 1). The plumes of Boca A and Boca B were sampled at ground level by extending the inlet tube horizontally and using the pump to purge the line before filling sample bags.

Direct sampling

On 30 April, direct samples were collected in replicates of five within the floor of the pit crater from the monitoring fumarole, from a tube inserted into warm ground, and from a bubbling pool (Figure 1). A titanium tube or funnel was connected to less than 1 meter of silicon tubing, and a 1000 ml syringe and 3-way valve were used to flush the line of ambient air prior to collecting the sample. Each 12 ml vial was then flushed three times and filled to overpressure.

Isotopic analysis

All samples from 25 to 30 April were analyzed within 24 hours on a Picarro G2201-i CRDS at the geochemistry lab of the Observatorio Vulcanológico y Sismológico de Costa Rica (OVSICORI) in Heredia, Costa Rica, following the methods of (Malowany et al., 2017). A copper tube filled with fine copper wire cuttings was used to remove any interference from H_2S, and three in-house standards (-43.15‰, -15.6‰, and -11.4‰) were used to define a calibration curve (Figure S1). Any samples above 5000 ppm CO_2 were diluted with zero air administered

from a tank using a gas-tight syringe. A standard was run every 5 to 12 samples at concentrations ranging from 450 to 1050 ppm CO_2 to monitor instrument drift (Table S1). Carbon isotopic results are reported using the per mil notation which provides values relative to the Vienna Pee Dee Belmenite (VPDB) reference standard. Repeat analysis of standards shows that uncertainties are ~0.3 ‰.

Results

UAS and ground-based $\delta^{13}C$ results of April 2019

Results of all carbon isotopic measurements collected at Poás during 25-30 April 2019 are reported in Table S1 and direct samples from 2017 to 2019 are reported in Table S2. A background flight and unaffected ground samples ranged from 406 to 411 ppm and $\delta^{13}C$ of -9.5 to -10.4 ‰. Therefore, average background in this location during the time of sampling was 408 pm and -9.8 ‰. This is within an acceptable range for the tropospheric region, whose atmospheric signature varies, even at remote summits, due to diurnal fluctuations from biogenic respiration and altitude (Takahashi et al., 2002; Araujo et al., 2008). On 25 April, 16 dilute plume samples were collected by distal UAS sampling, with CO_2 concentrations ranging from 408 ppm to 491 ppm, and $\delta^{13}C$ of -9.7 to -11.4 ‰. On 30 April, 8 dilute plume samples were collected by proximal UAS sampling, with CO_2 concentrations ranging from 477 ppm to 528 ppm, and $\delta^{13}C$ of -8.2 to -9.1 ‰. On 26 and 30 April, we collected a total of 37 ground-based samples from the ambient plumes of Boca A, Boca B, and the fumarole field, with CO_2 concentrations ranging from 570 ppm to 5280 ppm and $\delta^{13}C$ of -3.2 to -10.4 ‰. Direct samples from 30 April taken from the monitoring fumarole, bubbling spring, and diffusely degassing soil range from -3.9 to -4.7 ‰. Concentrations exceed 40,000 ppm CO_2 for all direct samples.

The results of both the UAS proximal sampling and ground-based sampling are compared in Figures 3A and 3B. We used a Keeling approach (Keeling, 1958) to model a binary mixing line between background air and the volcanic source in order to estimate the volcanic source $\delta^{13}C$. Using this method, we performed regression analysis for proximal UAS samples (n=10, -3.97 ± 1.94 ‰, R^2 of 0.81), Boca A samples (n=6, intercept of -3.42 ± 0.49 ‰, R^2=0.99), Boca B samples (n=3, intercept of -4.76 ± 1.5 ‰, R^2=0.96), and ground-based sampling of the plume above the fumarole field (n=11, intercept of -2.38 ± 1.5 ‰, R^2=0.86). Errors on the intercepts are calculated at 95% confidence. In Figure 3A, the intercept of the proximal UAS-based sampling falls within the range of source values estimated for Boca A, Boca B, and the fumarole field, indicating the UAS was sampling a mixed plume. The proximal UAS intercept (-3.97 ‰) is nearly identical to the direct sampling $\delta^{13}C$ (average -4.01 ‰). In Figure 3B, all ground-based samples from April 2019 (Boca A, Boca B, ground-based samples above fumarole field, and direct samples) are grouped together as a mixed population to compare with the UAS results. The mean $\delta^{13}C$ estimated for all ground-based samples is -3.64 ± 0.48 ‰ (n=33, R^2 of 0.83), a difference of 0.33 ‰ from the source value based on the proximal UAS samples. Also in Figure 3B, we compare proximal UAS samples (all of which are greater than 50 ppm above background) with distal UAS samples greater than 50 ppm above background. We performed a linear regression on distal UAS samples of 25 April, to delineate a ternary source (-14.6 ± 4.4 ‰, R^2 = 0.67, n=4). As the distal samples were collected in less dense volcanic plume up to 100 metres above the vents, we postulate that these samples are a mixture of volcanic emissions (-4‰, this work), soil respiration from the crater floor (-17 to -27 ‰; (Glamoclija et al., 2004), forest or pasture respiration from adjacent areas (-27 or -21 ‰, respectively; (Powers, 2006), and

stable atmosphere (-8.5 ‰; (White et al., 2015). For this reason, these samples are plotted along with their own regression line, and are not included in the proximal regression.

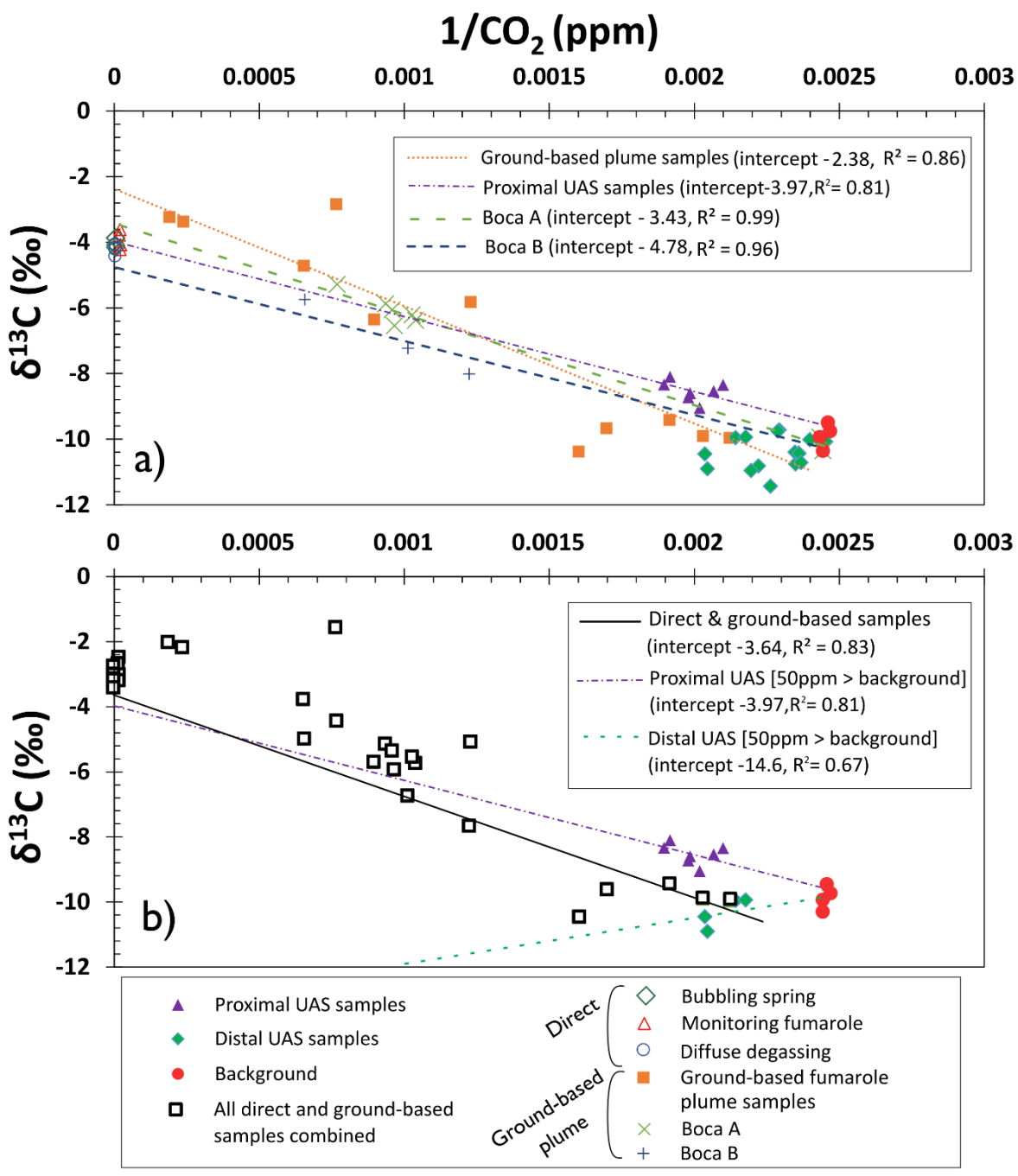

Figure 3: Plots showing inverse CO_2 concentration versus $\delta^{13}C$ relative to Vienna Pee Dee Belemnite of gas samples collected at Poás volcano in April-May 2019. a) Proximal UAS sampling (solid triangles), Boca A (x's), Boca B (crosses), and fumarole field plume samples

(solid squares) are shown along with their line of best fit. Also shown are samples from the distal UAS (solid diamonds), along with measurements of background air taken at the site (solid circles). Lastly, direct samples with very high concentrations are plotted as diffuse degassing (open circles), bubbling spring (open diamonds), and monitoring fumarole (open triangles). b) All ground-based sampling, including direct samples and samples of diffuse plumes taken from the ground, are plotted together (open squares) for comparison with proximal UAS sampling (triangles) and distal UAS samples (diamonds) greater than 50 ppm above background along with their respective linear regression lines of best fit.

In Figure 4, ground-based sampling from the three direct sampling sites in 2019 are compared to Boca A and B plumes. There is no statistically significant variation of $\delta^{13}CO_2$ for sites at Poás volcano measured in our study within the same 5-day span. This is consistent with the lack of significant $\delta^{13}CO_2$ variation among three fumaroles sampled from 2001 to 2008 (Hilton et al., 2010) and lack of systematic differences in major gas geochemistry from the same three sites (Fischer et al., 2015). However, de Moor et al. (2016) showed that SO_2/CO_2 varies between sources within the crater mostly due to variations in SO_2 flux. While we cannot rule out the possibility that the sites sampled in our study are isotopically distinct, we use the average $\delta^{13}C$ (-4.1 ± 0.5 ‰) collected in our study to represent the carbon isotopic signature of Poás volcano in April 2019 for temporal comparison with results from previous sample periods.

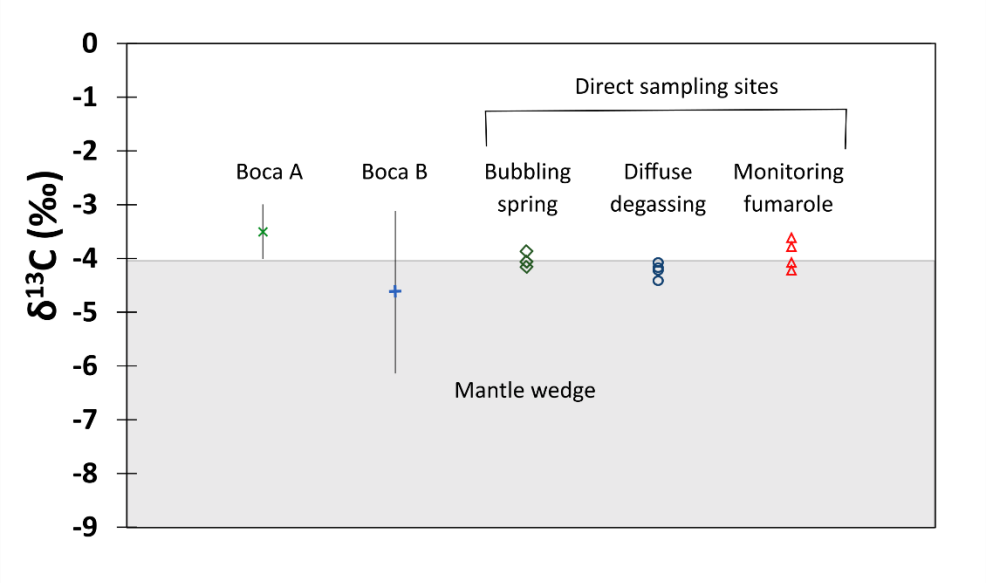

Figure 4: Spatial comparison of $\delta^{13}C$ in gas samples amongst sampling sites within the pit crater at Poás. Individual samples are shown for the monitoring fumarole (open triangles), bubbling spring (open diamonds) and diffuse degassing (open circles). Due to the comparatively dilute samples, the intercept of a linear regression of samples are shown for Boca A (green x's) and Boca B (blue crosses) along with the associated 95% confidence interval for each intercept (vertical lines). Mantle value shown is world-wide MORB (Sano and Marty, 1995).

Direct sampling results of January 2017 to April 2019

Direct samples range from -3.7 to -6.2 ‰ during 2017 to 2019, with the lightest value of -6.2 ‰ observed one week before the initiation of the April 2017 phreatic to phreatomagmatic activity (Fig. 5) during a ramping up phase of unrest associated with increasing SO_2 flux, increasing SO_2/CO_2 ratio, elevated seismicity, and inflation (Salvage et al., 2018; De Moor et al., 2019). These values lie within the range obtained for 2001 to 2008 samples (-1.3 to -6.8 ‰) from Hilton et al. (2010) and within the range of those obtained for 2000 to 2004 samples (-2.6 to -6.2 ‰) from Vaselli et al. (2019). With the exception of the April 2017 value of -6.2 ‰, a baseline during 2017 to 2019 appears to range between -3.4 and -5.1 ‰ for our dataset. The notably low value in April 2017 falls within the range of $\delta^{13}C$ recorded by Hilton et al. (2010) in January to

July 2001 (-5.6 to -6.8 ‰). Fischer et al. (2015) interpreted unstable fluctuations in gas ratios during 1998 to 2001 as the result of an influx of magmatic volatiles that occurred prior to 2001 along with increased infiltration of surface waters due to hydrofracturing events.

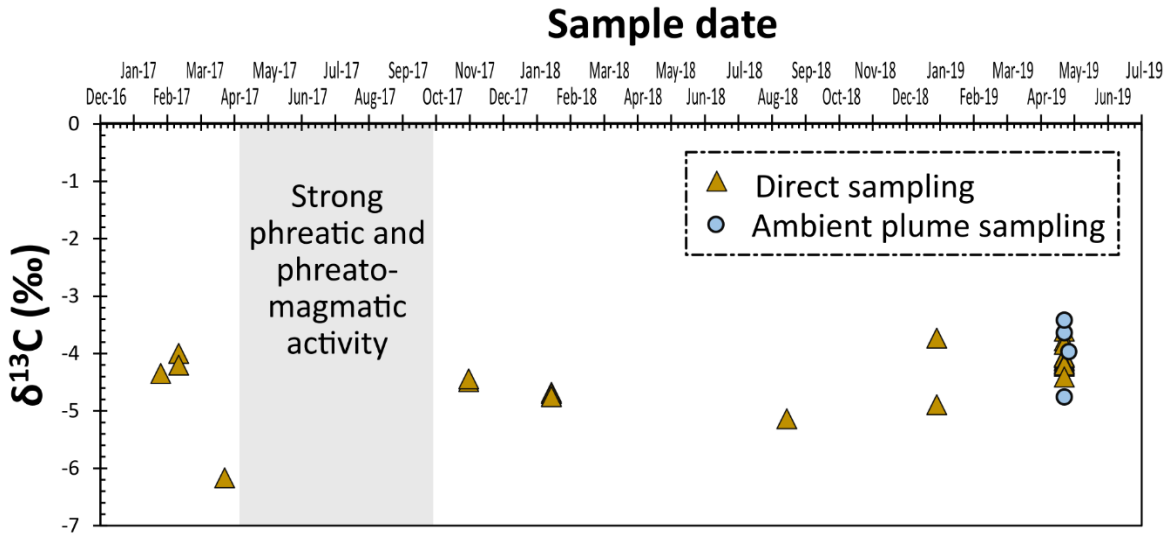

Figure 5: Carbon isotopic ratios relative to Vienna Pee Dee Belemnite from 2017 to 2019 at Poás volcano. Triangles represent direct sampling points collected from fumaroles, bubbling point source, or diffuse degassing through crater soil and measured by CRDS or IRMS. Circles represent estimates of source $\delta^{13}C$ for various plumes sampled by ground-based or UAS methods and extrapolated using the Keeling method (1958).

Discussion

Certain phreatic and phreatomagmatic eruptions are inherently linked to failure of a semi-permeable mineralized cap known as a hydrothermal seal (Stix and de Moor, 2018; Mick et al., 2021). This porosity-reducing mineralization has been considered by Rowe et al. (1992), notably for native sulfur deposits, in their model of a fractured magma carapace at Poás volcano. One caveat to consider when monitoring for magmatic changes at volcanoes with hydrothermal systems is the possibility of gases and their isotopic ratios being buffered by the hydrothermal system (Tassi et al., 2016). This further highlights the need to recognize which results indicate magmatic unrest and which are indicative of hydrothermal buffering. Our work attempts to

unravel this issue, laying the foundation for future studies exploring this interaction at Poás and elsewhere. Given the explosive nature of these eruptions, we first discuss how the use of UAS can improve monitoring at volcanoes with dynamic magmatic-hydrothermal systems. Next, we discuss the possible controls on carbon which could be related to magmatic fluids and sources, degassing, or hydrothermal sealing and unsealing at Poás. Finally, we integrate each of these controls into a new model incorporating the carbon isotope and gas ratio data from the 2005-2006 and 2017-2019 activity.

Drone-based and direct CO_2 sampling for same-day stable carbon isotopic analysis

An inherent challenge to airborne $\delta^{13}CO_2$ sampling of plumes is dictated by the need to sample a relatively high concentration plume, which is usually turbulent and risky to sample by UAS. Our work demonstrates that sampling dilute volcanic plumes by UAS can be a feasible volcano monitoring tool, which could supplement time-intensive ground sampling from crater floors. While the low CO_2 flux at Poás limited the concentration of dilute plume samples we collected in April 2019 (406 ppm to 528 ppm CO_2), we sampled higher concentrations and mole fractions of volcanic CO_2 (120 ppm above background, 23%, this work) as compared to other UAS carbon isotopic sampling campaigns at Manam volcano, Papua New Guinea ((Liu et al., 2020) and at Aso volcano, Japan (98 ppm above background, 19%; (Tsunogai et al., 2022). Using linear regression, we found remarkably similar $\delta^{13}C$ volcanic source values with the drone gas sampling assembly as compared to high concentration direct sampling. To further cross-validate our source estimate, we compared the linear regression using all proximal UAS samples (-3.97 ± 1.95 ‰, $R^2 = 0.81$) to that of only proximal samples with CO_2 concentrations greater than 500 ppm (-3.88 ± 1.55 ‰, $R^2 = 0.93$,) which are in agreement to within 0.09 ‰. Finally, we use a weighted mean of individual estimates based on proximal samples with CO_2 concentrations

greater than 500 ppm (Schipper et al., 2017), which estimates the volcanic signature to be -3.22 ± 0.86 ‰, thus within the acceptable error range produced by either regression calculation (Table S3). With caution and good sampling conditions, UAS plume sampling for isotopic analysis of carbon can be a reliable means by which to estimate the carbon signature at the source of a volcanic vent.

Controls on carbon isotopic systematics

Our data from 2017 to 2019 shows a marked change in baseline CO_2 in the lead-up to the April 2017 eruptive period. We propose that a steady-state convecting magma chamber replenished by deep injections governs the observed range in $\delta^{13}C$ baseline values (3.4 to -5.1 ‰). Minor variations in supply and increased magmatic fluids could potentially account for the slight rise in the baseline $\delta^{13}C$ leading up to the 2017 activity. However, this model alone cannot explain the major drop in $\delta^{13}C$ (from baseline to -6.2‰) observed at Poás in the immediate weeks leading up to the April 2017 opening eruptive phase. There are three main types of controls on carbon which we consider to interpret this drop in $\delta^{13}C$: deep sources of carbon, fractionation during magmatic degassing, and fractionation during shallow hydrothermal processes.

The simplest mechanism to begin with is based purely on fingerprinting the sources of carbon that supply the magmatic system from which the CO_2 is derived. The relative abundances of mantle wedge, sediment, and limestone accrued during subduction can be estimated based upon $\delta^{13}CO_2$ and $CO_2/^3He$ (Sano and Marty, 1995). Based upon further $^3He/^4He$ records, Hilton et al. (2010) postulated that beyond these three endmembers, crustal-derived CO_2 from the Caribbean plate could have caused the observed increase in $\delta^{13}CO_2$ in fumaroles at Poás from 2001 to 2005. Isotopically light compositions were attributed to relatively higher mantle contribution to the magmatic system. However, this model does not apply to our 2017 to 2019 data given the

evidence for a lack of deep magma involved in the eruption. The evolved composition of the juvenile magma erupted in the 2017 eruption (De Moor et al., 2019) and high SO_2/CO_2 concurrent with phreatic-phreatomagmatic eruptions reported during 2014 to 2017 at Poás (Moor et al., 2016; De Moor et al., 2019) together provide evidence for remobilization of pre-emplaced magma rather than injection of a fresh CO_2-rich intrusion spawning the 2017 activity. Finally, deep supply of CO_2 from increased magmatic fluids in 2017 would be expected to supply a more positive $\delta^{13}C$, so we instead seek other processes to explain the negative $\delta^{13}C$ excursion of April 2017.

The second mechanism is fractionation during magma degassing. Experimental studies have shown that $\delta^{13}CO_2$ decreases as a magma becomes progressively more degassed (Holloway and Blank, 1994), due to the preferential exsolution of heavier carbon into the vapour phase (Javoy et al., 1978). In Hawaii, Gerlach and Taylor (Gerlach and Taylor, 1990) demonstrated that closed-system equilibrium degassing can account for carbon isotope fractionation leading to the more negative $\delta^{13}CO_2$ of the Kilauea East Rift zone (-7.8‰) as compared to less fractionated summit crater gases (-3.4‰). At Etna, several authors have noted decadal or annual variations in $\delta^{13}CO_2$ which have been attributed to a combination of either deep and shallow magmatic endmembers of different stages of degassing being tapped, carbonate assimilation over time, or mantle metasomatism of carbon-rich fluids (Martelli et al., 2008; Chiodini et al., 2011; Paonita et al., 2012). Short-term variations in $\delta^{13}CO_2$ at Etna spanning 5 days were attributed solely to degassing-associated fractionation (Rizzo et al., 2015). A dual magmatic source has been extensively studied at Stromboli volcano (Aiuppa et al., 2010) whereby explosive periods are supplied by CO_2-rich gas bubbles from a deep source while degassing of a shallow magma contributes to quiescent degassing. Injection of deeply sourced CO_2 from undegassed basaltic

magma would be expected to produce isotopically heavier CO_2 (more positive $\delta^{13}CO_2$ than baseline) (Javoy et al., 1978) rather than the observed negative $\delta^{13}CO_2$ of -6.2 ‰. Our sample from April 2017 shows an anomalously light $\delta^{13}C$ consistent with the idea that the CO_2 was released from a largely degassed magma (de Moor et al., 2019) which was emplaced at shallow levels in 2000 – 2005 (Rymer et al., 2009).

There is a third mechanism of potentially equal importance at Poás: shallow buffering of carbon. In a hydrothermal setting, carbon can theoretically exist in gaseous, solid (bound in minerals), or aqueous (dissolved in solution) form. Preferential uptake of carbon during exchange from one form to another can result in fractionation corresponding to a fractionation factor, ε, which is dependent on temperature. In systems where pH is neutral or higher, calcite deposition in hydrothermal alteration areas is a mechanism by which CO_2 is removed from solution (Giggenbach, 1984). Assuming precipitation at temperatures less than 192°C, hydrothermal calcite deposited in the hydrothermal system will be isotopically heavy with respect to the gas (Ray et al., 2009; Barry et al., 2019). If calcite were dissolved back into hydrothermal fluids and released as a gas phase, we would expect an increasingly heavy signature. However, Laguna Caliente at Poás is highly acidic (Martínez et al., 2000), and no calcite has been found in a recent study which surveyed the alteration minerals in the surficial area (Rodríguez and van Bergen, 2017). Carbon dioxide exsolved from a magma body can remain in gaseous form or become dissolved in hydrothermal fluids according to Henry's law of solubility (Vogel et al., 1970). In the low pH settings of active craters, the aqueous form will be almost exclusively dissolved carbon, as bicarbonate and carbonate speciation is negligible. The ^{13}C partitions preferentially into the vapor phase according to a fractionation factor, $\alpha^{13}CO_2^{\text{vapor-solution}}$ which is temperature-dependent. As the core acid part of the hydrothermal system expands and is heated, fluid-gas

fractionation could contribute isotopically heavy C to the gas emissions. This has been postulated for hydrothermal areas exhibiting heavier $\delta^{13}CO_2$ as compared to higher-temperature crater areas at Turrialba volcano (Malowany et al., 2017). We propose that this hydrothermal process could potentially account for the slight rise in the baseline $\delta^{13}C$ leading up to the 2017 activity.

We now formulate our model of the activity at Poás in relation to the sealing and unsealing of the hydrothermal cap while drawing upon the fundamental mechanisms discussed above.

Spatio-temporal evolution of carbon isotopic variations at Poás from 2017 to 2019

We first discuss the implications of our results in terms of spatial variation at the study site, then discuss temporal evolution. While we cannot say for certain whether the different sources in the Poás crater are isotopically homogeneous due to the overlap in error amongst Boca A, Boca B, and the fumaroles (Figure 4), we can see that these sites may be supplied with gases from a common source with $\delta^{13}CO_2$ of -4.1 ± 0.5 ‰. The limited spatial variation could indicate a common permeable conduit source which is comprised of a network of interconnected fractures, as has been proposed to explain intra-crater spatial variation elsewhere, e.g., Cerro Negro (Lucic et al., 2014). This aligns well with the proposed structure of the magmatic plumbing system at Poás proposed by (Rymer et al., 2005), wherein gravimetric data point to a common magmatic carapace that is overlain by finger-like intrusions of shallower magma <100 m beneath the pit crater and dome. Keeping in mind the uncertainty of spatial variations, we now compare temporal results of carbon isotopes collected from various locations at Poás in this campaign (2017 to 2019) to previous campaigns (2001 to 2014).

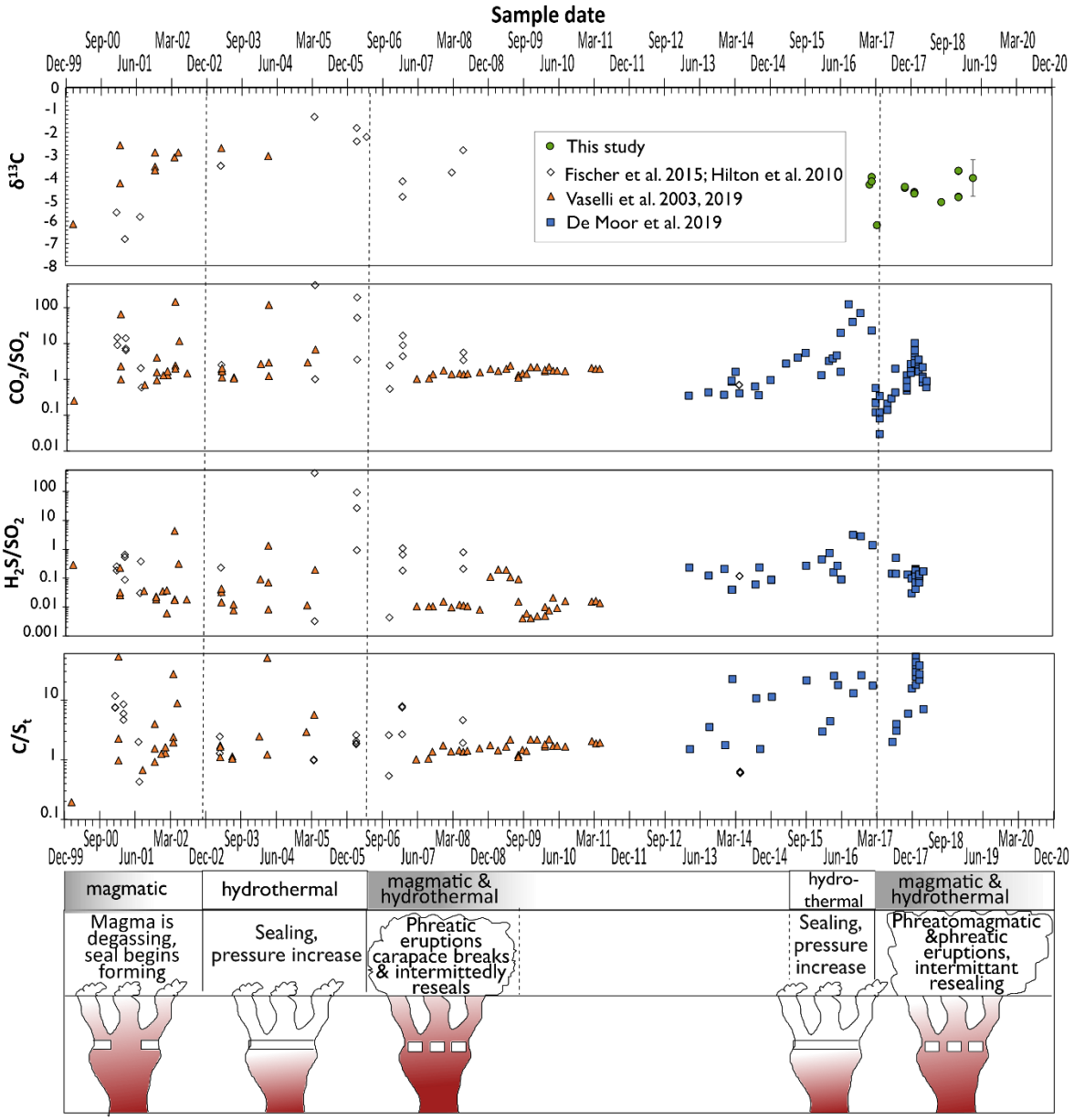

Figure 6: Comparison of gas geochemistry from 1999 to 2019 at Poás volcano, Costa Rica, with a schematic model shown at the bottom. We have not applied our model to activity at Poás from 2009 to 2016 due to a lack of carbon isotopic data spanning this timeframe.

The first stage of activity which our data cover is January to March 2017, when the gases were supplied by a convecting magma chamber overlain by a relatively well-sealed hydrothermal system. High H_2S/SO_2 and increasing C/S indicate hydrothermal sealing processes associated

with sulfur deposition, while $\delta^{13}C$ remains within baseline values. Failure of the hydrothermal seal in April 2017 likely caused sudden depressurization of previously emplaced shallow magma and was associated with increased degassing (de Moor et al., 2019). The next stage of activity is the April 2017 phreatomagmatic episodes and subsequent eruptions through August 2017. The onset of the eruption caused the hydrothermal seal to break, allowing the shallow magmatic gas which had been accumulating in the volatile-rich zone of the magma carapace to escape. Since the magma carapace was emplaced pre-2006 (Rymer et al., 2009; Fischer et al., 2015), the magma had already been degassing for several years. These observations agree with our results, wherein the $\delta^{13}C$ dipped to a more negative value (-6.2 ‰) consistent with a greater influence from a degassed magma. By November 2017, the $\delta^{13}C$ had returned to within baseline values (-4.5 ‰), indicating a return to steady state conditions as the hydrothermal seal was steadily rebuilding.

Extending our model further into the past, we now provide a new interpretation of the 2001-2008 evolution of carbon isotope systematics at Poás. In Figure 6 we compare data taken from gases at the Naranja/Norte fumarole, Official/Este fumarole, and Monitoring fumarole (Vaselli et al., 2003, 2019; Hilton et al., 2010; Fischer et al., 2015) with our data. Firstly, the lowest $\delta^{13}C$ of 2001 (-4.3 to -6.8 ‰) was collected from the Official/Este fumarole (Fischer et al., 2015; Vaselli et al., 2019) and is equivalent to the April 2017 isotopic signature (-6.2 ‰) of degassed magma with little or no hydrothermal influence. H_2S/SO_2 was low in 2001, consistent with a lesser influence of the hydrothermal system, though spatial heterogeneity is apparent. Scatter in the carbon isotopic values also reflects spatial heterogeneity in those fumaroles closer to the lake which likely underwent some buffering during gas-fluid exchange processes. The $\delta^{13}C$ then increased from January 2001 to June 2005, peaking at -1.3 ‰ in June 2005, 9 months before the

first phreatic eruption in 2006. This was followed by a steady decrease in $\delta^{13}C$ during phreatic activity post-June 2005, reaching -4.0 ‰ by 2008. This could be explained by either the shallow (fluid-gas interaction) or deep (degassing fractionation) mechanisms considered in our model. The first scenario suggests that the peak in $\delta^{13}C$ of -1.3‰ in 2005 was a response to increased heat, expansion of the acidic hydrothermal system and an increasing fluid-gas fractionation prior to the current extended eruption period. The second scenario would suggest that the increasing $\delta^{13}C$ was caused by progressively greater influence from the deeper system as slab and mantle carbon has a $\delta^{13}C$ of -0.5‰ ((Barry et al., 2019). As injections of undegassed magma enter into the deep convecting magma chamber with associated emplacement of shallow dikes, $\delta^{13}C$ would increase, while the subsequent decrease in $\delta^{13}C$ would be due to degassing fractionation as $CO_2$is lost from those same dikes. Both these scenarios align well with the model suggested by Fischer et al. (2015) in which injection of magma or magmatic volatiles in 1998 to 2005 were marked by increased C/S (Figure 6), which progressively formed a hydrothermal seal and subsequent pressure buildup under the seal. According to these authors, the post-2006 magma was continuously degassing and the hydrothermal seal became fractured as phreatic eruptions occurred in 2006 and 2008, with intermittent re-sealing. In late 2006, $\delta^{13}C$ values were -4 to -5 ‰, indicating a transition between partly hydrothermal and partly magmatic influence. More recently, Vaselli et al. (2019) suggested overpressuring and rupture of the hydrothermal seal in 2005-2006 as the system switched from hydrothermal to more magmatic dominated. Our model strengthens previous models by incorporating a mechanism by which carbon isotope systematics can be accounted for during both magmatic-dominated eruptive phases and baseline hydrothermal activity. With this new insight, we can now better understand and recognize the

cycles of hydrothermal seal formation and pressurization leading up to phreatomagmatic activity using carbon isotope monitoring.

Conclusions

Our new UAS approach to volcano monitoring could fill the gap left by current techniques, as rapid and repeated deployment of sampling drones, with same-day isotopic analysis, can be used prior to, during, and after eruptive phases to detect small isotopic changes occurring in the magmatic-hydrothermal plumbing system which would otherwise be overlooked. We have combined direct sampling of fumaroles with ground-based and UAS-based sampling of volcanic plumes at Poás volcano, Costa Rica, to characterize the stable carbon isotopic variations in the volcanic CO_2. We found markedly similar $\delta^{13}C$ between the two techniques. Near-synchronous sampling across multiple sites at Poás has demonstrated little spatial variation in $\delta^{13}C$, allowing for multi-decadal comparison of carbon isotope systematics at Poás. We present results of $\delta^{13}C$ from fumarolic sampling spanning 2017 to 2019. A comparatively negative carbon isotopic value of -6.2 ‰ immediately prior to the April 2017 phreatomagmatic episode can be explained by our conceptual model, in which a broken hydrothermal seal allows volatiles from a degassed, pre-2006 magma to emit carbon with an isotopically light signature. Post-eruptive values return to pre-eruptive baseline values of –3.4 to -5.1 ‰. In 2018 to 2019, the values tend towards more positive $\delta^{13}C$ due to fluid-gas exchange governed by increasing temperature of the hydrothermal system as the seal reformed and periodic phreatic explosions provided fractures for fluid infiltration.

Acknowledgments

The authors would like to thank the staff of the Parque Nacional Volcán Poás for coordinating our entry to the field site. FD is grateful for support from Vanier Canada. FD and JS were also

supported by Discovery Grant funding from the Natural Sciences and Engineering Research Council of Canada, and by a seed grant from McGill University to purchase UAS. This work was also supported by funding from the Costa Rican Ley Transitorio 8933 and from Universidad Nacional, Costa Rica. Tobias Fischer and Geoffroy Avard are thanked for help in the field.

References

Aiuppa, A., Bertagnini, A., Métrich, N., Moretti, R., Di Muro, A., Liuzzo, M., and Tamburello, G., 2010, A model of degassing for Stromboli volcano: Earth and Planetary Science Letters, v. 295, p. 195–204, doi: 10.1016/j.epsl.2010.03.040.

Araujo, A., Kruijt, B., Nobre, A., Dolman, A., Waterloo, M., Moors, E., and De Souza, J., 2008, Nocturnal Accumulation of CO2 Underneath a tropical forest canopy along a topographical gradient: Ecological Applications, v. 18, p. 1406–1419.

Barry, P.H., de Moor, J.M., Giovannelli, D., Schrenk, M., Hummer, D.R., Lopez, T., Pratt, C.A., Segura, Y.A., Battaglia, A., Beaudry, P., Bini, G., Cascante, M., D'Errico, G., di Carlo, M., et al., 2019, Forearc carbon sink reduces long-term volatile recycling into the mantle: Nature, v. 568, p. 487–492, doi: 10.1038/s41586-019-1131-5.

Battaglia, A., de Moor, J.M., Aiuppa, A., Avard, G., Bakkar, H., Bitetto, M., Mora Fernández, M.M., Kelly, P., Giudice, G., Delle Donne, D., and Villalobos, H., 2019, Insights into the mechanisms of phreatic eruptions from continuous high frequency volcanic gas monitoring: Rincón de la Vieja Volcano, Costa Rica: Frontiers in Earth Science, v. 6, p. 1–20, doi: 10.3389/feart.2018.00247.

Boudoire, G., Rizzo, A.L., Di Muro, A., Grassa, F., and Liuzzo, M., 2018, Extensive CO2 degassing in the upper mantle beneath oceanic basaltic volcanoes: First insights from Piton de la Fournaise volcano (La Réunion Island): Geochimica et Cosmochimica Acta, v. 235, p. 376–401, doi: 10.1016/j.gca.2018.06.004.

Chiodini, G., Caliro, S., Aiuppa, A., Avino, R., Granieri, D., Moretti, R., and Parello, F., 2011, First 13C/12C isotopic characterisation of volcanic plume CO2: Bulletin of Volcanology, v.

73, p. 531–542, doi: 10.1007/s00445-010-0423-2.

Chiodini, G., Pappalardo, L., Aiuppa, A., Caliro, S., Nazionale, I., and Bologna, S., 2015, The geological CO 2 degassing history of a long-lived caldera: Geology, v. 43, p. 767–770, doi: 10.1130/G36905.1.

Christenson, B.W., Reyes, A.G., Young, R., Moebis, A., Sherburn, S., Cole-Baker, J., and Britten, K., 2010, Cyclic processes and factors leading to phreatic eruption events: Insights from the 25 September 2007 eruption through Ruapehu Crater Lake, New Zealand: Journal of Volcanology and Geothermal Research, v. 191, p. 15–32, doi: 10.1016/j.jvolgeores.2010.01.008.

Fischer, T.P., and Lopez, T.M., 2016, First airborne samples of a volcanic plume for δ13C of CO2 determinations: Geophysical Research Letters, v. 43, p. 3272–3279, doi: 10.1002/2016GL068499.Received.

Fischer, T.P., Ramírez, C., Mora-amador, R.A., Hilton, D.R., Barnes, J.D., Sharp, Z.D., Brun, M. Le, Moor, J.M. De, Barry, P.H., Füri, E., and Shaw, A.M., 2015, Temporal variations in fumarole gas chemistry at Poás volcano , Costa Rica: Journal of Volcanology and Geothermal Research, v. 294, p. 56–70, doi: 10.1016/j.jvolgeores.2015.02.002.

Gerlach, T.M., and Taylor, B.E., 1990, Carbon isotope constraints on degassing of carbon dioxide from Kilauea Volcano: Geochimica et Cosmochimica Acta, v. 54, p. 2051–2058, doi: 10.1016/0016-7037(90)90270-U.

Giggenbach, W.F., 1975, A simple method for the collection and analysis of volcanic gas samples: Bulletin Volcanologique, v. 39, p. 132–145, doi: 10.1007/BF02596953.

Giggenbach, W.F., 1984, Mass transfer in hydrothermal alteration systems-A conceptual approach: Geochimica et Cosmochimica Acta, v. 48, p. 2693–2711, doi: 10.1016/0016-7037(84)90317-X.

Glamoclija, M., Garrel, L., Berthon, J., and López-García, P., 2004, Biosignatures and bacterial diversity in hydrothermal deposits of Solfatara Crater, Italy: Geomicrobiology Journal, v. 21, p. 529–541, doi: 10.1080/01490450490888235.

Hanson, M.C., Oze, C., Werner, C., and Horton, T.W., 2018, Soil δ 13 C-CO 2 and CO 2 fl ux in

the H 2 S-rich Rotorua Hydrothermal System utilizing Cavity Ring Down Spectroscopy: Journal of Volcanology and Geothermal Research, v. 358, p. 252–260, doi: 10.1016/j.jvolgeores.2018.05.018.

Hilton, D.R., Ramírez, C.J., Mora-Amador, R., Fischer, T.P., Furi, E., Barry, P.H., and Shaw, A.M., 2010, Monitoring of temporal and spatial variations in fumarole helium and carbon dioxide characteristics at Poás and Turrialba volcanoes , Costa Rica (2001 – 2009): v. 44, p. 431–440.

Holloway, J.., and Blank, J.., 1994, Application of experimental resultsto C-O-H species in natural melts, *in* Carroll, M.. and Holloway, J.. eds., Volatiles in Magmas, Washington, D.C., Mineral Society of America, p. 187–230.

James, M., Carr, B., D'Arcy, F., Diefenbach, A., Dietterich, H., Fornaciai, A., Lev, E., Liu, E., Pieri, D., Rodgers, M., Smets, B., Terada, A., von Aulock, F., Walter, T., et al., 2020, Volcanological applications of unoccupied aircraft systems (UAS): Developments, strategies, and future challenges: Volcanica, v. 3, p. 67–114, doi: 10.30909/vol.03.01.67114.

Javoy, M., Pineau, F., and Iiyama, I., 1978, Experimental determination of the isotopic fractionation between gaseous CO2 and carbon dissolved in tholeiitic magma - A preliminary study: Contributions to Mineralogy and Petrology, v. 67, p. 35–39, doi: 10.1007/BF00371631.

Keeling, C., 1958, The concentration and isotopic abundances of atmospheric carbon dioxide in rural areas: Geochimica et Cosmochimica Acta, v. 13, p. 322–334, doi: 10.1016/0016-7037(58)90033-.

Liu, E.J., Aiuppa, A., Alan, A., Arellano, S., Bitetto, M., Bobrowski, N., Carn, S., Clarke, R., Corrales, E., de Moor, J.M., Diaz, J.A., Edmonds, M., Fischer, T.P., Freer, J., et al., 2020, Aerial strategies advance volcanic gas measurements at inaccessible, strongly degassing volcanoes: Science Advances, v. 6, p. eabb9103, doi: 10.1126/sciadv.abb9103.

Lucic, G., Stix, J., Sherwood Lollar, B., Lacrampe-Couloume, G., Muñoz, A., and Carcache, M.I., 2014, The degassing character of a young volcanic center: Cerro Negro, Nicaragua:

Bulletin of Volcanology, v. 76, p. 1–23, doi: 10.1007/s00445-014-0850-6.

Malowany, K., Stix, J., de Moor, J.M., Chu, K., Lacrampe-Couloume, G., and Sherwood Lollar, B., 2017, Carbon isotope systematics of Turrialba volcano, Costa Rica, unsing a portable cavity ring-down spectrometer: Geochemistry, Geophysics, Geosystems, v. 18, p. 2769–2784, doi: 10.1002/2017GC006856.

Martelli, M., Caracausi, A., Paonita, A., and Rizzo, A., 2008, Geochemical variations of air-free crater fumaroles at Mt. Etna: New inferences for forecasting shallow volcanic activity: Geophysical Research Letters, v. 35, p. 2–7, doi: 10.1029/2008GL035118.

Martínez, M., Fernández, E., Valdés, J., Barboza, V., Van Der Laat, R., Duarte, E., Malavassi, E., Sandoval, L., Barquero, J., and Marino, T., 2000, Chemical evolution and volcanic activity of the active crater lake of Poas volcano, Costa Rica, 1993-1997: Journal of Volcanology and Geothermal Research, v. 97, p. 127–141, doi: 10.1016/S0377-0273(99)00165-1.

Mick, E., Stix, J., de Moor, J.M., and Avard, G., 2021, Hydrothermal alteration and sealing at Turrialba volcano, Costa Rica, as a mechanism for phreatic eruption triggering: Journal of Volcanology and Geothermal Research, v. 416, p. 107297, doi: 10.1016/j.jvolgeores.2021.107297.

Moor, J.M. De, Aiuppa, A., Pacheco, J., Avard, G., Kern, C., Liuzzo, M., Martínez, M., Giudice, G., and Fischer, T.P., 2016, Short-period volcanic gas precursors to phreatic eruptions : Insights from Poás Volcano , Costa Rica: Earth and Planetary Science Letters, v. 442, p. 218–227, doi: 10.1016/j.epsl.2016.02.056.

De Moor, J.M., Stix, J., Avard, G., Muller, C., Corrales, E., Diaz, J.A., Alan, A., Brenes, J., Pacheco, J., Aiuppa, A., and Fischer, T.., 2019, Insights on Hydrothermal - Magmatic Interactions and Eruptive Processes at Poás Volcano (Costa Rica) From High - Frequency Gas Monitoring and Drone Measurements: Geophysical Research Letters, v. 46, p. 1293–1302, doi: 10.1029/2018GL080301.

Paonita, A., Caracausi, A., Iacono-Marziano, G., Martelli, M., and Rizzo, A., 2012, Geochemical evidence for mixing between fluids exsolved at different depths in the magmatic system of

Mt Etna (Italy): Geochimica et Cosmochimica Acta, v. 84, p. 380–394, doi: 10.1016/j.gca.2012.01.028.

Powers, J.S., 2006, Spatial variation of soil organic carbon concentrations and stable isotopic composition in 1-ha plots of forest and pasture in Costa Rica: Implications for the natural abundance technique: Biology and Fertility of Soils, v. 42, p. 580–584, doi: 10.1007/s00374-005-0054-5.

Ray, M.C., Hilton, D.R., Muñoz, J., Fischer, T.P., and Shaw, A.M., 2009, The effects of volatile recycling, degassing and crustal contamination on the helium and carbon geochemistry of hydrothermal fluids from the Southern Volcanic Zone of Chile: Chemical Geology, v. 266, p. 38–49, doi: 10.1016/j.chemgeo.2008.12.026.

Rizzo, A.L., Jost, H.J., Caracausi, A., Paonita, A., Liotta, M., and Martelli, M., 2014, Real-time measurements of the concentration and isotope composition of atmospheric and volcanic CO2 at Mount Etna (Italy): Geophysical Research Letters, v. 41, p. 2382–2389, doi: 10.1002/2014GL059722.Received.

Rizzo, A.L., Liuzzo, M., Ancellin, M.A., and Jost, H.J., 2015, Real-time measurements of δ13C, CO2 concentration, and CO2/SO2 in volcanic plume gases at Mount Etna, Italy, over 5 consecutive days: Chemical Geology, v. 411, p. 182–191, doi: 10.1016/j.chemgeo.2015.07.007.

Rizzo, A.L., Pelorosso, B., Coltorti, M., Ntaflos, T., Bonadiman, C., Matusiak-Małek, M., Italiano, F., and Bergonzoni, G., 2018, Geochemistry of noble gases and co2 in fluid inclusions from lithospheric mantle beneath wilcza góra (Lower silesia, southwest Poland): Frontiers in Earth Science, v. 6, doi: 10.3389/feart.2018.00215.

Rodríguez, A., and van Bergen, M.J., 2017, Superficial alteration mineralogy in active volcanic systems: An example of Poás volcano, Costa Rica: Journal of Volcanology and Geothermal Research, v. 346, p. 54–80, doi: 10.1016/j.jvolgeores.2017.04.006.

Rouwet, D., Mora-amador, R., Ramirez-umana, C.J., Gonzalez, G., and Inguaggiato, S., 2017, Dynamic fluid recycling at Laguna Caliente (Poa and during the 2006 – ongoing phreatic eruption cycle (2005 – 10), *in* Ohba, T., Capaccioni, B., and Caudron, C. eds.,

Geochemistry and Geophysics of Active Volcanic Lakes, London, Geological Society, Special publications, 437, p. 73–96.

Rowe, G.L., Brantley, S.L., Fernandez, M., Fernandez, J.F., Borgia, A., and Barquero, J., 1992, Fluid-volcano interaction in an active stratovolcano: the crater lake system of Poás volcano, Costa Rica: Journal of Volcanology and Geothermal Research, v. 49, p. 23–51, doi: 10.1016/0377-0273(92)90003-V.

Rymer, H., Locke, C.A., Borgia, A., Martinez, M., Brenes, J., Van Der Laat, R., and Williams-Jones, G., 2009, Long-term fluctuations in volcanic activity: Implications for future environmental impact: Terra Nova, v. 21, p. 304–309, doi: 10.1111/j.1365-3121.2009.00885.x.

Rymer, H., Locke, C.A., Brenes, J., and Williams-Jones, G., 2005, Magma plumbing processes for persistent activity at Poás volcano, Costa Rica: Geophysical Research Letters, v. 32, p. 1–4, doi: 10.1029/2004GL022284.

Rymer, H., van Wyk de Vries, B., Stix, J., and Williams-Jones, G., 1998, Pit crater structure and processes governing persistent activity at Masaya Volcano, Nicaragua: Bulletin of Volcanology, v. 59, p. 345–355, doi: 10.1007/s004450050196.

Salvage, R.O., Avard, G., Moor, J.M. De, and Pacheco, J.F., 2018, Renewed Explosive Phreatomagmatic Activity at Poás Volcano , Costa Rica in April 2017: Frontiers in Earth Science, v. 6, p. 1–18, doi: 10.3389/feart.2018.00160.

Sandoval-Velasquez, A., Rizzo, A.L., Aiuppa, A., Remigi, S., Padrón, E., Pérez, N.M., and Frezzotti, M.L., 2021, Recycled crustal carbon in the depleted mantle source of El Hierro volcano, Canary Islands: Lithos, v. 400–401, doi: 10.1016/j.lithos.2021.106414.

Sano, Y., and Marty, B., 1995, Origin of carbon in fumarolic gas from island arcs: Chemical Geology, v. 119, p. 265–274.

Schipper, C.I., Moussallam, Y., Curtis, A., Peters, N., Barnie, T., Bani, P., Jost, H.J., Hamilton, D., Aiuppa, A., Tamburello, G., and Giudice, G., 2017, Isotopically (δ13C and δ 18 O) heavy volcanic plumes from Central Andean volcanoes: a field study: Bulletin of Volcanology, v. 79, doi: 10.1007/s00445-017-1146-4.

Shingubara, R., Tsunogai, U., Ito, M., Nakagawa, F., Yoshikawa, S., Utsugi, M., and Yokoo, A., 2021, Development of a drone-borne volcanic plume sampler: Journal of Volcanology and Geothermal Research, v. 412, p. 107197, doi: 10.1016/j.jvolgeores.2021.107197.

Stix, J., and de Moor, J.M., 2018, Understanding and forecasting phreatic eruptions driven by magmatic degassing: Earth, Planets and Space, v. 70, doi: 10.1186/s40623-018-0855-z.

Takahashi, H.A., Konohira, E., Hiyama, T., Minami, M., Nakamura, T., and Yoshida, N., 2002, Diurnal variation of CO 2 concentration, Δ 14 C and δ 13 C in an urban forest: Estimate of the anthropogenic and biogenic CO 2 contributions: Tellus, Series B: Chemical and Physical Meteorology, v. 54, p. 97–109, doi: 10.1034/j.1600-0889.2002.00231.x.

Tassi, F., Agusto, M., Vaselli, O., and Chiodini, G., 2016, Copahue Volcano, *in* Tassi, F., Vaselli, O., and Caselli, A.T. eds., Copahue Volcano, Berlin-Heidelberg, Springer-Verlag Berlin Heidelberg, p. 119–139, doi: 10.1007/978-3-662-48005-2.

Troll, V.R., Hilton, D.R., Jolis, E.M., Chadwick, J.P., Blythe, L.S., Deegan, F.M., Schwarzkopf, L.M., and Zimmer, M., 2012, Crustal CO2 liberation during the 2006 eruption and earthquake events at Merapi volcano , Indonesia: Geophysical Research Letters, v. 39, p. 1–6, doi: 10.1029/2012GL051307.

Tsunogai, U., Shingubara, R., Morishita, Y., Ito, M., Nakagawa, F., Yoshikawa, S., Utsugi, M., and Yokoo, A., 2022, Sampling Volcanic Plume Using a Drone-Borne SelPS for Remotely Determined Stable Isotopic Compositions of Fumarolic Carbon Dioxide: Frontiers in Earth Science, v. 10, p. 1–12, doi: 10.3389/feart.2022.833733.

Vaselli, O., Tassi, F., Fischer, T., Tardani, D., Fernandez, E., Martinez, M. del M., de Moor, J.M., and Bini, G., 2019, The Last Eighteen Years (1998–2014) of Fumarolic Degassing at the Poás Volcano (Costa Rica) and Renewal Activity, *in* Tassi, F., Vaselli, O., and Mora-Amador, R.A. eds., Poás Volcano: The Pulsing Heart of Central America Volcanic Zone, Switzerland, Springer International Publishing, p. 235–260, doi: 10.1007/978-3-319-02156-0_10.

Vaselli, O., Tassi, F., Minissale, A., Montegrossi, G., Duarte, E., Fernández, E., and Bergamaschi, F., 2003, Fumarole migration and fluid geochemistry at Poás Volcano (Costa

Rica) from 1998 to 2001, *in* Oppenheimer, C., Pyle, D.., and Barclay, J. eds., Volcanic Degassing, London, Geological Society, v. 213, p. 247–262, doi: 10.1144/GSL.SP.2003.213.01.15.

Venturi, S., Tassi, F., Bicocchi, G., Cabassi, J., Capecchiacci, F., Capasso, G., Vaselli, O., Ricci, A., and Grassa, F., 2017, Fractionation processes affecting the stable carbon isotope signature of thermal waters from hydrothermal / volcanic systems : The examples of Campi Flegrei and Vulcano Island (southern Italy): Journal of Volcanology and Geothermal Research, v. 345, p. 46–57, doi: 10.1016/j.jvolgeores.2017.08.001.

Vogel, J.C., Grootes, P.M., and Mook, W.G., 1970, Isotopic fractionation between gaseous and dissolved carbon dioxide: Zeitschrift für Physik, v. 230, p. 225–238, doi: 10.1007/BF01394688.

White, J.W.C., Vaughn, B.H., and Michel, S.E., 2015, Institute of Arctic and Alpine Research (INSTAAR), Stable Isotopic Composition of Atmospheric Carbon Dioxide (13C and 18O) from the NOAA ESRL Carbon Cycle Cooperative Global Air Sampling Network, 1990-2014, Version: 2015-10-26: University of Colorado, ftp://aftp.cmdl.noaa.gov/data/trace_gases/co2c13/flask/.

Preface to chapter 2

In the previous chapter, I show that carbon isotopes can be sampled safely at volcanic summits by remote means with introduction of the first Compact Aerial Receiver-Initiated Gas-Sampling Operation (CARGO) for UAS-based sampling. We demonstrate the utility of carbon isotopes as forecasting tools at a wet volcano, that is to say, one with a strong hydrothermal system. In this chapter, we seek to answer the question of whether carbon isotopes are also variable at an open-vent volcano and how that can aid in eruption forecasting. We also seek to delineate the advantages and disadvantages of this type of gas monitoring, and test improvements we made to the original sampling systems with first usage of the CARGO 4.0. We derive a carbon signature of the volcanic source of Stromboli volcano in June 2019 using samples collected with CARGO 4.0. We use these along with carbon signatures spanning previous studies and 2018 (this work) to model degassing regimes at the volcano. Chapter 2 has been published in Geophysical Research Letters and is authored by Fiona D'Arcy, Alessandro Aiuppa, Fausto Grassa, Andrea Rizzo, and John Stix.

Citation:

D'Arcy, F., Aiuppa, A., Grassa, F., Rizzo, A.L., Stix, J. (2024). Large isotopic shift in volcanic plume CO_2 prior to a basaltic paroxysmal explosion. *Geophysical Research Letters*, 51, e2023GL107474, doi.org/10.1029/2023GL107474.

Chapter 2

Large isotopic shift in volcanic plume CO_2 prior to a basaltic paroxysmal explosion

Fiona D'Arcy[1], Alessandro Aiuppa[2], Fausto Grassa[3], Andrea Luca Rizzo[4,5], John Stix[1]

[1] Department of Earth & Planetary Sciences, McGill University, Montreal, Canada

[2] Dipartimento DiSTeM, Università degli Studi di Palermo, Palermo, Italy

[3] Istitutio Nazionale di Geofisica e Vulcanologia, Palermo, Palermo, Italy

[4] Department of Earth and Environmental Sciences, University of Milano-Bicocca, Piazza della Scienza 4, 20126, Milan, Italy

[5] Istitutio Nazionale di Geofisica e Vulcanologia, Sezione di Milano, Via Alfonso Corti 12, Milan, Italy

Corresponding author: Fiona D'Arcy (fiona.darcy@mail.mcgill.ca)

Key Points:

- Rapid collection of volcanic plume CO_2 enabled by Uncrewed Aerial Systems
- A carbon isotopic anomaly was present two weeks prior to the Stromboli 2019 paroxysm
- High CO_2 concentrations, elevated CO_2/S_t, and light $\delta^{13}C$-CO_2 may precede paroxysms on timescales of months to weeks

Abstract

Carbon dioxide is a key gas to monitor at volcanoes because its concentration and isotopic signature can indicate changes to magma supply and degassing behaviour prior to eruptions, yet carbon isotopic fluctuations at volcanic summits are not well constrained. Here we present $\delta^{13}C$ results measured from plume samples collected at Stromboli volcano, Italy, by Uncrewed Aerial Systems (UAS). We found contrasting volcanic $\delta^{13}C$ signatures in 2018 during quiescence (-0.36 ± 0.59 ‰) versus 10 days before the July 3rd 2019 paroxysm (-5.01 ± 0.56 ‰). Prior to the eruption, an influx of CO_2-rich magma began degassing at deep levels (~100 MPa) in an open-system fashion, causing strong isotopic fractionation and maintaining high CO_2/S_t ratios in the gas. This influx occurred between 10 days and several months prior to the event, meaning that isotopic changes in the gas could be detected weeks to months before unrest.

Plain Language Summary

Volcanoes produce gases which change composition depending on how active the volcano is. One of these gases, carbon dioxide, is known to change relative to other gases before an eruption occurs, but little is known about how the isotopes of carbon change leading up to an eruption. Using drones to reach the gaseous plume of Stromboli volcano, Italy, we have captured carbon dioxide both during an inactive phase in 2018 and during the lead-up to a highly explosive eruption called a paroxysm. There is a stark difference in the carbon isotopes measured 10 days before the July 3rd 2019 paroxysm as opposed to those measured in 2018. This is caused by the arrival of CO_2-rich magma which progressively degassed, leading to more negative carbon isotopes in the residual magma over time. This process could have started anywhere from 10 days to several months before the paroxysm. This provides a warning signal which can be picked up weeks to months before an active period begins.

Introduction

Volcanoes play a significant role in the global cycle of carbon (Burton et al., 2013; Mather, 2015; Werner et al., 2019). This is because carbon is the second major species dissolved in a magma, it is transferred from the lithosphere to the atmosphere during eruption, and more significantly, during quiescence between eruptions at open-vent volcanoes (Edmonds et al., 2022). Carbon isotopes provide information complementary to gas ratios and fluxes, as the isotopes can be used to constrain degassing pathways (Barry et al., 2014; Boudoire et al., 2018; Gerlach and Taylor, 1990), distinguish magma sources (Fischer et al., 2015; Paonita et al., 2012; Troll et al., 2012), and monitor magmatic inputs to hydrothermal systems (D'Arcy et al., 2022; Federico et al., 2008; Federico et al., 2023).

Sampling of volcanic plumes provides a safe and fast alternative to directly collecting volcanic gases from fumarolic vents into sample bottles. The plume can be sampled at varying distances from the source vent depending on the topography and wind conditions, but it is crucial to sample CO_2 as close to the source as possible for isotopic characterisation. Sampling was first done by physically entering the plume and manually collecting samples (Chiodini et al., 2011) before evolving to plume traverses in ground vehicles (Rizzo et al., 2015), helicopters (Fischer & Lopez, 2016), and use of field laboratories (Malowany et al., 2017; Schipper et al., 2017). Such sampling has entered a new era with the onset of compact sensor arrays combined with lightweight pumps for targeted sampling of volcanic plumes by Uncrewed Aerial Systems (UAS) (D'Arcy et al., 2022; Liu et al., 2020; Shingubara et al., 2021; Tsunogai et al., 2022).

Stromboli volcano is part of the Aeolian arc of volcanoes in Italy, which results from the subduction of the African plate below the European plate (e.g., Gasparini et al., 1982). It has a well-studied volcanic gas composition, with up to ~35 mol% CO_2 during passive degassing and

up to 54 mol% CO_2 during syn-explosive degassing (Aiuppa et al., 2010; Burton et al., 2007; Pering et al., 2020). The plumbing system of the volcano comprises a deep magma storage zone at ~6-8 km, from which low-porphyritic (LP) materials are erupted. The magmas here are CO_2-rich, reflected by gases at the surface with elevated CO_2/S_T exceeding values of 20. A second shallower storage zone <3 km deep produces highly porphyritic (HP) eruptive products, with associated gases depleted in CO_2 and having CO_2/S_T values less than 10-15 (Metrich et al., 2010; Aiuppa et al., 2010, 2021). Prior to this study, carbon isotopes of CO_2 at the summit of Stromboli varied from -1.0 to -2.5 ‰ $\delta^{13}C$ (Capasso et al., 2005; Federico et al., 2008; Finizola et al., 2003; Di Martino et al., 2021; Rizzo et al., 2009), yet plume samples from the summit have never been captured during and immediately prior to paroxysms.

In this work, we have refined a series of custom UAS gas sampling assemblies to collect CO_2 from Stromboli for isotopic analysis. We show distinct differences in $\delta^{13}C$ of CO_2 between passive quiescent degassing vs. immediately before a devastating explosive paroxysm. We relate these changes to transitions between closed-system and open-system degassing, i.e., to whether the gas travels with or separates from the host melt, respectively. We demonstrate the potential utility of carbon isotopes to better understand these styles of degassing and their implications for eruption forecasting at open-vent volcanoes.

Materials and Methods

Sampling and isotopic analysis

We conducted 25 sampling flights in May 2018 and June 2019 at the summit of Stromboli. We used a series of UAS (Figure 1a and 1b) and Compact Aerial Receiver-initiated Gas-sampling Operations (CARGOs) which we developed over the course of this study, paired with ground-based plume samples, which are described in detail in the Supporting Information (Text S1).

Each sampling flight collected two to ten 600 ml bags of plume gas, while individual ground-based samples of plume gas were collected with a pump and portable Multi-GAS at the crater rim. Bags were closed with clamps upon landing the aircraft and immediately taken from the summit to the field lab at the end of the day for same-day $\delta^{13}C$ analysis (Supporting Information Text S2-S6).

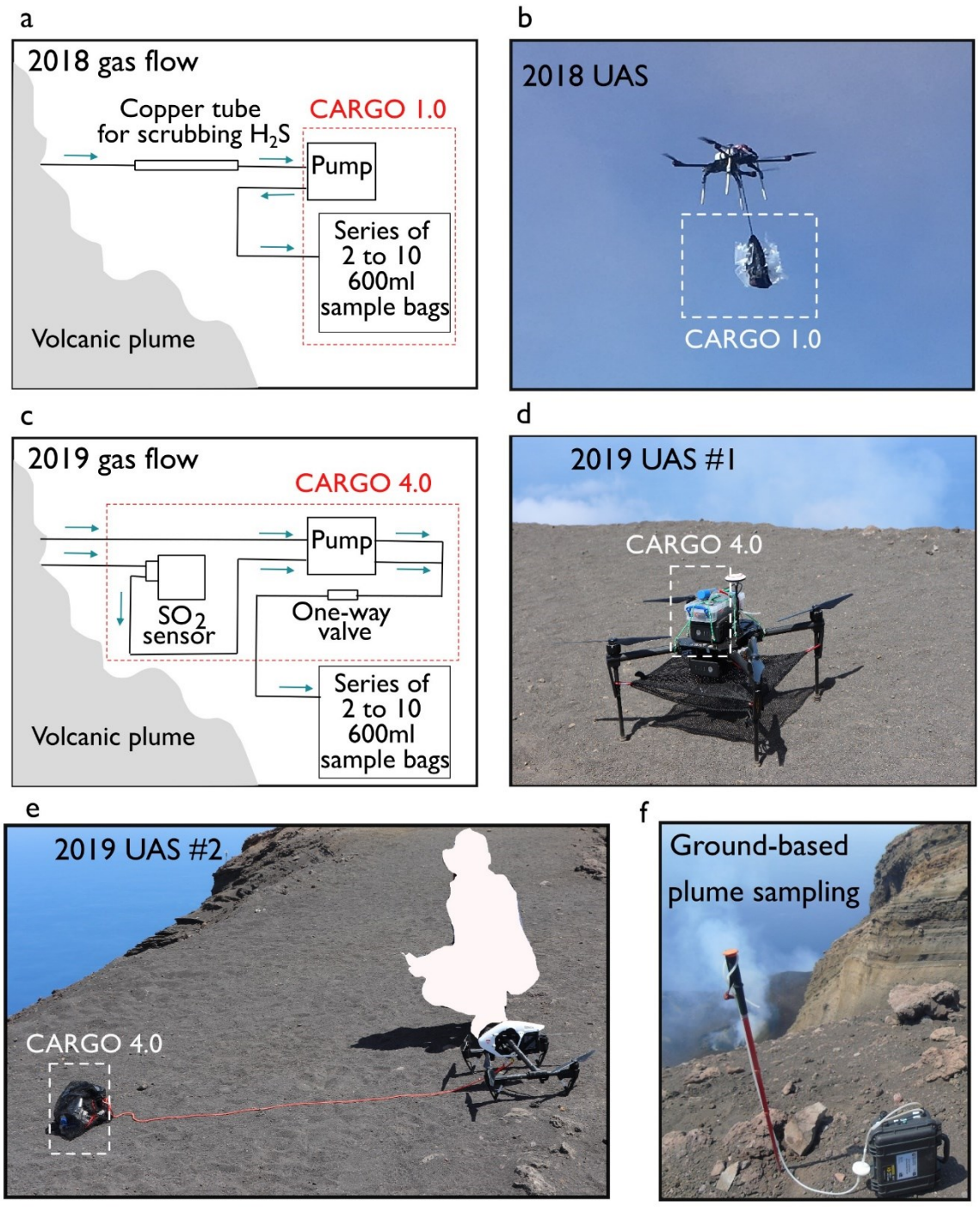

Figure 1: Sampling set-up for 2019 and 2018 samples. Gas flow schematics of the 2018 (a) and 2019 (c) Compact Aerial Receiver-initiated Gas-sampling Operations (CARGOs) along with the Uncrewed Aerial System (UAS) used to fly them in 2018 (b) and in 2019 (d, e). In (f), the general method used for ground-based sampling is pictured.

Estimates of the isotopic signature of magmatic carbon

Volcanic plumes are a mixture of atmosphere and volcanic gas, such that:

$$\delta^{13}C_p[CO_2]_p = f * \delta^{13}C_v[CO_2]_v + (1 - f) * \delta^{13}C_b[CO_2]_b \quad [1]$$

where f is the relative contribution from the volcanic source (Chiodini et al., 2011), and subscripts p, b, and v denote plume, background, and volcanic, respectively. To estimate the isotopic composition of the volcanic source of gas, isotopic results of plume samples must account for the presence of background air. A number of authors (Rizzo et al., 2014, 2015; Fischer and Lopez, 2016; Malowany et al., 2017; Liu et al., 2020; Shingubara et al., 2021; Tsunogai et al., 2022) have adopted the Keeling method (Keeling, 1958) to calculate the source $\delta^{13}C$ of volcanic plumes. This method uses linear regression to fit the observations of plume $\delta^{13}C$ against $1/CO_2$ to a line of best fit, wherein one endmember is background air and the other is the volcanic source. A linearization of equation [1] yields the equation of a line (equation [2]) wherein the y-axis intercept represents the theoretical composition of the volcanic source, $\delta^{13}C$ (Malowany et al., 2017):

$$\delta^{13}C_p = \frac{1}{[CO_2]_p}\,[CO_2]_b\,[\delta^{13}C_b - \delta^{13}C_v] + \delta^{13}C_v \quad [2]$$

There is a simplified method adapted from equation [1] which uses each discrete point sampled in a plume to estimate the $\delta^{13}C_v$ which takes the weighted mean of the combined estimates (Schipper et al., 2017):

$$[CO_2]_v \cdot \delta^{13}C_v = [CO_2]_p \cdot \delta^{13}C_p - CO_{2_b} \cdot \delta^{13}C_b \quad [3]$$

We applied both methods to calculate the volcanic source $\delta^{13}C$-CO_2.

Results and Discussion

First aerial samples of volcanic CO_2 capture an isotopically light data set

Average background from samples taken at the summit in 2018 was 401 ± 2 ppm CO_2 and -8.9 ± 0.2 ‰ $\delta^{13}C$-CO_2 (n=9), and 401 ± 2 ppm CO_2 and -9.9 ± 0.2 ‰ $\delta^{13}C$-CO_2 in 2019 (n=4). We discuss this background variation in the Supporting Information (Text S4). The concentration of CO_2 collected within the volcanic plume, during 14 flights from 12 - 17 May 2018, ranged from 405 to 490 ppm and $\delta^{13}C$ between -7.5 and -9.2 ‰ (Supporting Information Dataset S1). We also collected 16 ground-based plume samples on the crater rim which varied from 410 to 463 ppm CO_2 with $\delta^{13}C$ of -7.6 to -9.0 ‰. During 11 flights from 17 - 21 June 2019, we measured CO_2 concentrations ranging from 403 to 555 ppm and $\delta^{13}C$ between -8.3 and -9.8 ‰ (Dataset S1). We also collected 12 ground-based plume samples on the rim ranging from 408 to 501 ppm CO_2 with $\delta^{13}C$ -7.8 to -9.7 ‰.

Our volcanic plume concentrations are comparable to those collected by UAS at other volcanoes. Shingubara et al. (2021) achieved 531 ppm (maximum volcanic CO_2 of 61 ppm), while Tsunogai et al. (2022) reached 514 ppm (maximum volcanic CO_2 of 98 ppm) at Aso volcano in Japan. At Manam volcano in Papua New Guinea, plume samples from Liu et al. (2021) ranged from 421 to 494 ppm (maximum volcanic CO_2 of 85 ppm). At Poás volcano, D'Arcy et al. (2022) reached up to 528 ppm or 120 ppm volcanic CO_2.

The $\delta^{13}C_v$ estimated from the Keeling method for May 2018 and June 2019 are -0.36 ± 0.59 ‰ (R^2 = 0.67, p= 0.05, n=50) and -5.01 ± 0.56 ‰ (R^2 = 0.73, p= 0.05, n=51), respectively. Errors are reported as the standard error of the regression multiplied by 1.96 to give ±2σ (Figure 2). The estimates for the weighted mean method for 2018 and 2019 using samples with volcanic CO_2

concentration greater than 50 ppm are -0.78 ± 1.34 ‰ and -4.12 ± 1.71 ‰, respectively (Dataset S2).

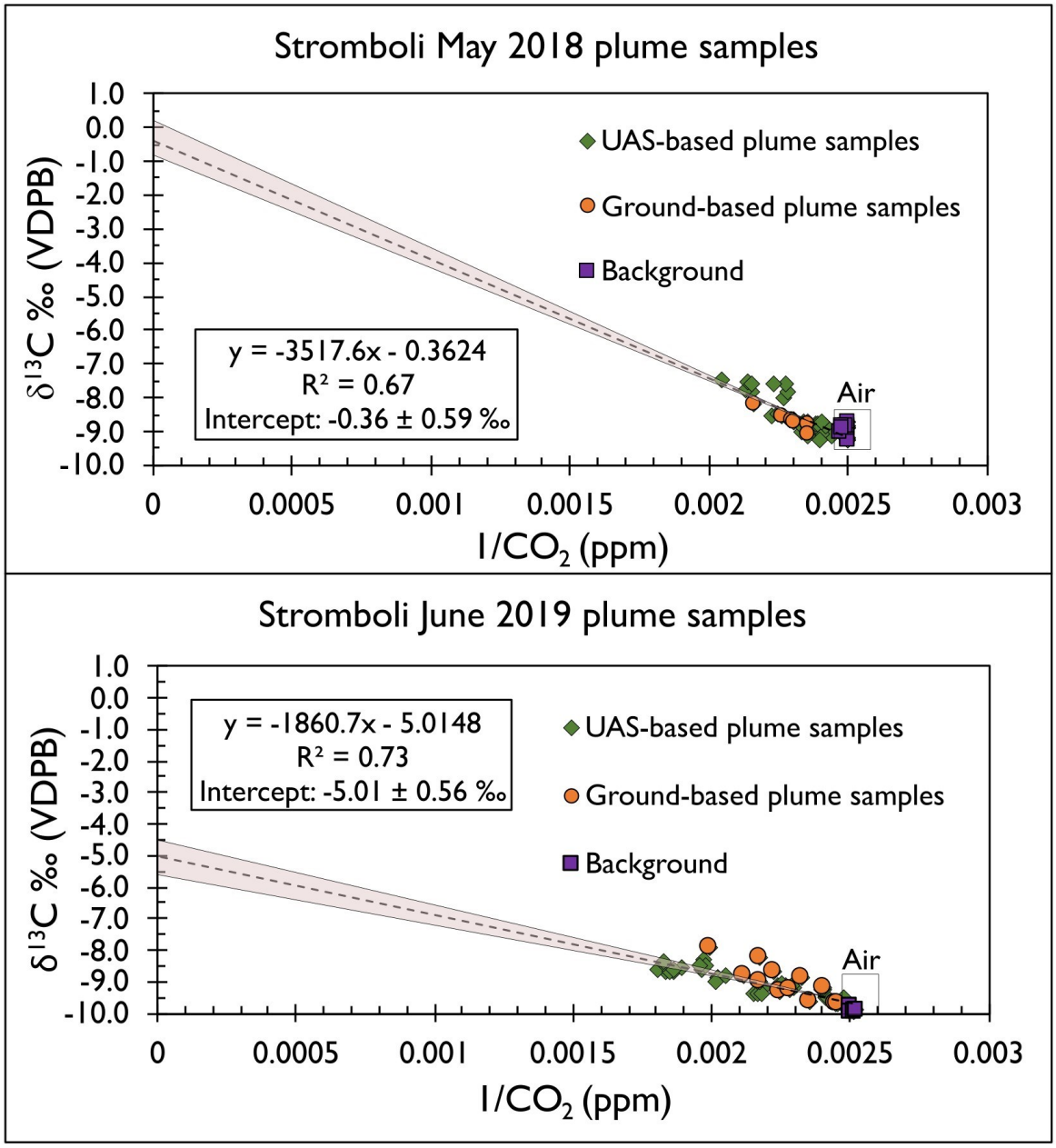

Figure 2: $\delta^{13}C$ values against inverse CO_2 concentrations of all plume samples during this study. UAS-based plume (green diamonds), ground-based plume (orange circles), and ground-based background (purple squares) samples are plotted and included in a linear regression analysis whose line of best fit (dashed line) is shown for 2018 (a) and 2019 (b). This line represents a mixing line between the volcanic source and background air which is extrapolated to the y-intercept in order to estimate the $\delta^{13}CO_2$ of the high concentration volcanic source.

The volcanic source $\delta^{13}C$-CO_2 composition we estimate for 2018 (-0.36 ± 0.59 ‰) is similar to albeit slightly heavier than the range of $\delta^{13}CO_2$ measured in summit fumaroles (-1.0 to -2.5 ‰) in previous years (Figure 3). The small difference between these past fumarole measurements (Capasso et al., 2005; Rizzo et al., 2009; Di Martino et al., 2021) and that of the plume we sampled in 2018 may be due to uncertainties in estimating $\delta^{13}C$, vent-specific differences, fumarole versus dense volcanic plume differences, and/or daily variations. Even more striking, the volcanic source in 2019 (-5.01 ± 0.56 ‰) is more than 2‰ lighter than the lowest $\delta^{13}C$ values usually measured at Stromboli in fumaroles (Figure 3). The large difference between the 2018 and 2019 isotopic signatures in the carbon dioxide sampled at Stromboli is a key finding, as the 2019 samples were collected two weeks prior to the July 3rd paroxysm, which was an unusually intense and fatal volcanic explosion (Andronico et al., 2021; Giordano & De Astis, 2021; Ripepe et al., 2021).

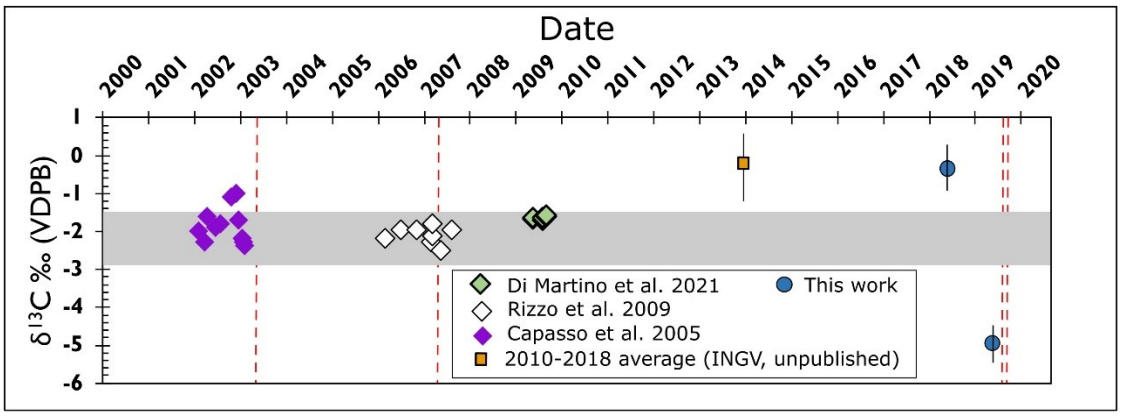

Figure 3: Carbon isotopes plotted against time on the x-axis, showing how 2018 and 2019 results compare with previous studies. The grey band represents the $\delta^{13}C$ range from fluid inclusions at Stromboli (Gennaro et al., 2017). The 2010-2018 average was calculated using a regression on passive gas samples taken at the summit during an 8-year period (n=49) with 4 blanks as background.

Carbon isotopes reveal changes in degassing state prior to paroxysmal activity

The significant divergence in $\delta^{13}C$ of the volcanic plume between 2018 (-0.36 ‰) and 2019 (-5.01‰) is unprecedented at Stromboli. Such a variation in $\delta^{13}C$ has never been observed in any fumarolic or hydrothermal sample. We sampled the plume close to the vent during two fortuitous sampling windows: (a) during a quiescent period and (b) just two weeks before a highly energetic paroxysmal eruption. Our analytical procedures using two different instruments and employing two different statistical methods (Supporting Information Text S1 – S6) demonstrate that these results represent true volcanic variations.

The well-studied magma source at Stromboli consists of a volatile-rich, deep-derived magma and a volatile-poor, shallow magma (Métrich et al., 2009). The most intuitive explanation for the nearly 5 ‰ difference in $\delta^{13}CO_2$ is a new magmatic source with a distinct carbon isotopic composition supplying the 2019 eruption. However, the major and trace element geochemistry of

the 2019 eruptive products (Andronico et al., 2021; Métrich et al., 2021; Petrone et al., 2022) is indistinguishable from that of pyroclastic materials erupted during other recent paroxysms on Stromboli in 2003 and 2007 (Métrich et al., 2005, 2009). This indicates that all these events (2003, 2007 and 2019) were charged by compositionally similar magma sourced from the same metasomatically altered mantle source (Peccerillo and Frezzotti, 2015). Furthermore, there is no evidence for a magma source in the region with $\delta^{13}CO_2$ as light as our 2019 data (-5.01 ‰). Studies from fumarolic emissions of volcanoes in the Aeolian arc range from -2.5 to -1.0 ‰ at Stromboli (Capasso et al., 2005; Federico et al., 2008; Rizzo et al., 2009) and -3.2 to +0.7 ‰ at Vulcano (Capasso et al., 1997; Venturi et al., 2017). Thus, there is no evidence for the existence of a light carbon component in the mantle, both at a local scale (Gennaro et al., 2017) and regionally.

Another plausible mechanism is isotopic fractionation during degassing of the volatile-rich deep-derived magma associated with past paroxysms at Stromboli (Metrich et al., 2009). During release of gases from magma, the heavier ^{13}C isotope concentrates in the gas phase compared to the lighter ^{12}C isotope. As magma degasses, the remaining carbon in the melt becomes lighter (^{13}C-depleted), as does the gas phase released at later stages of degassing (Holloway & Blank, 1994). This depletion can occur during closed-system degassing when the melt stays in contact with the gas, or to a much greater extent during open-system degassing (Raylegh fractionation) conditions when the gas is removed from the melt (Rayleigh, 1896; Brown et al., 1985). Hence, magma degassing under open-system conditions can lower $\delta^{13}C$ of the resulting gas to levels that could explain our 2019 gas data.

Dynamic carbon isotopes at arc volcanoes

On Stromboli, as in other open-vent volcanoes (Edmonds et al., 2022), both closed- and open-system degassing conditions can occur, and even coexist. During ordinary Strombolian activity (Harris & Ripepe, 2007; Rosi et al., 2013), both quiescent and explosive degassing occur, in which the former is caused by shallow gas release from convectively circulating magma in the upper conduits, effectively acting as closed-system degassing (Allard et al., 2008). Explosive bursting at the surface reflects rapid, separate ascent of deeply sourced gas bubbles undergoing open-system degassing (Burton et al., 2007). Important in this context is that high CO_2/SO_2 ratios have typically been observed in the bulk plume (passive + explosive) before paroxysms (Aiuppa et al., 2010, 2021) and major explosions (Aiuppa et al., 2011). This indicates that open-system conditions prevail in such conditions, resulting in the release of deeply sourced gas that is not in equilibrium with resident shallow conduit magma.

Geochemical and geophysical evidence indicates that a deeply derived gas was being emitted in the months prior to the July 3rd paroxysm. First, increased CO_2 concentrations and high CO_2/SO_2 ratios were noted in the plume beginning 8 months prior (Aiuppa et al. 2021), indicative of a deeply sourced magma (> 4 km) due to the low solubility and deeper exsolution level of CO_2 as compared to SO_2. Second, elevated CO_2 flux from summit soil began in October 2018, accelerating to July 2019 as higher volatile input was supplied (Inguaggiato et al., 2020). Third, modelling the degassing behaviour as a combination of open- and closed-system conditions has been invoked to account for the bimodal CO_2/SO_2 gas ratios observed prior to the July 3rd paroxysm (Aiuppa et al. 2021). Fourth, a seismic precursor to the July 3rd paroxysm was noted in very long period (VLP) waveforms starting at least one month before the eruption, thought to be

caused by vigorous (deep-sourced?) gas jetting activity sustaining the Strombolian activity (Giudicepietro et al., 2020).

We now test and model if a switch from closed-system to open-system degassing conditions can explain the distinct $\delta^{13}CO_2$ plume composition in 2018 and 2019 (Fig. 4). Here, we use the model of Gerlach and Taylor (1990) to simulate carbon isotope fractionation during degassing in both closed-system and open-system conditions (Supporting Information). In order to estimate f, the fraction of residual carbon in the melt at each step of the degassing path (see equations 5-7 in the Supporting Information), we use the Chosetto model (Moretti et al., 2003; Moretti & Papale, 2004) to simulate degassing upon decompression of a Stromboli-like parental melt (same initial conditions as in Aiuppa et al., 2010; see Supporting Information Text S7). The model also outputs, at each degassing step (e.g., at each pressure of the modelled decompression path), the CO_2/S_{tot} ratios in the gas coexisting with the melt. These are plotted, along with the gas carbon isotope signature, in Figure 4.

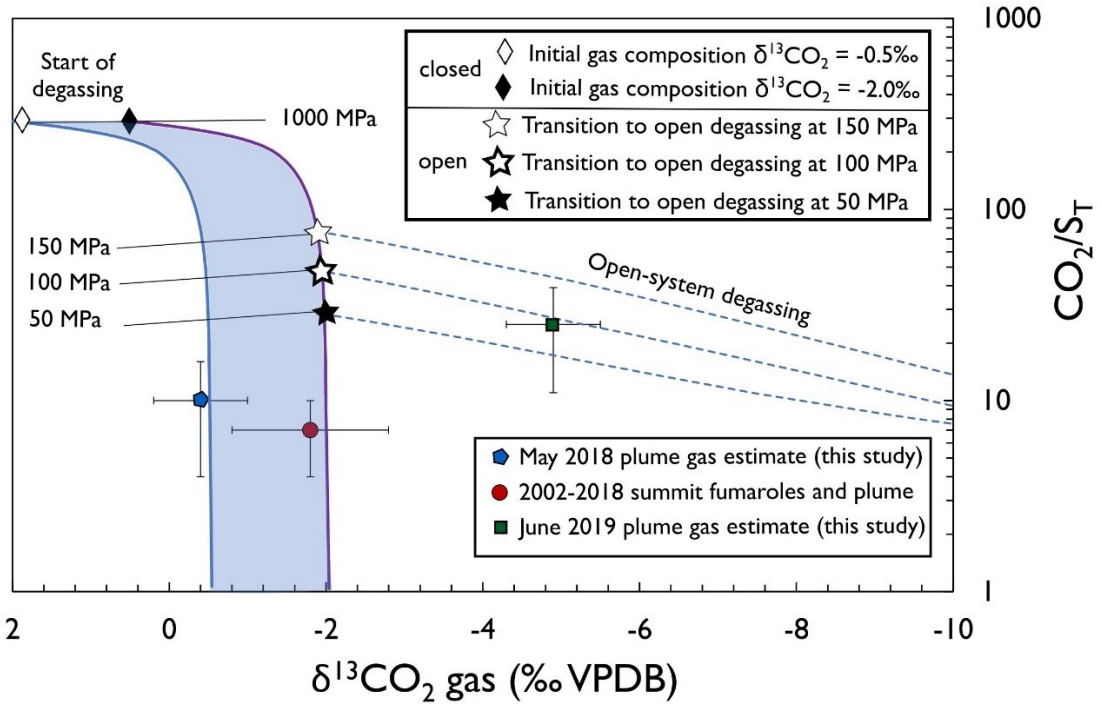

Figure 4: a) Modelled degassing paths of magma at Stromboli, showing carbon isotopic ratios on the x-axis and carbon dioxide to sulfur gas ratios on the y-axis. The solid purple and blue lines are closed-system degassing starting from 1000 MPa, while the dashed blue lines are open-system degassing starting from 150 MPa to 50 MPa switchover depths from closed to open (star symbols). This corresponds to a starting f value of 0.7 at 1000 MPa and f values of 0.03 to 0.006 at 50 to 150 MPa. Initial gas compositions are shown ranging from 2 ‰ (with a parental melt $\delta^{13}C$ of -0.5 ‰ (open diamond)) to 0.5 ‰ (with a parental melt $\delta^{13}C$ of -2 ‰ (solid diamond)). The green square represents June 2019 $\delta^{13}C$-CO_2 (this study) and CO_2/S (Aiuppa et al., 2021). The blue pentagon represents May 2018 $\delta^{13}C$-CO_2 (this study) and CO_2/S (Aiuppa et al., 2021). The red circle represents the average $\delta^{13}CO_2$ of 2002-2007 direct samples (n = 25) of summit fumaroles (Rizzo et al., 2009; Capasso et al., 2015; Di Martino et al., 2021) and the source estimate based on linear regression of 2010-2018 $\delta^{13}C$-CO_2 of summit plume gases collected from the crater rim (INGV, unpublished). The CO_2/S for the red circle is an average based on Aiuppa et al. (2011, 2017b) for 2006-2012.

Our results indicate that the plume 2018 results, as well as the 2010-2018 fumarole data, result from degassing under closed-system conditions up to 0.1 MPa (less than 1 km) of a parental magma with $\delta^{13}C$ of -0.5 to -2.0 ‰ informed by melt inclusion studies (Gennaro et al., 2017) (Figure 4). This confirms that degassing of shallow convecting magma dominates the degassing budget during ordinary Strombolian activity (Allard et al., 2008; Aiuppa et al., 2010). In contrast, we see that the 2019 plume data diverge from the closed-system degassing lines due to their light (^{13}C-poor) carbon signature. Specifically, our June 2019 carbon isotopic results can be reproduced from a degassing path that switches from closed to open (Figure 4). We propose that closed-system degassing takes place as magma decompresses from 1000 MPa (~40 km) to ~150-50 MPa (6-2 km depth). At this point, magma reaches a ponding zone (a geological or rheological discontinuity), at which point accumulating gas bubbles separate from melt (Aiuppa et al., 2021), and the system switches to open-system degassing. This "switchover depth" from closed to open-system degassing may be variable rather than constant, resulting in variable yet high CO_2/SO_2 (~20-35) observed before the July 3rd paroxysm. Vent-specific changes in CO_2/SO_2 (6.8 to 25.4) were noted at Stromboli during small explosive events in 2018 and attributed to differences in gas-melt separation (Pering et al., 2020). A variable switchover depth could indicate multiple levels of magma storage and/or multiple foam layers accumulating at different depths within the magma plumbing system prior to a paroxysm (Aiuppa et al., 2021). In any case, we postulate that the gas separated from the magma at 2-6 km depth then rapidly ascends toward the surface, preserving its high CO_2/SO_2 signature of 25 ± 14 (Aiuppa et al., 2021) and furthermore a strongly depleted isotopic signature in $\delta^{13}C$-CO_2 caused by fractional

equilibrium degassing (open-system degassing). These are exactly the features we observe in the June 2019 plume (Figure 4).

Recent applications of carbon isotopes as monitoring tools at Stromboli assume that small increases in $\delta^{13}C$-CO_2 would indicate unrest due to injection of a fresh, CO_2-rich magma (Federico et al., 2008; Federico et al., 2023). By contrast, our work shows that a decrease in $\delta^{13}C$ may be indicative of gas accumulation and overpressure as a foam layer builds over time. In the same way that patterns of precursory CO_2/SO_2 increases are being documented prior to basaltic eruptions across many arcs (Werner et al., 2019), now is the time to build a similar repository for precursory $\delta^{13}C$ changes for Stromboli and other volcanic systems.

At Stromboli in 2018, the observed low CO_2/SO_2 and heavy $\delta^{13}C$ resulted from CO_2 remaining in equilibrium with the magma until shallow levels, thereby efficiently lowering the gas ratios. In 2019, high CO_2/SO_2 and light $\delta^{13}C$ were the result of the gas decoupling and separating from the deeper magma at pressures of ~100 MPa (~4 km depth). By Rayleigh fractionation, the CO_2 was depleted in ^{13}C, while CO_2/SO_2 remained high. The early onset of deep gas supply many months before the July 3rd event caused the system to pressurize, as seen in other volcanic systems host to paroxysmal activity such as Villarica (Aiuppa et al., 2017a).

What is the "recipe" for forecasting large eruptive events at Stromboli? Based on previous work (Aiuppa et al., 2021) and ours, we propose that a combination of high CO_2 concentrations (maximum volcanic CO_2 > 50 ppm) and elevated CO_2/S_t (values > 20) as measured by Multi-GAS at the summit, combined with anomalously light $\delta^{13}C$ (e.g., less than -2 to -3 ‰), may indicate a heightened probability of a paroxysm. The longer the timescale of anomalous CO_2 characteristics, the greater the thickness of the foam layer(s) developing at depth (Aiuppa et al., 2021), hence the more powerful the eruption may be. Geophysical data may enhance this

geochemical forecasting recipe, e.g., anomalously elevated VLP seismicity on weekly to monthly timescales (Giudicepietro et al., 2020). An integrated geochemical-geophysical approach will improve our understanding of Stromboli and our ability to successfully forecast large eruptive events.

Conclusions

Our principal conclusions are the following:

1. Robust measurements of $\delta^{13}C\text{-}CO_2$ in volcanic plumes can be made with sampling by UAS in the plume and same-day isotopic analysis with portable spectrometers.

2. A large negative shift in plume $\delta^{13}C\text{-}CO_2$ was observed at Stromboli from quiescent degassing in May 2018 (-0.36 ± 0.59 ‰) to June 2019 (-5.01 ± 0.56 ‰), just prior to a large paroxysmal eruption.

3. We interpret this isotopic shift as a change from closed-system degassing in 2018, typical of ordinary strombolian activity, to a situation in 2019 where closed-system degassing prevailed at deep levels and transitioned to open-system degassing at 50-150 MPa (2-6 km depth). This transition allowed bubbles to separate from the melt and rise rapidly to the surface.

4. Prior to large eruptions, we hypothesize that (a) plume gas will have high CO_2 concentrations, anomalously light $\delta^{13}C\text{-}CO_2$, and high CO_2/S_T.

We observed some potential daily variations in $\delta^{13}C\text{-}CO_2$ during our work (see Figure S9). Future work could examine more detailed temporal and spatial variability of $\delta^{13}C\text{-}CO_2$, e.g., timescales of days to weeks and sampling of individual vents.

Acknowledgements

We thank Alfredo Alan for technical advice on the wiring schematics of the gas-sampling devices. FD is grateful for funding from Vanier Canada. JS is supported by funding from an NSERC Discovery grant. AA and ALR acknowledge funding from the Italian Ministero Ricerca e Università (PRIN projects 2017LMNLAW and 2022HA8XCS). AA also acknowledges funding from the RETURN Extended Partnership funded by the European Union Next-GenerationEU (National Recovery and Resilience Plan – NRRP, Mission 4, Component 2, Investment 1.3 – D.D. 1243 2/8/2022, PE0000005), and from Istituto Nazionale di Geofisica e Vulcanologia under research agreement "SVILUPPO DEL SISTEMA UNICO (INGV - UNIVERSITÀ) DI MONITORAGGIO VULCANICO E RILEVAMENTO PRECOCE DEI MAREMOTI E DELLE ESPLOSIONI PAROSSISTICHE DI "STROMBOLI".

Open Research

The data used in the study are available for download in the Earthchem repository (D'Arcy at al. 2024). The Chosetto code used for the CO_2 modelling was downloaded from https://github.com/charlesll/chosetto and is freely available from Github.(R. Moretti et al., 2003; Roberto Moretti & Papale, 2004).

References

Aiuppa, A., Bitetto, M., Donne, D.D., la Monica, F.P., Tamburello, G., Coppola, D., et al. (2021). Volcanic CO_2 tracks the incubation period of basaltic paroxysms. *Science Advances*, *7*, eabh0191. https://doi.org/10.1126/sciadv.abh0191

Aiuppa, A., Bitetto, M., Francofonte, V., Velasquez, G., Parra, C.B., Giudice, G., et al. (2017a). A CO_2 - gas precursor to the March 2015 Villarrica volcano eruption. *Geochemistry, Geophysics, Geosystems, 18*, 2120–2132. https://doi.org/10.1002/2017GC006892

Aiuppa, A., Bertagnini, A., Métrich, N., Moretti, R., Di Muro, A., Liuzzo, M., & Tamburello, G. (2010). A model of degassing for Stromboli volcano. *Earth and Planetary Science Letters*, *295*(1–2), 195–204. https://doi.org/10.1016/j.epsl.2010.03.040

Aiuppa, A., Burton, M., Allard, P., Caltabiano, T., Giudice, G., Gurrieri, S., et al. (2011). First observational evidence for the CO_2-driven origin of Stromboli's major explosions. *Solid Earth*, *2*(2), 135–142. https://doi.org/10.5194/se-2-135-2011

Aiuppa, A., Burton, M., Caltabiano, T., Giudice, G., Guerrieri, S., Liuzzo, M., et al. (2010). Unusually large magmatic CO_2 gas emissions prior to a basaltic paroxysm. *Geophysical Research Letters*, *37*, L17303. https://doi.org/10.1029/2010GL043837

Aiuppa, A., Giudice, G., Liuzzo, M., Burton, M., Caltabiano, T., & Salerno, G. (2017b). Volcanic gas plume data from Stromboli volcano (Italy), Version 1.0 [Dataset]. Interdisciplinary Earth Data Alliance (IEDA). https://doi.org/10.1594/IEDA/100642

Allard, P., Aiuppa, A., Burton, M., Caltabiano, T., Federico, C., Salerno, G., & La Spina, A. (2008). Crater gas emissions and the magma feeding system of Stromboli volcano. In S. Calvari, S. Inguaggiato, G. Puglisi, M. Ripepe, M. Rosi (Eds.), *The Stromboli volcano: an integrated study of the 2002–2003 eruption, Geophysical Monograph Series* (Vol. 182, pp. 65-80). Washington, DC: American Geophysical Union. https://doi.org/10.1029/182GM07

Andronico, D., Del Bello, E., D'Oriano, C., Landi, P., Pardini, F., Scarlato, P., et al. (2021). Uncovering the eruptive patterns of the 2019 double paroxysm eruption crisis of Stromboli volcano. *Nature Communications*, *12*(1), 1–14. https://doi.org/10.1038/s41467-021-24420-1

Aubaud, C. (2022). Carbon stable isotope constraints on CO_2 degassing models of ridge, hotspot and arc magmas. *Chemical Geology*, *605*, 120962. https://doi.org/10.1016/j.chemgeo.2022.120962

Barry, P.H., Hilton, D.R., Füri, E., Halldórsson, S.A., & Grönvold, K. (2014). Carbon isotope and abundance systematics of Icelandic geothermal gases, fluids and subglacial basalts with implications for mantle plume-related CO_2 fluxes. *Geochimica et Cosmochimica Acta*, *134*, 74–99. https://doi.org/10.1016/j.gca.2014.02.038

Boudoire, G., Rizzo, A.L., Di Muro, A., Grassa, F., & Liuzzo, M. (2018). Extensive CO_2 degassing in the upper mantle beneath oceanic basaltic volcanoes: first insights from Piton de la Fournaise volcano (La Réunion Island). *Geochimica et Cosmochimica Acta*, *235*, 376–401. https://doi.org/10.1016/j.gca.2018.06.004

Branca, S., Coltelli, M., De Beni, E. *et al.* Geological evolution of Mount Etna volcano (Italy) from earliest products until the first central volcanism (between 500 and 100 ka ago) inferred from geochronological and stratigraphic data. *Int J Earth Sci (Geol Rundsch)* **98**, 239 (2009). https://doi.org/0.1007/s00531-006-0152-0

Brown, P.E., Bowman, J.R., & Kelly, W.C. (1985). Petrologic and stable isotopic constraints on the source and evolution of skam-forming fluids at Pine Creek, California: *Economic Geology, 80*(1), 72–95. https://doi.org/10.2113/gsecongeo.80.1.72

Burton, M.R., Allard, P., Mure, F., & La Spina, A. (2007). Magmatic gas composition reveals the source depth of slug-driven strombolian explosive activity. *Science*, *317*(5835), 227-230. https://doi.org/10.1126/science.1141900

Burton, M.R., Sawyer, G.M., & Granieri, D. (2013). Deep carbon emissions from volcanoes. In R.M. Hazen, A.P. Jones, J.A. Baross (Eds.), *Carbon in Earth, Reviews in Mineralogy and Geochemistry* (Vol. 75, pp. 323–354). Washington, DC: Mineralogical Society of America, Geochemical Society. https://doi.org/10.2138/rmg.2013.75.11

Capasso, G., Carapezza, M.L., Federico, C., Inguaggiato, S., & Rizzo, A. (2005). Geochemical monitoring of the 2002-2003 eruption at Stromboli volcano (Italy): precursory changes in the carbon and helium isotopic composition of fumarole gases and thermal waters. *Bulletin of Volcanology*, *68*(2), 118–134. https://doi.org/10.1007/s00445-005-0427-5

Capasso, G., Favara, R., & Inguaggiato, S. (1997). Chemical features and isotopic composition of gaseous manifestations on Vulcano Island, Aeolian Islands, Italy: An interpretative model of fluid circulation. *Geochimica et Cosmochimica Acta*, *61*(16), 3425–3440. https://doi.org/10.1016/S0016-7037(97)00163-4

Chiodini, G., Caliro, S., Aiuppa, A., Avino, R., Granieri, D., Moretti, R., & Parello, F. (2011). First $^{13}C/^{12}C$ isotopic characterisation of volcanic plume CO_2. *Bulletin of Volcanology*, *73*(5), 531–542. https://doi.org/10.1007/s00445-010-0423-2

D'Arcy, F., Aiuppa, A., Grassa, F., Rizzo, A.L., Stix, J. (2024). Volcanic gas plume isotopic ratios of carbon dioxide from Stromboli volcano, 2018-2019, Version 1.0 [Dataset]. Interdisciplinary Earth Data Alliance (IEDA). https://doi.org/10.60520/IEDA/113060

D'Arcy, F., de Moor, J. M., Stix, J., Alan, A., Bogue, R., Corrales, E., et al. (2022). New insights into carbon isotope systematics at Poás volcano, Costa Rica. *Journal of Volcanology and Geothermal Research*, *431*, 107639. https://doi.org/10.1016/j.jvolgeores.2022.107639

Di Martino, R.M.R., Gurrieri, S., & Camarda, M. (2021). Continous monitoring of hydrogen and carbon dioxide at Stromboli volcano (Aeolian Islands, Italy). *Italian Journal of Geosciences*, *140*(1), 79–94. https://doi.org/10.3301/IJG.2020.26

Edmonds, M., Liu, E. J., & Cashman, K. (2022). Open-vent volcanoes fuelled by depth-integrated magma degassing. *Bulletin of Volcanology*, *84*(3), 1-28. https://doi.org/10.1007/s00445-021-01522-8

Federico, C., Brusca, L., Carapezza, M.L., Cigolini, C., Inguaggiato, S., Rizzo, A., & Rouwet, D. (2008). Geochemical prediction of the 2002 – 2003 Stromboli eruption from variations in CO_2 and Rn emissions and in helium and carbon isotopes. In S. Calvari, S. Inguaggiato, G. Puglisi, M. Ripepe, M. Rosi (Eds.), *The Stromboli volcano: an integrated study of the 2002–2003 eruption, Geophysical Monograph Series* (Vol. 182, pp. 117-128). Washington, DC: American Geophysical Union. https://doi.org/10.1029/182GM11

Federico, C., Inguaggiato, S., Liotta, M., Rizzo, A.L., & Vita, F. (2023). Decadal monitoring of the hydrothermal system of Stromboli volcano, Italy. *Geochemistry, Geophysics, Geosystems, 24*, e2023GC010931. https://doi.org/10.1029/2023GC010931

Finizola, A., Sortino, F., Lénat, J. F., Aubert, M., Ripepe, M., & Valenza, M. (2003). The summit hydrothermal system of Stromboli. New insights from self-potential, temperature, CO_2 and fumarolic fluid measurements, with structural and monitoring implications. *Bulletin of Volcanology*, *65*(7), 486–504. https://doi.org/10.1007/s00445-003-0276-z

Fischer, T.P., & Lopez, T.M. (2016). First airborne samples of a volcanic plume for $\delta^{13}C$ of CO_2 determinations. *Geophysical Research Letters*, *43*, 3272–3279. https://doi.org/10.1002/2016GL068499

Fischer, T.P., Ramírez, C., Mora-Amador, R.A., Hilton, D.R., Barnes, J.D., Sharp, Z.D., et al. (2015). Temporal variations in fumarole gas chemistry at Poás volcano, Costa Rica. *Journal of Volcanology and Geothermal Research*, *294*, 56–70. https://doi.org/10.1016/j.jvolgeores.2015.02.002

Gasparini, C., Iannaccone, G., Scandone, P., & Scarpa, R. (1982). Seismotectonics of the Calabrian Arc. *Tectonophysics*, *84*(2-4), 267–286. https://doi.org/10.1016/0040-1951(82)90163-9

Gennaro, M.E., Grassa, F., Martelli, M., Renzulli, A., & Rizzo, A.L. (2017). Carbon isotope composition of CO_2-rich inclusions in cumulate-forming mantle minerals from Stromboli volcano (Italy): *Journal of Volcanology and Geothermal Research, 346*, 95–103. https://doi.org/10.1016/j.jvolgeores.2017.04.001

Gerlach, T. M., & Taylor, B. E. (1990). Carbon isotope constraints on degassing of carbon dioxide from Kilauea Volcano. *Geochimica et Cosmochimica Acta*, *54*(7), 2051–2058. https://doi.org/10.1016/0016-7037(90)90270-U

Giordano, G., & De Astis, G. (2021). The summer 2019 basaltic vulcanian eruptions (paroxysms) of Stromboli. *Bulletin of Volcanology*, *83*(1), 1-27. https://doi.org/10.1007/s00445-020-01423-2

Giudicepietro, F., López, C., Macedonio, G., Alparone, S., Bianco, F., Calvari, S., et al. (2020). Geophysical precursors of the July-August 2019 paroxysmal eruptive phase and their implications for Stromboli volcano (Italy) monitoring. *Scientific Reports*, *10*(1), 1–16. https://doi.org/10.1038/s41598-020-67220-1

Harris, A., & Ripepe, M. (2007). Temperature and dynamics of degassing at Stromboli. *Journal of Geophysical Research: Solid Earth*, *112*, B03205. https://doi.org/10.1029/2006JB004393

Holloway, J.R., & Blank, J.G. (1994). Application of experimental results to C-O-H species in natural melts. In J.R. Holloway, M.R. Carroll (Eds.), *Volatiles in magmas, Reviews in*

Mineralogy and Geochemistry (Vol. 30, pp. 187–230). Washington, DC: Mineralogical Society of America. https://doi.org/10.1515/9781501509674-012

Inguaggiato, S., Vita, F., Cangemi, M., & Calderone, L. (2020). Changes in CO_2 soil degassing style as a possible precursor to volcanic activity: the 2019 case of Stromboli paroxysmal eruptions. *Applied Sciences*, *10*(14), 4757. https://doi.org/doi:10.3390/app10144757

Javoy, M., Pineau, F., & Iiyama, I. (1978). Experimental determination of the isotopic fractionation between gaseous CO_2 and carbon dissolved in tholeiitic magma – a preliminary study. *Contributions to Mineralogy and Petrology*, *67*(1), 35–39. https://doi.org/10.1007/BF00371631

Keeling, C. (1958). The concentration and isotopic abundances of atmospheric carbon dioxide in rural areas. *Geochimica et Cosmochimica Acta*, *13*(4), 322–334. https://doi.org/10.1016/0016-7037(58)90033-4

Liu, E.J., Aiuppa, A., Alan, A., Arellano, S., Bitetto, M., Bobrowski, N., et al. (2020). Aerial strategies advance volcanic gas measurements at inaccessible, strongly degassing volcanoes. *Science Advances*, *6*(44), eabb9103. https://doi.org/10.1126/sciadv.abb9103

Malowany, K., Stix, J., de Moor, J. M., Chu, K., Lacrampe-Couloume, G., & Sherwood Lollar, B. (2017). Carbon isotope systematics of Turrialba volcano, Costa Rica, using a portable cavity ring-down spectrometer. *Geochemistry, Geophysics, Geosystems*, *18*, 2769–2784. https://doi.org/10.1002/2017GC006856

Malowany, K., Stix, J., Van Pelt, A., & Lucic, G. (2015). H_2S interference on CO_2 isotopic measurements using a Picarro G1101-i cavity ring-down spectrometer. *Atmospheric Measurement Techniques, 8*, 4075–4082. https://doi.org/10.5194/amt-8-4075-2015

Mather, T. A. (2015). Volcanoes and the environment: Lessons for understanding Earth's past and future from studies of present-day volcanic emissions. *Journal of Volcanology and Geothermal Research*, *304*, 160–179. https://doi.org/10.1016/j.jvolgeores.2015.08.016

Mattey, D. P. (1991). Carbon dioxide solubility and carbon isotope fractionation in basaltic melt. *Geochimica et Cosmochimica Acta*, *55*(11), 3467–3473. https://doi.org/10.1016/0016-7037(91)90508-3

Métrich, N., Bertagnini, A., Landi, P., Rosi, M., & Belhadj, O. (2005). Triggering mechanism at the origin of paroxysms at Stromboli (Aeolian Archipelago, Italy): the 5 April 2003 eruption. *Geophysical Research Letters*, *32*, L10305. https://doi.org/10.1029/2004GL022257

Métrich, N., Bertagnini, A., & Di Muro, A. (2009). Conditions of magma storage, degassing and ascent at Stromboli: New insights into the volcano plumbing system with inferences on the eruptive dynamics. *Journal of Petrology*, *51*(3), 603–626. https://doi.org/10.1093/petrology/egp083

Métrich, N., Bertagnini, A., & Pistolesi, M. (2021). Paroxysms at Stromboli volcano (Italy): source, genesis and dynamics. *Frontiers in Earth Science*, *9*, 593339. https://doi.org/10.3389/feart.2021.593339

Moretti, R., Papale, P., & Ottonello, G. (2003). A model for the saturation of C-O-H-S fluids in silicate melts. In C. Oppenheimer, D.M. Pyle, J. Barclay (Eds.), *Volcanic degassing, Special Publication* (Vol. 213, pp. 81–101). London: Geological Society of London. https://doi.org/10.1144/GSL.SP.2003.213.01.06

Moretti, R., & Papale, P. (2004). On the oxidation state and volatile behavior in multicomponent gas-melt equilibria. *Chemical Geology*, *213*(1–3), 265–280. https://doi.org/10.1016/j.chemgeo.2004.08.048

Paonita, A., Caracausi, A., Iacono-Marziano, G., Martelli, M., & Rizzo, A. (2012). Geochemical evidence for mixing between fluids exsolved at different depths in the magmatic system of Mt Etna (Italy). *Geochimica et Cosmochimica Acta*, *84*, 380–394. https://doi.org/10.1016/j.gca.2012.01.028

Peccerillo, A., & Frezzotti, M. L. (2015). Magmatism, mantle evolution and geodynamics at the converging plate margins of Italy. *Journal of the Geological Society*, *172*(4), 407–427. https://doi.org/10.1144/jgs2014-085

Pering, T. D., Liu, E. J., Wood, K., Wilkes, T. C., Richardson, T., Mcgonigle, A.J.S., & Aiuppa, A. (2020). Combined ground and aerial measurements resolve vent-specific gas fluxes from

a multi-vent volcano. *Nature Communications, 11*(1), 3039. https://doi.org/10.1038/s41467-020-16862-w

Petrone, C. M., Mollo, S., Gertisser, R., Buret, Y., Scarlato, P., Del Bello, E., et al. (2022). Magma recharge and mush rejuvenation drive paroxysmal activity at Stromboli volcano. *Nature Communications*, *13*(1), 7717. https://doi.org/10.1038/s41467-022-35405-z

Rayleigh, J.W.S. (1896). Theoretical considerations respecting the separation of gases by diffusion and similar processes. *The London, Edinburgh, and Dublin Philosophical Magazine and Journal of Science, 42*(259), 493-498. https://doi.org/10.1080/14786449608620944

Ripepe, M., Lacanna, G., Pistolesi, M., Silengo, M.C., Aiuppa, A., Laiolo, M., et al. (2021). Ground deformation reveals the scale-invariant conduit dynamics driving explosive basaltic eruptions. *Nature Communications*, *12*(1), 1683. https://doi.org/10.1038/s41467-021-21722-2

Rizzo, A., Grassa, F., Inguaggiato, S., Liotta, M., Longo, M., Madonia, P., et al. (2009). Geochemical evaluation of observed changes in volcanic activity during the 2007 eruption at Stromboli (Italy). *Journal of Volcanology and Geothermal Research*, *182*(3–4), 246–254. https://doi.org/10.1016/j.jvolgeores.2008.08.004

Rizzo, A.L., Jost, H.J., Caracausi, A., Paonita, A., Liotta, M., & Martelli, M. (2014). Real-time measurements of the concentration and isotope composition of atmospheric and volcanic CO_2 at Mount Etna (Italy). *Geophysical Research Letters*, *41*(7), 2382–2389. https://doi.org/10.1002/2014GL059722

Rizzo, A.L., Liuzzo, M., Ancellin, M.A., & Jost, H.J. (2015). Real-time measurements of $\delta^{13}C$, CO_2 concentration, and CO_2/SO_2 in volcanic plume gases at Mount Etna, Italy, over 5 consecutive days. *Chemical Geology*, *411*, 182–191. https://doi.org/10.1016/j.chemgeo.2015.07.007

Rosi, M., Pistolesi, M., Bertagnini, A., Landi, P., Pompilio, M., & Di Roberto, A. (2013). Stromboli volcano, Aeolian Islands (Italy): Present eruptive activity and hazards. *Geological Society Memoir*, *37*, 473–490. https://doi.org/10.1144/M37.14

Schipper, C. I., Moussallam, Y., Curtis, A., Peters, N., Barnie, T., Bani, P., et al. (2017). Isotopically ($\delta^{13}C$ and $\delta^{18}O$) heavy volcanic plumes from Central Andean volcanoes: a field study. *Bulletin of Volcanology*, *79*, 1-15. https://doi.org/10.1007/s00445-017-1146-4

Shingubara, R., Tsunogai, U., Ito, M., Nakagawa, F., Yoshikawa, S., Utsugi, M., & Yokoo, A. (2021). Development of a drone-borne volcanic plume sampler. *Journal of Volcanology and Geothermal Research*, *412*, 107197. https://doi.org/10.1016/j.jvolgeores.2021.107197

Troll, V.R., Hilton, D.R., Jolis, E.M., Chadwick, J.P., Blythe, L.S., Deegan, F.M., et al. (2012). Crustal CO_2 liberation during the 2006 eruption and earthquake events at Merapi volcano, Indonesia. *Geophysical Research Letters*, *39*, L11302. https://doi.org/10.1029/2012GL051307

Tsunogai, U., Shingubara, R., Morishita, Y., Ito, M., Nakagawa, F., Yoshikawa, S., et al. (2022). Sampling volcanic plume using a drone-borne SelPS for remotely determined stable isotopic compositions of fumarolic carbon dioxide. *Frontiers in Earth Science*, *10*, 833733. https://doi.org/10.3389/feart.2022.833733

Venturi, S., Tassi, F., Bicocchi, G., Cabassi, J., Capecchiacci, F., Capasso, G., et al. (2017). Fractionation processes affecting the stable carbon isotope signature of thermal waters from hydrothermal / volcanic systems: the examples of Campi Flegrei and Vulcano Island (southern Italy). *Journal of Volcanology and Geothermal Research*, *345*, 46–57. https://doi.org/10.1016/j.jvolgeores.2017.08.001

Werner, C., Fischer, T.P., Aiuppa, A., Edmonds, M., Cardellini, C., Carn, S., et al. (2019). Carbon dioxide emissions from subaerial volcanic regions: two decades in review. In B. Orcutt, I. Daniel, R. Dasgupta (Eds.), *Deep Carbon: Past to Present* (pp. 188–236). Cambridge: Cambridge University Press. https://doi.org/10.1017/9781108677950

Preface to chapter 3

In the previous two chapters, I present two case studies for monitoring volcanic gases by use of carbon signatures of volcanic plumes. In this chapter, we venture to a different use for carbon

isotopes in relation to volcanic plumes. We seek to answer the question of whether carbon isotopes are also useful in tree rings which have been fumigated with volcanic gases. We analyze stable carbon and radiocarbon in tree rings on the south-east flank of Etna volcano, Italy. We use these along with soil gas measurements and ring width indices to correlate volcanic gas fluctuations (SO_2 flux) and tree response while factoring in climate variations. Chapter 3 is in preparation for publication in the Journal of Geophysical Research: Biogeosciences and is authored by Fiona D'Arcy, Robert Bogue, Etienne Boucher, Sergio Calabrese, Peter Douglas, and John Stix.

Citation:

D'Arcy, F., Bogue, R., Boucher, E., Calabrese, S., Douglas, P., and Stix, J. (In prep). Stable and radiogenic carbon isotopes in tree rings as a record of degassing at Etna volcano, Italy. Journal of Geophysical Research: Biogeosciences.

Chapter 3

Stable and radiogenic carbon isotopes in tree rings as a record of degassing at Etna volcano, Italy

Fiona D'Arcy[1], Robert Bogue[1], Etienne Boucher[2], Sergio Calabrese[3], Peter Douglas[1], and John Stix[1]

[1] Department of Earth & Planetary Sciences, McGill University, Montréal, Québec

[2] Département de Géographie, Université du Québec à Montréal, Montréal, Québec

[3] Dipartimento DiSTeM, Università di Palermo, Palermo, Italy

Abstract

Past fluctuations of gas output in volcanic areas can be studied by examining chemical changes in tree rings of surrounding vegetation. Recent studies have shown that stable isotopes of carbon are particularly useful due to the fact that the isotopic composition of trees can be altered by prolonged exposure to sulfur dioxide. However, in order for this to be a useful proxy, tree uptake of volcanic carbon dioxide must also be constrained. Radiogenic carbon in tree rings has been used to infer magmatic CO_2 emissions in geothermally active regions, and we propose that they can similarly be used to infer volcanic CO_2 uptake from a gas plume. In this study, we combine radiocarbon analysis with stable carbon isotope analysis of tree rings at Etna volcano to assess whether trees downwind of a volcanic plume record volcanic activity. We perform dendrochronology to assess ring width indices of 21 tree cores from a species of pine growing 5 to 11 km from the volcanic summit and source of plume gases. In addition, soil gas samples were taken for stable carbon isotopic analysis to evaluate possible variability in each sample area. For two sites on the south-east flank most exposed to plumes gases, we perform dendrochemical isotopic analyses at an annual resolution for ^{14}C between 1998 and 2003 and for $\delta^{13}C$ between

1998 to 2018. We conduct a correlation analysis of our results to compare with climate and SO_2 flux data of Etna during the same time period. Our soil gas and ^{14}C results indicate a lack of magmatic CO_2 exposure, yet there is a low growth anomaly for 2005-2008 as well as a negative correlation between ring width and $\delta^{13}C$ for 2003 to 2013. For 2001 to 2015, we find positive but weak correlations between the SO_2 flux and ring width indices of site ET-03 at 5.7 km from the summit, and $\delta^{13}C$ trending inversely for that site as compared to the others during 2004 to 2006. While we speculate on a delayed response to the 2001 eruption which spanned the growth season for trees in the area, we conclude that there is not enough evidence to support a correlation between the strength of the volcanic degassing and the tree response. This work may none the less provide valuable information for those seeking to evaluate isotopes in tree rings as a biomonitoring tool for volcanic plume surveillance or paleo reconstruction.

Introduction

Carbon isotopes in tree rings have been studied for a variety of environmental applications such as dating of paleoclimate events (D'Arrigo et al., 2003), reconstruction of water use efficiency (Saurer et al., 2004) and gauging response to industrial pollution (Savard et al., 2002). In recent decades, carbon isotopes (expressed in delta notation as $\delta^{13}C$) have been applied to study trees exposed to volcanic activity in the form of plume and ash deposition (D'Arcy et al., 2019; Alfaro-Sánchez et al., 2020), soil degassing (Bogue et al., 2018), and lava flows (Seiler et al., 2021). The $\delta^{13}C$ in trees can be affected by SO_2 exposure from either anthropogenic (Savard et al., 2002) or volcanic (D'Arcy et al., 2019) sources, which interfere with or damage stomata, causing fractionation. However, the fractionation caused by volcanic exposure can be difficult to

quantify due to the potential interference of magmatic emissions of CO_2 from plumes or soil. Volcanic CO_2 has an isotopic signature that is enriched in ^{13}C relative to atmospheric CO_2, which can also affect the isotopic composition of the tree rings.

Radiocarbon, or ^{14}C, in tree rings has been used to infer magmatic CO_2 emissions in geothermally active regions. Volcanic CO_2 contains no radiocarbon, while atmospheric CO_2 has relatively high amounts of ^{14}C derived from natural cosmogenic nuclide production and atomic weapons testing. Thus, ^{14}C is a very sensitive measure of plant uptake of volcanic CO_2. Radiocarbon depletion was identified in trees following the onset of diffuse soil CO_2 emissions at Mammoth Mountain, California (Cook et al., 2001; Lewicki et al., 2014) and Yellowstone caldera, Wyoming (Evans et al., 2010). Another study by Holdaway et al., (2018) found that magmatic carbon in groundwater was significant enough to cause biased radiocarbon ages in the Taupo volcanic zone, New Zealand. Hence high CO_2 flux zones in active volcanic areas contain magmatic CO_2 which is traceable with depleted radiocarbon amounts.

Until recently, studies combining both stable carbon and radiocarbon were rare. Seiler et al. (2021) analyzed $\delta^{18}O$, $\delta^{13}C$, and C^{14} in tree rings at Etna volcano, Italy, at the site of a fissure eruption on the northeast rift zone. As with previous radiocarbon studies, they examined trees in an area where CO_2 was diffusing from the ground. No study has combined tree ring analysis of radiocarbon and stable carbon to study a volcanic plume. Here, we examine trees close to the Valle del Bove, a valley on the southeast side of Etna volcano where summit gases are commonly funneled down the slopes of the volcano. We examine trees from four sites at increasing radial distance from the southeast flank of Etna where trees are persistently exposed to the quiescent degassing of Etna. We test the limits of applying a combined radiocarbon and stable carbon dendrochemical technique for volcanic surveillance of plume chemistry.

Study area

Etna is a large stratovolcano, 60 km wide at its base, on the island of Sicily. The volcano is highly active, with unrest in the last 20 years ranging from explosive summit eruptions to fissure-style flank eruptions (Liuzzo et al., 2013). Interestingly, Etna also has a strong passive degassing profile from CO_2 emissions along faults (Allard et al., 1991), as well as persistent summit degassing which can be channeled into the Valle del Bove (Aiuppa et al., 2004; Allen et al., 2006). Etna is mostly forested from 1000 to 2100 masl (Chester et al., 1985), with the exception of touristic areas as well as valleys and plateaus where recent lava flows have destroyed vegetation. Along with a variety of hardwood and softwood species, one of the most abundant trees growing in the area is the Corsican pine tree (*Pinus Nigra*). The seasonal rings produced by this species, as well as the geochemical variations within the rings, have been the subject of several studies concerning volcanic activity at Etna (Watt et al., 2007; Seiler et al., 2017, 2021).

Methods

Field sampling

Four sites were selected for this study at increasing distance from the Valle del Bove (Table 1 and Figure 1). Background (ET-02) is the background location, sampled on 18 July 2019 near Santa Maria, on the northwest flank of Etna, 10.5 km from the summit and 1160 m elevation. Piano Provenzano (ET-07) is located adjacent to the flank eruption of 2002-2003 on the northeast side at 1800 m and 7.0 km from the summit. Sites Citelli (ET-03 and ET-04) are located adjacent to a 2006 lava flow at an elevation of 1737 m and 5.7 km from the summit, while Monte Fontana (ET-05 and ET-06) are closest to the Valle del Bove and most likely to receive plume fumigation at 1204 m and 8.2 km from the summit. In July 2019, a total of 21 tree cores from 8 *Pinus Nigra* trees were collected. From each tree, one to two cores were sampled with a 12 mm increment borer, and one to two cores sampled with a 5.15 mm increment borer, at

1.5 m height. Cores were taken at 90 degree angles from each other where possible. At each site, we sampled one to two trees and chose a spot in the middle to assess soil degassing.

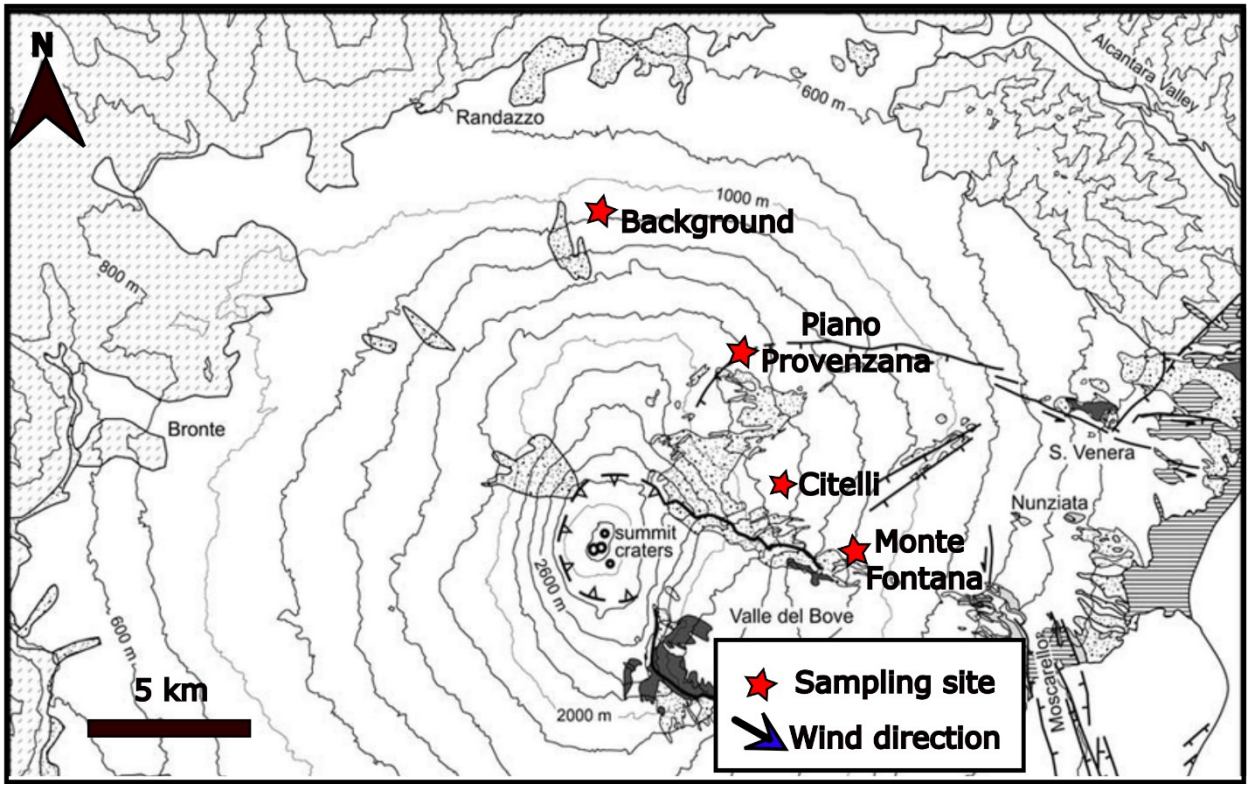

Figure 1: Map of sampling sites on Etna volcano in Italy, with scale at bottom left. Red stars represent sample collection sites of *Pinus Nigra* trees. Modified from Branca et al (2009).

Site	Northing	Easting	Elevation	Trees	Description
Background	37.8439	14.98831	1160 m	PIN1-ET02 & PIN2-ET02	This is a lower elevation area on the north side of the volcano. We later found that these trees have an inconsistent growth pattern with banded latewood.
Piano Provenzana	37.79912	15.04047	1797 m	PIN1-ET07 & PIN2-ET07	These trees are 3 to 18 metres from the 2002-2003 lava flow on the northeast rift, adjacent to the Seiler et al. (2021) study area

Citelli	37.76736	15.05487	1737 m	ET-03 & ET-04	These trees are 10 metres upslope from the 2006 lava flow on the edge of the Valle del Bove
Monte Fontana	37.74099	15.08455	1204 m	ET-05 & ET-06	These trees are 10 metres upslope from an old lava flow on the edge of the Valle del Bove

Table 1: Overview of sampling sites with GPS data, number of trees sampled, and description. Locations are in decimal degrees using the WGS84 datum.

Soil gas analysis

A soil probe was used to sample soil gas from 30 cm depth at each site along with samples of ambient air. A barbed connector on the top of the soil probe was connected to tygon tubing connected to a CO_2 meter. The low flow pump of the CO_2 meter was used to purge the line for 5 minutes before the outlet was attached in-line to an Altaf gas bag. The bag was subsequently purged twice before filling for approximately 2 minutes. Duplicate gas bags were taken at each site along with ambient air samples which were analyzed each evening on a Picarro G2201i-cavity ring-down spectrometer.

Dendrochronological analysis

All cores were dried in an oven at 60C overnight. The 5.15 mm cores were glued to wooden slats, and all cores were sanded and scanned at high resolution. Ring widths were measured and counted using Coorecorder and Cdendro software before being cross-dated manually and with PAST5 (Axiem, Austria) software. Missing and extra rings were identified between cores of the same tree and then between trees of the same site before the master chronology was made. The overall chronology and site chronologies were each validated by comparison with a master chronology spanning 1793-2014 located on the flanks of Etna (Seiler et al., 2021) obtained from

the International Tree Ring Data Bank of the World Data Centre for Paleoclimatology (ITRDB). The two chronologies had a 112 year overlap, with significant cross-correlation values including a t-value of T_{BP} of 7.96 (Baillie and Pilcher, 1973), THO of 8.19 (Hollstein, 1980), and Gleichläufigkeit of 70 (Eckstein and Bauch, 1969). After this initial chronology was created, the ring widths underwent a second phase of dendrochronological analysis using the open-source package of dplR (Bunn, 2008, 2010; Bunn et al., 2023) in the R program (R Core Team, 2023). As is common practice in the literature (Cook et al., 1990), the individual ring widths were detrended to remove low frequency trends (using cubic spline) and to create ring width indices (RWi) for each series. The detrended ring widths were used to create a master chronology in dplR using Tukeys biweight robust mean.

Species	Number of trees	Length	Years	Mean series intercorrelation	Mean first order autocorrelation
Pinus Nigra	5	116	1903 - 2018	0.44 +/- 0.09	0.49 +/- 0.28

Table 2: Dendrochronological statistics obtained from dplR for the five pine trees selected for this study. The length refers to the age of the oldest tree.

Cellulose preparation

Samples were prepared at the Centre des études de la forêt, the Laboratoire dendrologie, and the Stable Isotope Laboratory of the Geotop centre for the dynamics of the Earth, all at the Université du Québec à Montréal. Trees ET_03 from Citadelli and ET_06 from the Monte Fontana site were chosen for geochemical analysis due to their proximity to the Valle del Bove and their excellent correlation with the local master chronology (correlation coefficients of 0.94 and 0.84, respectively). Chronologies from two 12 mm cores for the period 1998-2018 were

dissected with a scalpel under a binocular microscope. The glass plate and scalpel were wiped down with methanol between each ring. Each ring was split into wafers encompassing even proportions of the earlywood to latewood, and a fraction of these wafers was set aside for radiocarbon sample preparation. The remaining fraction was ground to a fine powder with a steel-ball mill (Retsch 400). The wood powders were placed in filter bags (Ankom F57), sealed, and labelled with a coded label to distinguish each sample. To isolate holocellulose, the samples underwent a three-stage process of lignin extraction: 90 minutes in a 1:1 solution of ethanol:toluene, 60 minutes in ACS-grade acetone, 60 minutes in boiling water, and 180 minutes in a solution of progressively stronger glacial acetic acid and $NaClO_2$. This was followed by an acid-base stripping process to isolate alpha-cellulose: 60 minutes in 17% NaOH, rinsing in deionized water, and 15 minutes in 10% acetic acid followed by rinsing in deionized water. Samples were dried in an oven at 60°C for 6 to 18 hours, then air-dried afterward until analysis.

Stable carbon isotopes

All 42 samples were processed at the Geotop Stable Isotope Laboratory. Aliquots of 0.07 mg were weighed into tin capsules and combusted in an Elemental Analyser (Elementar Vario Microcube in continuous flow mode) connected to an Isotope Ratio Mass Spectrometer (Micromass model Isoprime 100 isotope ratio mass spectrometer). A duplicate was weighed every 10 samples, and two internal standards ($\delta^{13}C$=-28.74±0.02‰, -11.80±0.03‰) were used to normalize results. A third standard ($\delta^{13}C$=-17.06±0.02‰) was measured to check the fit of the data. The overall 1σ analytical uncertainty is better than ±0.1‰. Results are reported in delta notation, $\delta^{13}C$, in per mil units, ‰, relative to VPDB. To account for the annual incremental increase of CO_2 sourced from fossil fuels in global background atmospheric CO_2, we corrected the $\delta^{13}C$ values to account for this Suess effect (McCarroll and Loader, 2004). We used values of

background $\delta^{13}CO_2$ from Graven et al., (2017) and Belmecheri and Lavergne, (2020) and the following equation:

$$\delta^{13}C = \delta^{13}C_{measured} - (\delta^{13}C_{atmosphere} + 6.61)$$

Radiocarbon analysis

A preliminary sample of pooled wood from wafers of equal weight was prepared for radiocarbon analysis in June 2023, followed by a second batch of 10 samples of individual rings in August 2023. The pooled sample covered two years, 2002 to 2003, for site ET-06, while the individual samples covered the years 1998 to 2001 for ET-03 and years 1998 to 2003 for ET-06 (Table 5). Two standards were processed alongside the samples, a radiocarbon-free AVR wood and a known dated ring from the MAG-C63. All samples followed the same protocol outlined above. Radiocarbon analysis was performed at the Lalonde AMS radiocarbon laboratory, University of Ottawa. Aliquots of 2.5 mg were weighed into tin capsules for each sample, as well as duplicates of each standard. Samples were combusted in an Elemental Analyser (Thermo Flash 1112) at 1000°C, and pure CO_2 was collected in a liquid nitrogen-cooled trap before being collected into a break seal yielding approximately 1 mg carbon. Samples were then graphitized according to Crann et al. (2017) and analyzed on an Ionplus AG MICADAS (Mini Carbon Dating System). Results are reported as the fraction modern carbon, F14C, calculated and normalized to a standard measured in the same data block and corrected for background variation.

Results

Soil gas

Results of the soil gas samples from the four sites are presented in Table 3. The CO_2 concentrations at the background site range from 971 to 2733 ppm, and from 2070 to 3776 ppm at the target sites. The $\delta^{13}C$ at the background site ranges from -18.4 to -20.6 ‰, and from -19.8 to -22.6 ‰ at the target sites. Therefore, at the time of sampling, the target areas and background

fell within a similar range of CO_2 concentrations and $\delta^{13}C$ (Figure 2). This indicates biogenic activity with little to no influence from magmatic gases percolating upward through the soil. Soil flux measurements taken during 2009 to 2012 at site Ripenaca, an area located between our sites Citelli and Monte Fontana, recorded maximum CO_2 flux of 69 $g/m^2/d$ (Liuzzo et al., 2013). Their site is located along the Ripe della Naca fault, which could elicit increased soil gas emanations. Our soil gas results indicate that magmatic CO_2 from diffuse soil emanations was unlikely to be affecting the carbon isotopic signatures of trees ET-06 and ET-03 at the time of our sampling.

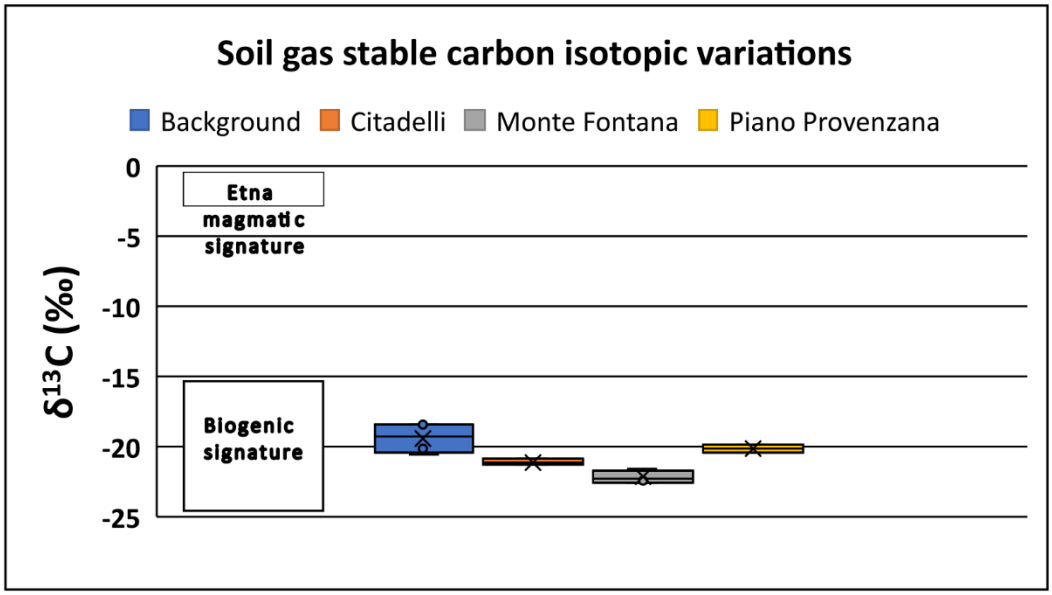

.

Figure 2: Soil gas $\delta^{13}CO_2$ values for different localities

Sample	Date	Time	CO_2 ppm	CO_2 stdev	$\delta^{13}C_{CO2}$	$\delta^{13}C_{CO2}$ stdev	CH_4
McGill std (-15.6) A	18/07/19	16:02-16:06	1151	2.1	-15.91	0.41	1.969
McGill std (-15.6) B	18/07/19	16:10-16:15	1005	0.6	-16	0.44	1.916
McGill std -43.15 A	18/07/19	16:50-16:55	999.6	3.7	-43.08	0.47	1.874
McGill std -43.15 B	18/07/19	16:59-17:04	1180	2.3	-43.29	0.4	1.889
McGill std -11.4 A	18/07/19	17:12-17:17	1362	4.5	-10.97	0.39	1.958
McGill std -11.4 B	18/07/19	17:20-17:25	1154	2.2	-11.02	0.42	1.894
Gas-ET-01-A	18/07/19	17:38-17:42	2315	5.2	-20.17	0.34	1.639
Gas-ET-01-B	18/07/19	17:45-17:49	971.3	3.3	-18.51	0.41	1.739
Air-ET-01-A	18/07/19	17:52-17:57	404.6	0.9	-9.87	0.75	1.818
Air-ET-01-B	18/07/19	17:59-18:03	388.2	0.9	-9.31	0.76	1.447
Gas-ET-02-A	18/07/19	18:05-18:10	1269	2.6	-18.45	0.43	1.271
Gas-ET-02-B	18/07/19	18:15-18:20	2733	3.4	-20.59	0.37	0.356
Air-ET-02-A	18/07/19	18:25-18:30	392.4	4.1	-9.33	0.74	1.816
Air-ET-02-B	18/07/19	18:37-18:41	390.6	2.1	-8.87	0.78	1.821
McGill std (-11.4) A	19/07/19	16:30-16:36	1312	3.1	-11	0.47	1.921
McGill std (-15.6) A	19/07/19	16:39-16:43	988.9	0.6	-15.66	0.45	1.902
Gas-ET-03-A	19/07/19	16:47-16:51	2788	2.6	-20.93	0.38	0.653
Gas-ET-03-B	19/07/19	16:54-16:58	3094	3.8	-21.3	0.4	0.867
Air-ET-03-A	19/07/19	17:01-17:05	412.7	5.2	-10.13	0.73	1.803

Air-ET-03-B	19/07/19	17:08-17:12	413.9	1.3	-9.65	0.76	1.819
Air-ET-05-A	19/07/19	17:19-17:23	400.2	1.7	-9.3	0.7	1.792
Air-ET-05-B	19/07/19	17:27-17:32	393.2	1	-9.22	0.74	1.787
Gas-ET-05-A	19/07/19	17:36-17:40	1483	3.5	-21.65	0.41	1.169
Gas-ET-05-B	19/07/19	17:45-17:50	3474	3.2	-22.48	0.37	0.25
Air-ET-06-A	19/07/19	17:59-18:03	417.4	3.1	-10.25	0.69	1.789
Air-ET-06-B	19/07/19	18:07-18:11	396.1	1.1	-9.28	0.72	1.788
Gas-ET-06-A	19/07/19	18:15-18:19	1799	3.3	-22.08	0.38	1.022
Gas-ET-06-B	19/07/19	18:22-18:26	1888	2.6	-22.62	0.45	1.243
McGill std (-15.6) A	19/07/19	18:32-18:36	1139	3	-15.77	0.44	1.917
McGill Std (-15.6) A	20/07/19	12:50-12:54	1235	2.4	-15.82	0.39	1.85
McGill Std (-15.6) B	20/07/19	12:58-13:02	1270	0.82	-15.78	0.35	1.856
Air-ET-07-A	20/07/19	13:06-13:10	391.8	1.2	-9.19	0.67	1.823
Air-ET-07-B	20/07/19	13:13-13:17	386.3	0.3	-8.893	0.77	1.813
Gas-ET-07-A	20/07/19	13:22-13:26	2389	3	-20.45	0.38	0.767
Gas-ET-07-B	20/07/19	13:29-13:33	2070	1.5	-19.83	0.34	0.802
McGill std (-43.15) A	20/07/19	13:36-13:40	1244	2.8	-43.03	0.41	1.855
McGill std (-43.15) B	20/07/19	13:44-13:48	1392	2.5	-42.79	0.37	1.864

Table 3: Soil gas CO_2 concentrations and stable isotopic values

Dendrochronology

Of the 8 trees sampled in this study, we found that 3 trees did not have consistent intra-tree chronologies between the cores taken at different directions from one another. These trees were not included in the master chronology, whose statistics are presented in table 2. The detrended ring widths from the five trees and their master chronology for the study period when all 5 series overlap (1976 to 2018) are presented in table 3. The medians of each ring width series range from 296 mm to 531 mm, while the interquartile ranges are from 147 to 413 mm for the 25^{th} percentile and 275 to 702 mm for the 75^{th} percentile. The series' chronology, along with the ring width index for each tree that was used to create it, is plotted from 1976 to 2018 when ring width for all series is available (Figure 3). We also plot the chronology of Seiler et al. (2021) for comparison. Qualitatively, we note that the trees from the same site behave similarly, e.g., ET-04 and ET-03 as well as ET-05 and ET-06 appear to mirror each other. Quantitatively, there are significant positive correlations between ET-04 and ET-03 and ET-05 and ET-06 (Pearson's r value of 0.69, $p < 0.05$ and 0.61, $p < 0.05$, respectively). There is a reduction in growth between 2005 and 2008 in all samples, and an apparent large ring anomaly in ET-05 in 2010.

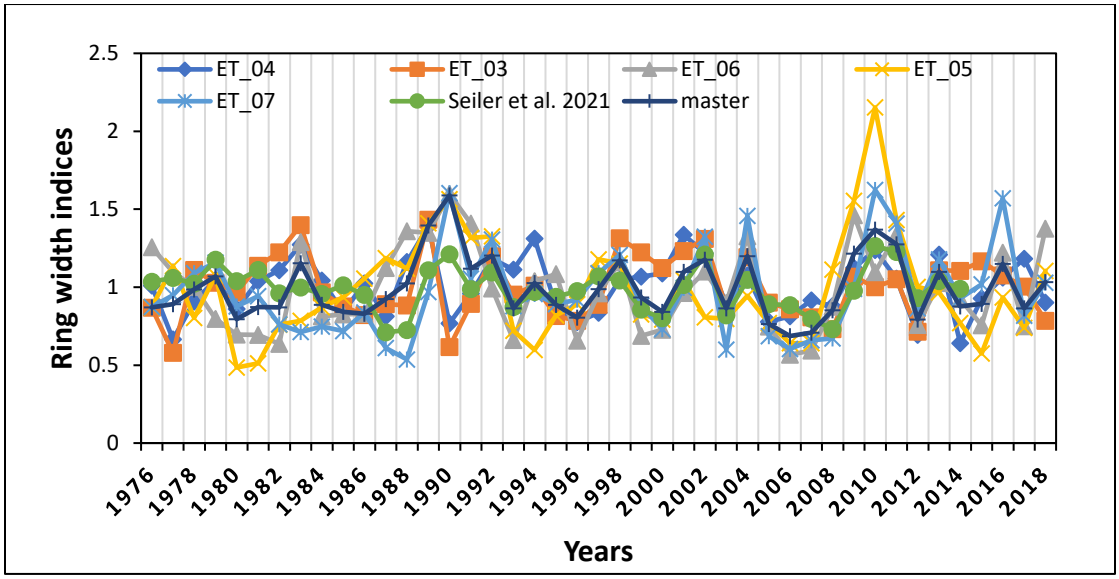

Figure 3: Detrended ring widths and series chronology for the 1976-2018 timeseries.

Years	ET_master	PIN_ET_04	PIN_ET_03	PIN_ET_06	PIN_ET_05	PIN2_ET_07
1976	275	313	345	442	346	162
1977	262	209	230	420	428	174
1978	281	290	442	415	288	198
1979	302	341	411	356	368	208
1980	224	286	388	334	159	156
1981	250	352	458	356	162	166
1982	261	384	495	348	234	133
1983	318	450	569	750	237	123
1984	279	376	395	500	260	128
1985	273	309	360	533	278	122
1986	294	384	339	559	314	141
1987	303	310	370	784	354	102
1988	343	450	369	973	336	89
1989	456	547	602	981	427	160
1990	432	306	261	1166	478	263
1991	417	386	380	1020	405	172
1992	434	481	514	706	412	212
1993	324	456	411	459	226	142
1994	381	540	438	700	190	154
1995	333	363	355	704	264	143
1996	285	321	343	410	292	147
1997	346	346	390	574	394	174
1998	423	433	579	664	394	192
1999	346	440	540	378	290	140
2000	331	446	495	384	286	116
2001	403	544	541	491	389	158
2002	410	491	572	545	310	210
2003	291	356	376	434	316	95
2004	412	424	513	630	388	231
2005	275	302	384	351	328	109
2006	250	311	361	266	282	96
2007	258	345	336	281	292	105
2008	299	326	301	420	522	107
2009	435	409	434	718	748	158
2010	485	443	401	553	1058	260
2011	434	371	417	694	714	226
2012	281	239	280	406	505	139
2013	385	408	428	569	491	190

2014	**310**	**212**	**421**	**531**	**392**	**150**
2015	**312**	**301**	**438**	**451**	**294**	**165**
2016	**407**	**337**	**398**	**758**	**479**	**255**
2017	**318**	**367**	**366**	**483**	**380**	**133**
2018	**380**	**274**	**282**	**921**	**568**	**168**

Table 4: Raw ring widths in millimetres for the study period

Stable carbon isotopes

The results of the stable carbon analysis are presented in Figure 4a. The correlation coefficient between sites ET-03 and ET-06 is 0.14. The $\delta^{13}C$ of site ET-03 ranges from -21.7 to -23.0 ‰ while that of site ET-06 ranges from -22.9 to -24.4 ‰. This is comparable to the $\delta^{13}C$ of trees analyzed by Seiler et al. (2021) which range from -20.3 to -24.7 ‰. Our two sites appear to be distinct, with almost no overlap between the two series, with ET-06 being consistently more negative. We also note the high value for ET-06 in 2012, and the high values for both in 2017. In Figure 4b, we compare our $\delta^{13}C$ data with those of Seiler et al. (2021) spanning 1998 to 2006. Interestingly, the cross-correlation for the 8-year window of the Seiler data and our site ET-03 is 0.64, while the cross-correlation is only 0.32 with our site ET06. The $\delta^{13}C$ of individual years at site ET-03 is also within 1 ‰ of each corresponding datapoint of the Seiler data, while the entire ET-06 series is 2 ‰ more negative.

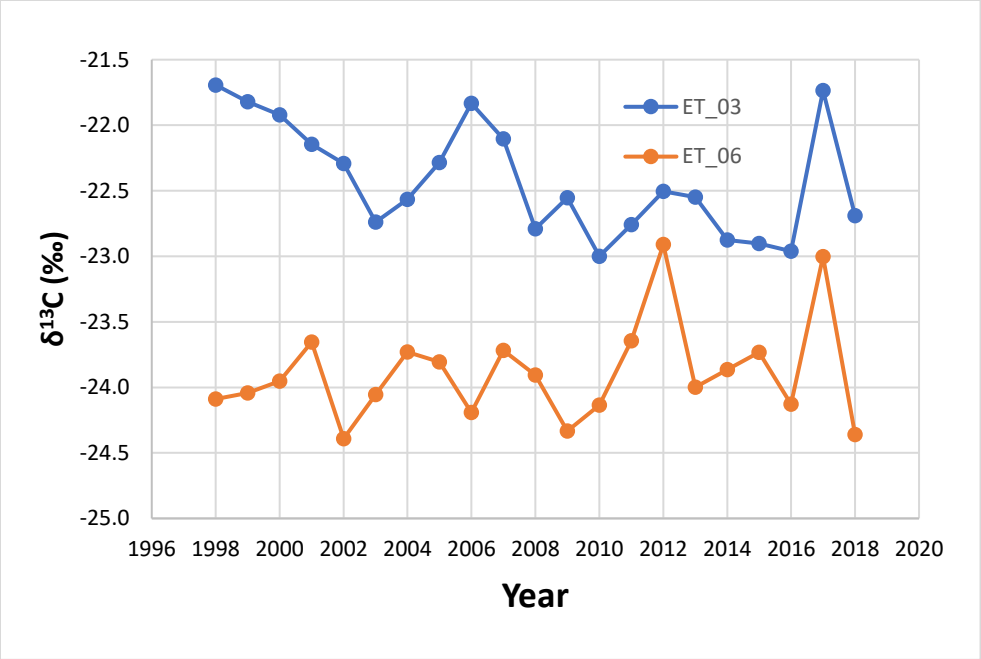

Figure 4a: $\delta^{13}C$ in annual tree rings from two sites at Etna volcano for 1998 to 2018. Raw data have been corrected to account for increasing $\delta^{13}C$ in the atmosphere due to anthropogenic activity as in McCarrol and Loader, 2004.

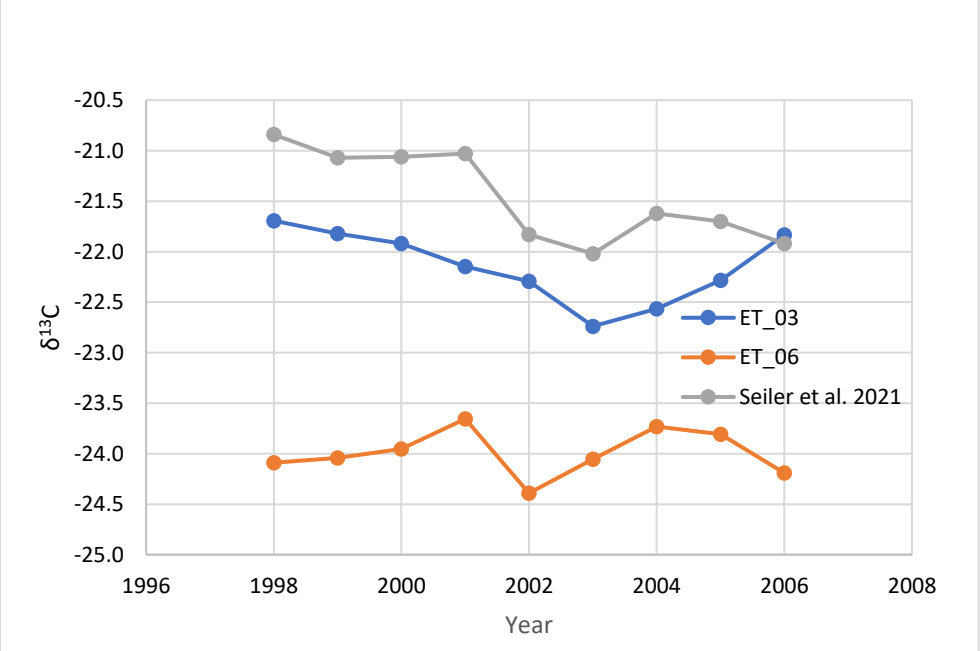

Figure 4b: $\delta^{13}C$ in annual tree rings from three sites at Etna volcano for 1998 to 2006. This is the same data as in 4a but with a shorter timespan to compare with data available from Seiler et al. 2021 (also plotted).

Sample ID	Year	d13C	Average d13C	d13C_atm*	d13C_corrected
ET_03C_1998	1998	-23.1	-23.1	-8.03	-21.7
ET_03C_1999	1999	-23.3	-23.3	-8.06	-21.8
ET_03C_2000	2000	-23.4	-23.4	-8.06	-21.9
ET_03C_2001	2001	-23.6	-23.6	-8.07	-22.1
ET_03C_2002	2002	-23.8	-23.8	-8.11	-22.3
ET_03C_2003	2003	-24.3	-24.3	-8.15	-22.7
ET_03C_2004	2004	-24.1	-24.1	-8.19	-22.6
ET_03C_2005	2005	-23.9	-23.9	-8.21	-22.3
ET_03C_2006	2006	-23.5	-23.5	-8.24	-21.8
ET_03C_2007	2007	-23.8	-23.8	-8.26	-22.1
ET_03C_2008	2008	-24.5	-24.5	-8.28	-22.8
ET_03C_2009	2009	-24.2	-24.2	-8.29	-22.6
ET_03C_2010	2010	-24.7	-24.7	-8.31	-23.0
ET_03C_2011	2011	-24.5	-24.5	-8.33	-22.8
ET_03C_2012	2012	-24.3	-24.3	-8.36	-22.5
ET_03C_2013	2013	-24.3	-24.3	-8.39	-22.5
ET_03C_2014	2014	-24.7	-24.7	-8.42	-22.9
ET_03C_2015	2015	-24.7	-24.7	-8.44	-22.9
ET_03C_2016	2016	-24.8	-24.8	-8.48	-23.0
ET_03C_2017	2017	-23.6	-23.6	-8.51	-21.7
ET_03C_2018	2018	-24.6	-24.6	-8.55	-22.7
ET_06B_1998	1998	-25.5	-25.5	-8.03	-24.1
ET_06B_1999	1999	-25.5	-25.5	-8.06	-24.0
ET_06B_2000	2000	-25.4	-25.4	-8.06	-24.0
ET_06B_2001	2001	-25.1	-25.1	-8.07	-23.7
ET_06B_2002	2002	-25.9	-25.9	-8.11	-24.4
ET_06B_2003	2003	-25.6	-25.6	-8.15	-24.1
ET_06B_2004	2004	-25.3	-25.3	-8.19	-23.7
ET_06B_2005	2005	-25.4	-25.4	-8.21	-23.8
ET_06B_2006	2006	-25.9	-25.8	-8.24	-24.2
ET_06B_2007	2007	-25.4	-25.4	-8.26	-23.7
ET_06B_2008	2008	-25.6	-25.6	-8.28	-23.9
ET_06B_2009	2009	-26.0	-26.0	-8.29	-24.3
ET_06B_2010	2010	-25.8	-25.8	-8.31	-24.1
ET_06B_2011	2011	-25.4	-25.4	-8.33	-23.6
ET_06B_2012	2012	-24.7	-24.7	-8.36	-22.9
ET_06B_2013	2013	-25.8	-25.8	-8.39	-24.0
ET_06B_2014	2014	-25.7	-25.7	-8.42	-23.9

ET_06B_2015	2015	-25.6	-25.6	-8.44	-23.7
ET_06B_2016	2016	-26.0	-26.0	-8.48	-24.1
ET_06B_2017	2017	-24.9	-24.9	-8.51	-23.0
ET_06B_2018	2018	-26.3	-26.3	-8.55	-24.4

Table 5: $\delta^{13}C$ in annual tree rings from two sites at Etna volcano for 1998 to 2006. Average $\delta^{13}C$ uses the mean value for those samples which were analyzed in duplicate (n=5). The column for $\delta^{13}C$_atm represents $\delta^{13}C$ values of background atmospheric CO_2 from Graven et al., (2017) for 2008 to 2015 and from Belmecheri and Laverne (2020) for 2016 to 2018. The d13C_corrected column uses those values to correct for the Suess effect as described in the Methods. All units are ‰ relative to VPDB.

Radiocarbon

The results of the radiocarbon analysis are presented in Figure 5. The fraction modern ranges from 1.07 to 1.10, which is within the range of modern atmospheric values. In order to assess whether there is a depletion in ^{14}C from volcanic CO_2 uptake, we must account for the global atmospheric value of ^{14}C which decreases each year. We calculate the concentration of magmatic CO_2 in air (C mag) according to the mass balance equation of Sharma and Williams (2009), using the atmospheric ^{14}C values of (Levin and Kromer, 2004; Levin et al., 2008) and the CO_2 concentrations from Keeling et al., (2009). Both sites ET-06 and ET-03 yield C mag values between -0.8 and 0.75 ppm. For comparison, we have plotted data for C_{mag} from two other studies examining volcanic carbon in 2001 to 2002. Trees from the Piano Provenzana site along the northeast rift of Etna volcano exhibit C_{mag} up to 13.3 ppm (Seiler et al., 2021), while trees at Mammoth Mountain in Long Valley caldera exhibit C_{mag} values up to 35.2 ppm (Lewicki et al. 2014). These C_{mag} values are 5.5 and 14.6 times higher respectively than those of our study, and these areas likely received significant carbon fluxing through diffuse soil emission. Therefore, we find no evidence of volcanic carbon uptake from either diffuse soil emissions nor the gas plume of Etna in trees at the Monte Fontana (ET-05, ET-06) or Citadelli (ET-03, ET-04) sites.

Hence we assume that any volcanic influence on ^{13}C results is due to other factors such as SO_2 damage and dry deposition following ash emissions.

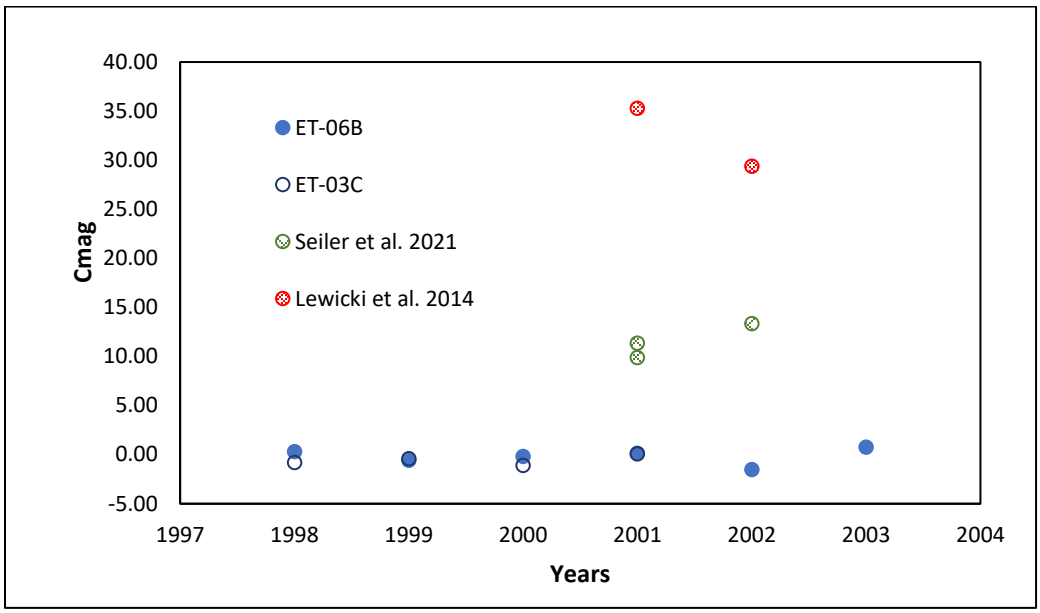

Figure 5: Magnitude of magmatic CO_2 in air (C mag) for 1998 to 2003 using tree rings from two sites at Etna (this study), and for 2001 to 2003 for a third site at Etna (Seiler et al. 2021) and a fourth site at Mammoth Mountain (Lewicki et al. 2014), Values calculated using radiocarbon values measured in tree rings and using the atmospheric ^{14}C values of (Levin and Kromer, 2004; Levin et al., 2008) and the CO_2 concentrations from Keeling et al., (2009) for 1998 to 2003 at Etna and comparative sources

Sample	Year	F14C	±	^{14}C atm	Difference	C atm (ppm)	Cmag
ET-06B-1998	1998	1.1031	0.0023	1.104	-0.0009	367.9	0.31
ET-06B-1999	1999	1.0997	0.0023	1.098	0.0017	369.4	-0.57
ET-06B-2000	2000	1.0936	0.0023	1.093	0.0006	370.4	-0.20
ET-06B-2001	2001	1.0876	0.0023	1.088	-0.0004	372.1	0.13
ET-06B-2002	2002	1.0865	0.0023	1.082	0.0045	374.1	-1.54
ET-06B-2003	2003	1.0739	0.0023	1.076	-0.0021	376.9	0.75
ET-03C-1998	1998	1.1065	0.0023	1.104	0.0025	367.9	-0.83
ET-03C-1999	1999	1.0993	0.0023	1.098	0.0013	369.4	-0.43
ET-03C-2000	2000	1.0963	0.0023	1.093	0.0033	370.4	-1.12
ET-03C-2001	2001	1.0878	0.0023	1.088	-0.0002	372.1	0.08

Table 6: Radiocarbon values for 1998 to 2003 as measured in tree rings from two sites at Etna volcano. Measurements are reported in fraction modern (F14C) as described in the methods. Atmospheric radiocarbon values data (Levin and Kromer, 2004; Levin et al., 2008) are used to calculate the difference between our measured values and those expected should the trees be incorporating solely atmospheric CO_2. We calculate the concentration of magmatic CO_2 in air (C mag) according to the mass balance equation of Sharma and Williams (2009), using the atmospheric CO_2 concentrations from Keeling et al., (2009).

Discussion

The Valle del Bove is a depression which predates Etna volcano itself, having formed 10 000 years ago during the collapse of an extinct volcano (Calvari et al., 2004). It is the ideal site to study the influence of a volcanic plume on nearby trees, as the gas from the volcano is commonly channelled down the eastern flank. Furthermore, many aspects of plume exposure in this area have been examined in the last two decades. Aiuppa et al. (2004) found evidence of volcanic gases funneling down into the Valle del Bove during the summer 2002 based on passive gas samplers. They found that SO_2 fumigation rates were significant extensing to 4 km downwind of the craters, with up to 7% of plume SO_2 scavenged by dry deposition. Again in summer 2004, plume aerosols were funneled down the Valle del Bove and vicinity on the southeast flank and detected at ground level as far away as 10 km from the summit (Allen et al., 2006). On the other hand, a study by Watt et al., (2007) found no significant correlations

between metal concentrations in foliage around the Valle del Bove and plume exposure. While HYSPLIT trajectory modelling indicated that the plume did not often reach altitudes below 2500 masl during their study period (June to July 2005), their study site at 1000 masl at the bottom of the Valle del Bove nonetheless had high foliar cation concentrations.

Our study assesses the effect of prolonged volcanic plume exposure on trees flanking the Valle del Bove. We set out to find a site and method allowing us to isolate the effect of gaseous uptake of the plume, which is different from other mechanisms which have been previously explored. We now discuss the significance of our time series of ring widths, stable carbon isotopes, and radiocarbon.

Volcanic CO_2 in tree rings

We seek evidence of volcanic gas fluctuations, in particular that of the volcanic plume, archived within tree rings. There are two main ways in which this evidence could manifest in tree rings: (1) direct CO_2 uptake, wherein carbon of magmatic or volcanic origin can be traced from the trees to their source by means of isotopic signatures, and (2) indirect evidence of volcanic fumigation, as indicated by reduction of growth and physiological alterations from tree response to stress.

Our results indicate a lack of evidence for direct volcanic plume CO_2 uptake at our two main sites of expected volcanic gas exposure: ET-06 and ET-03. At high levels of CO_2 exposure, we would expect the trees to be visibly damaged or dying, as in the co-called “dead zones” in other volcanic regions. At lower levels, we look to our soil gas and radiocarbon results for more subtle indications. The soil gas results do not indicate magmatic CO_2 reaching our study areas during the year of sampling (2019). Considering that diffuse degassing around Etna is found principally

along the many fault zones around the flank, none of which are located on our study sites ET-03 and ET-06, this likely indicates that there has not been strong magmatic soil degassing at these locations in recent decades. At these same two locations, our radiocarbon results do not show anomalously low values associated with magmatic CO_2 uptake for the period 1998 to 2003. Therefore, there is no evidence for volcanic carbon uptake into the tree rings, whether at the soil or canopy level, during 1998-2003 nor 2018. However, the stable carbon series we report spans 1998 to 2018. Could the plume still be reaching these sample areas and imprinting upon the trees a chemical trace of their presence? We now investigate whether volcanic influence has some control over the $\delta^{13}C$ values measured, and to what extent the climate, volcanic SO_2 emissions, and soil changes govern the $\delta^{13}C$ values observed.

Correlation between ring-width indices, stable carbon, and climate

Before we can begin to seek out indirect evidence of volcanic influence in either ring width or $\delta^{13}C$, we must first take a comprehensive look at all external factors affecting these indices. In carbon climatology studies, tree ring $\delta^{13}C$ has been shown to correlate to various climate parameters such as summer precipitation and summer temperature (McCarroll and Loader, 2004; Johnstone et al., 2013). In addition, the amount of sunshine reaching the trees can also affect their growth and therefore their CO_2 assimilation, so cloud cover can also in principle correlate to trends in $\delta^{13}C$. These studies tend to involve chronologies that span several decades to centuries and require several layers of statistical analysis and detrending. On shorter timescales, previous studies which have sought to correlate volcanic activity with local tree ring $\delta^{13}C$ have used a variety of statistical techniques to first account for any climate variations. In examining activity 3 km from Popocatepetl volcano, Mexico, Alfaro-Sánchez et al., (2020) performed a series of Pearson correlations between both seasonal and monthly precipitation, mean temperature, and

cloud cover from the KNMI climate explorer webpage with tree ring width and stable isotopes. Their results were incorporated into a Principal Component Analysis (PCA) to determine the factors influencing the rings, and a subsequent linear mixed-effects model (LMEM) was calibrated with two growth periods to estimate RWi for a third period. Battipaglia et al., (2007) sampled trees 40 km from Vesuvius volcano, Italy, and compared ring width and stable isotopes with climate variables as well as eruption chronologies.

In this study, our twenty-year chronology underwent a two-stage statistical analysis. In the first stage, we perform 8-year running correlations using Pearson's correlation between ring-width indices and $\delta^{13}C$ (figure 6). For our two individual trees, intratree variations between RWi and $\delta^{13}C$ are poorly correlated ($r < 0.7$, $P < 0.05$) with the exception of the 2011 to 2018 period for ET-06 ($r = -0.71$, $P < 0.05$). For the master chronology rwi (n=5 pooled trees), the correlation with the $\delta^{13}C$ of the two measured trees (ET-06 and ET-03) is significant between 2003 and 2013 ($-0.73 < r < -0.77$, $p < 0.05$). While we see correlations in figure 6, we must be cautious in interpreting these, as autocorrelations have not been accounted for as in other studies (Johnstone et al., 2013), and long-term variations may be obscuring shorter-term fluctuations (Alfaro-Sánchez et al., 2020). However, given the short timescale of our data, we can reasonably assume that long-term variations are minimal, and detrending would have a minor affect on the raw $\delta^{13}C$, as observed in a similar study at Etna (Seiler et al., 2017).

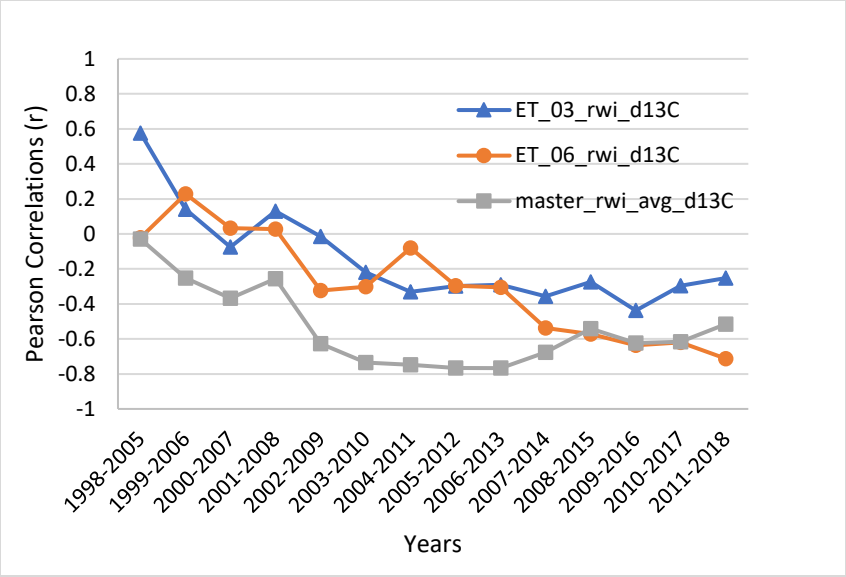

Figure 6: Running correlations between ring width indices and $\delta^{13}C$ for site ET_03, site ET_06, and the master chronology. Running correlations are spanning 8-year windows and are calculated using Pearson Correlations. Significant correlation for n=7 degrees of freedom is 0.7.

In the second stage of our statistical analysis, we did a correlation analysis between climate variables, ring width indices, and $\delta^{13}C$ of our samples. Monthly precipitation and maximum temperatures for Mt. Etna were obtained from the Climatic Research Unit (CRU) TS 4.07 dataset from the KNMI climate explorer webpage at 0.5 degree spatial resolution (Harris et al., 2014; Koninklijk Nederlands Meteorologisch Instituut). We use Pearson's correlation coefficient to compare both raw RWi and detrended RWi as well as the suess-corrected $\delta^{13}C$ from both individual trees and averages (master ring width chronology and average $\delta^{13}C$) with monthly precipitation (Figure 7) and maximum temperatures (Figure 8). In general, the RWi shows both positive and negative correlations with precipitation, but none are significant except a negative correlation between February precipitation and RWi of ET-03 ($r < -0.52$ and $r < -0.53$ for raw and detrended RWi, respectively, $p < 0.05$). In terms of carbon isotopes, the $\delta^{13}C$ of ET-03 are negatively correlated with March precipitation ($r = -0.55$, $P < 0.05$) and the average $\delta^{13}C$ are

negatively correlated with March and October precipitation. Studies of nearby trees have similarly found little correlation with precipitation in the Etna area (Seiler et al., 2017), while in a moderately similar climate to Etna, Battiglia et al., (2007) found that total precipitation in April and May correlated well with the RWI, while $\delta^{13}C$ correlated with April precipitation. For maximum temperatures, ET-06 and the master chronology RWi correlate negatively with May and June temperatures ($-0.46 > r > -0.53$ and $-0.49 > r > -0.59$ for raw and detrended RWi, respectively, $p < 0.05$), while the $\delta^{13}C$ of ET-03 and the average $\delta^{13}C$ correlate with January maximum temperatures ($r = -0.48$, $P < 0.05$).

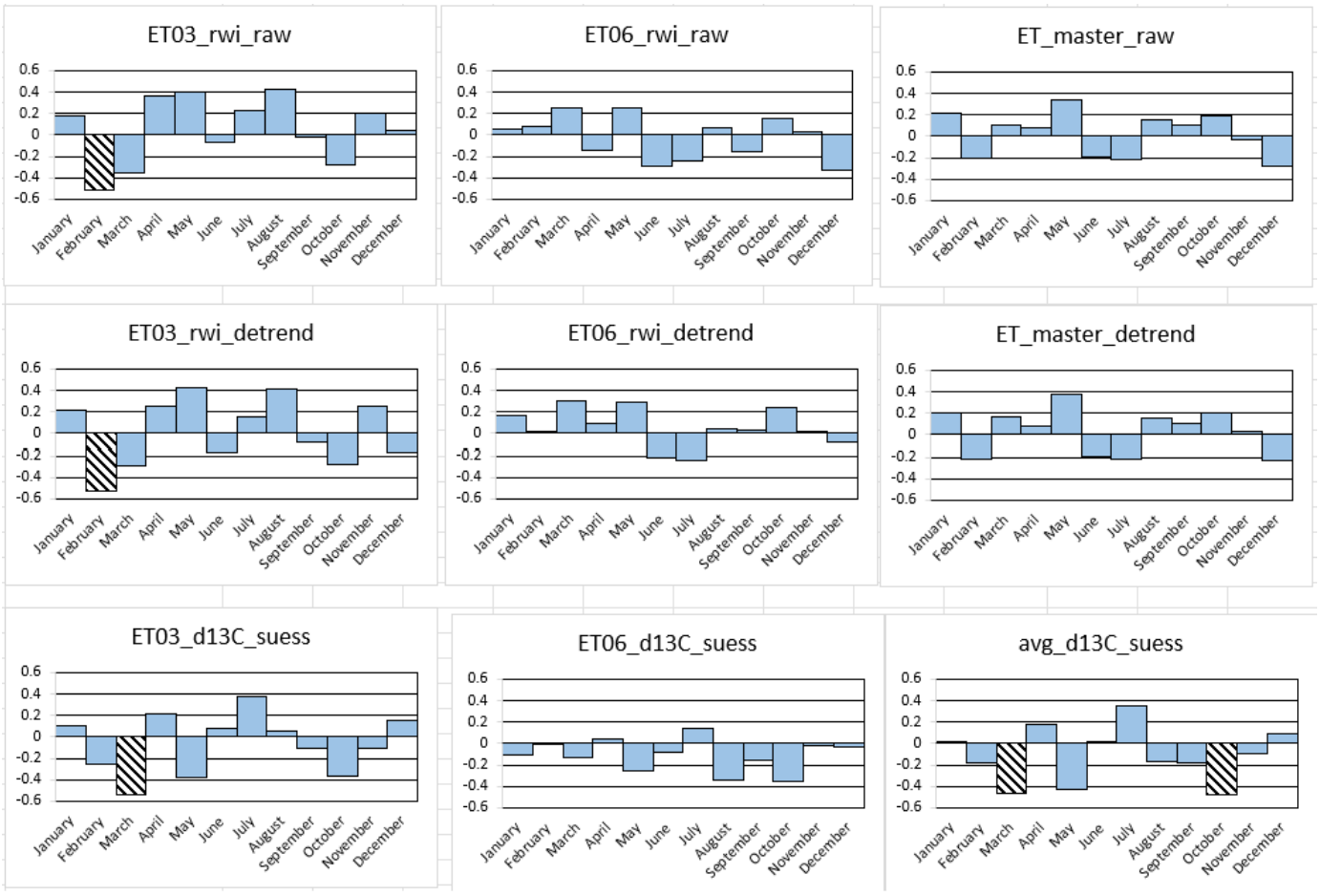

Figure 7: Correlation diagrams showing Pearson's correlation coefficient between ring width and monthly precipitation. The first and second rows compare the raw and detrended RWi of ET06, ET03, and the master chronology with the monthly precipitation. The third row compares the suess-detrended $\delta^{13}C$ of ET06, ET03, and their average with

precipitation. Precipitation data is from the Climatic Research Unit (CRU) TS 4.07 dataset from the KNMI climate explorer webpage at 0.5 degree spatial resolution (Harris et al., 2014; Koninklijk Nederlands Meteorologisch Instituut).

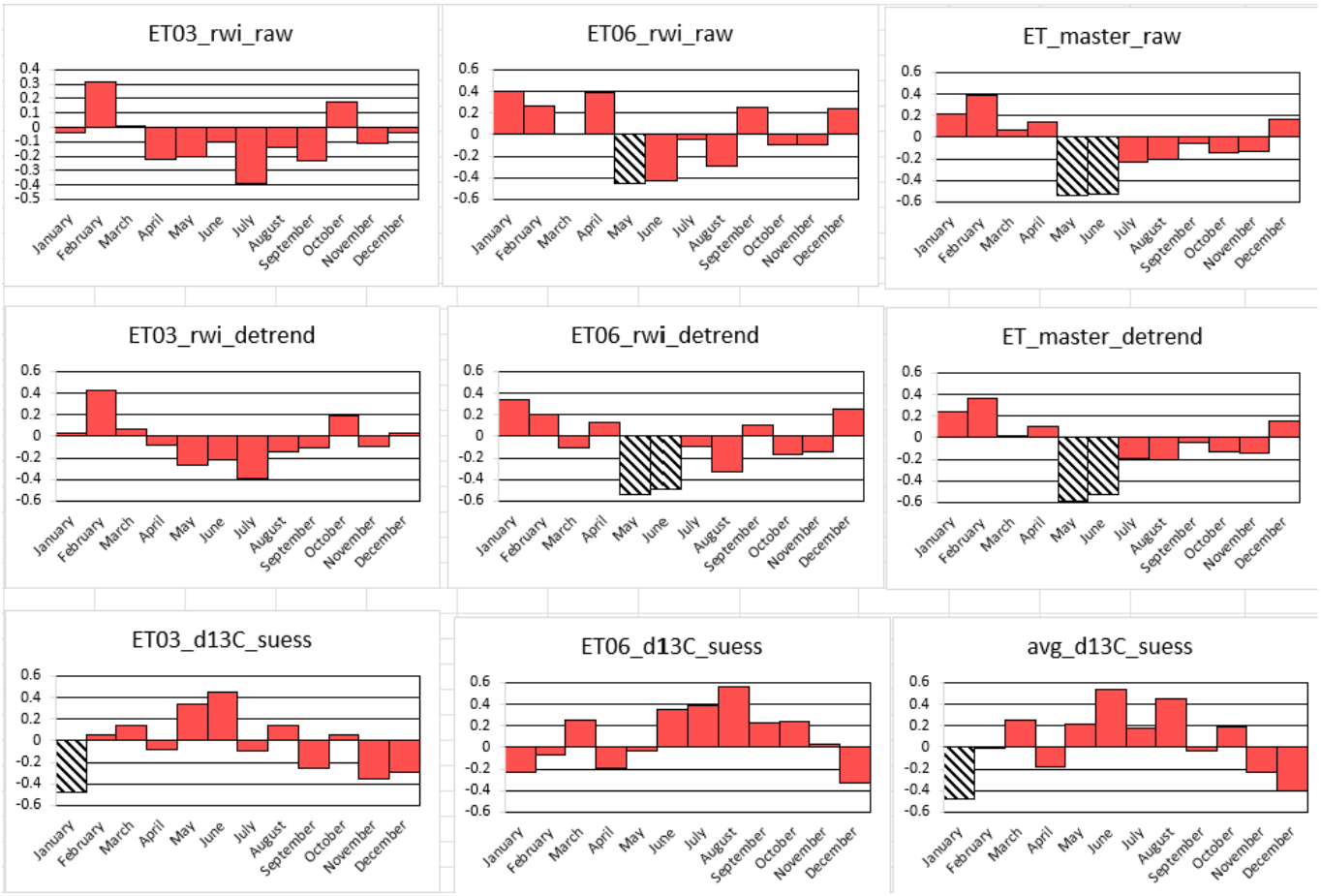

Figure 8: Correlation diagrams showing Pearson's correlation coefficient between ring width and monthly temperature. The first and second rows compare the raw and detrended RWi of ET06, ET03, and the master chronology with the monthly temperature. The third row compares the suess-detrended $\delta^{13}C$ of ET06, ET03, and their average with monthly temperature. Temperature data is from the Climatic Research Unit (CRU) TS 4.07 dataset from the KNMI climate explorer webpage at 0.5 degree spatial resolution (Harris et al., 2014; Koninklijk Nederlands Meteorologisch Instituut).

Indirect evidence of volcanic gases on tree rings

Mechanisms of indirectly imparting a volcanic signal on nearby trees, less than 50km from the volcanic area, fall into three broad categories. The first is increased photosynthesis and carbon

fixation related to positive changes in soil humidity. This has been investigated at Etna prior to rift-opening flank eruptions, wherein excess moisture from vapours seeping from the ground have been linked to decreased $\delta^{18}O$ in tree rings (Seiler et al., 2021) or increased plant productivity as indicated by satellite-based measurements of normalized difference vegetation indices (Houlié et al., 2006). In terms of $\delta^{13}C$ and RWi, high moisture would be expected to increase growth and decrease $\delta^{13}C$, while low moisture would lead to closing of stomata, decreased discrimination, and increased $\delta^{13}C$ along with smaller RWi from reduced growth (Francey and Farquhar, 1982). This mechanism does not concern us for the plume gas study, as our sites are not overlying faults and there is a lack of evidence for soil CO_2 emanations which would increase moisture. The second mechanism encompasses climate-related impacts from a volcanic dust-veil. This could reduce light intensity and photosynthetic activity, decreasing $\delta^{13}C$ and localized cooling (Farquhar et al., 1989). On the other hand, the feedback mechanism could lead to increased $\delta^{13}C$ if high diffusive radiation dominated, increasing air humidity and growth rates (Battiglia et al., 2007). The third mechanism is the ash or SO_2 content of a volcanic plume either closing or damaging stomata, the pores of tree leaves and needles through which gases are exchanged. At low concentrations, this would result in partial closure of the stomata and increased $\delta^{13}C$ or if concentrations are high enough to injure the photosynthetic metabolism, a decreased $\delta^{13}C$ would be expected (Martin et al., 1988). At Turrialba volcano in Costa Rica, an increase of 1.3 ‰ was noted in living trees 1.5 km from the summit craters after the onset of degassing (D'Arcy et al., 2019).

The negative correlations between ring width and $\delta^{13}C$ (figure 6) are not unlike those seen in other studies (Alfaro-Sanchez et al., 2020), where a decrease in ring width was recorded three years after a large eruption of Popocatapetl volcano in Mexico. Our results indicate that

during periods of decreased growth, there was an increase in $\delta^{13}C$ during 2003 to 2013. This may be reflecting reduced growth in the two or three years following the extensive 2001 and 2002-2003 eruptions. The 2001 eruption was preceded by lava effusions and activity at the Southeast Crater in early 2001, before cyclical paroxysmal activity took place in June to July 2001, followed by lava flows in July to August 2001 that extended down the flank as far as 1040 m elevation (Behncke and Neri, 2003; Pecoraino and Giammanco, 2005). The 2002-2003 eruption was equally as disruptive and SO_2 fluxes were elevated for several months; however, the eruption occurred from October 2002 through January 2003 after the growing season. Looking closer at our data, we see that RWi is low for 2005-2008 for all series (figure 3), while $\delta^{13}C$ of ET-03 and ET-06 trend in opposite directions for 2004 to 2006 (figure 4a). Specifically, during 2004 to 2006, the $\delta^{13}C$ of ET-03 increased, while both ET-06 and the average $\delta^{13}C$ of Seiler et al., (2021) decreased. During 2003 to 2013, we do not see consistent seasonal correlations between either ring width or precipitation (figures 7 and 8). Neither do we see significant correlations with annual SO_2 output from 2005 to 2015 (Carn et al., 2017), with Pearson's R coefficients between -0.37 and 0.43. To investigate this further, we now compare SO_2 output at Etna before, during, and after the period of 2001 to 2004, when a high sulfur load could be impacting the surrounding trees with a lag of two to three years.

Plume SO_2

Etna is one of the world's largest emitters of volcanic CO_2 (Burton et al., 2013) and SO_2 (Oppenheimer et al., 2011). Etna is a strong emitter both during quiescence as well as eruptive phases, with passive degassing dominant. It is estimated that the volcano produced 0.505 Tg SO_2 during eruptions from 1978 to 2014 based on satellite observations (Carn et al., 2017). The SO_2

flux record from Etna has evolved to encompass various instrumentation and methods over the years. From 1987 to 2000 SO_2 flux at Etna was monitored by ground spectrometry using COSPEC, averaging 5560 t/d (Caltabiano et al. 2000, 2004). During eruptions of summer 2001 and fall 2002, SO_2 flux was 9245 – 13200 t/d as measured by ASTER satellite radiometry (Pugnaghi et al. 2006) and 15200-46100 t/d as measured with an AIRS hyperspectral IR spectrometer, respectively (Carn et al., 2005). COSPEC measurements during these same eruptions peaked at 20000 t/d and 30000 t/d, respectively (Global Volcanism Program, 2002). In 2004, an automatic scanning network of UV spectrometers was installed, which calculated an average flux of 3530 t/d SO_2 from 2005 to 2008 (Salerno et al., 2009) and an average of 2400 to 2700 t/d (minimum 400 to 13500 t/d for quiescent degassing and 450 to 20000 t/d for eruptions) for 2008 to 2009 (Salerno et al., 2018). For 2005 to 2015, an average of 1277 t/d was measured by ground-based UV spectrometry (DOAS) traverses (Aiuppa et al., 2008) and 2039 t/d by satellite-based UV spectrometry (OMI) (Carn et al., 2017). These measurements included passive degassing. The daily emission rate can thus be highly variable, ranging from 612 to 5698 t/d in 2005 to 2007. Finally, near the end of our study period, estimates for 2018 were 2830 t/d by TROPOMI satellite-based spectrometry (Queißer et al., 2019). This variable record of SO_2 flux is displayed in figure 9.

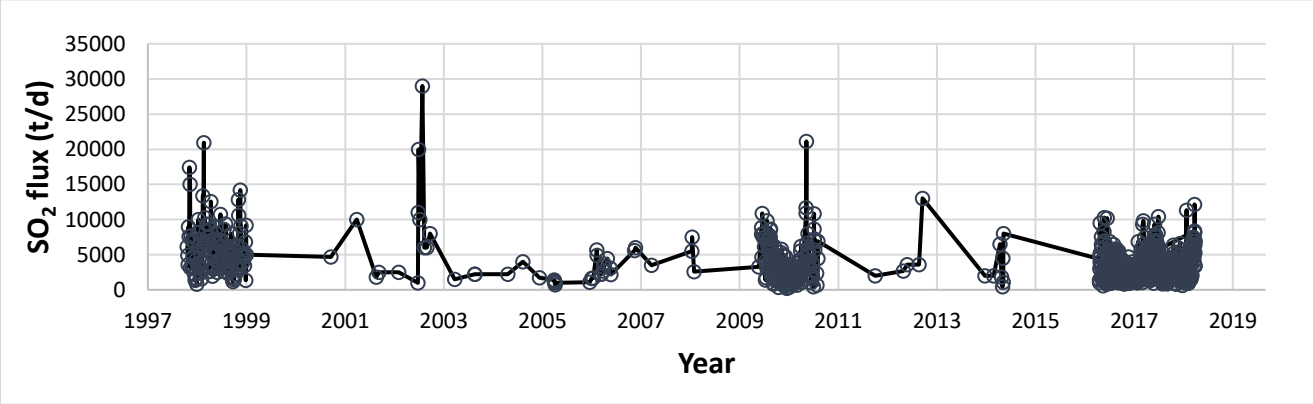

Figure 9: SO_2 fluxes at Mt. Etna, 1998-2018. Fluxes are compiled from Bruno et al. (2001), Giammanco et al. (2013), Salerno et al (2003), Andronico et al. (2005), Aiuppa et al. (2008), Salerno et al. (2018), Spaminato et al. (2015), Ferlito et al. (2017), Paonita et al. (2021). To estimate fluxes for time periods lacking high-resolution data, an average flux value from the literature was used. This value was plotted at both the start and end of each period, which spanned several weeks to months.

The SO_2 estimates give us a good range of baseline and eruptive emissions during our target study period of 1998 to 2018. However, there are several caveats to using the SO_2 data as a proxy for tree exposure to volcanic plume emissions. For example, does the plume reach the locations where our study trees are growing? We do not have atmospheric measurements taken beside the samples trees. Instead, the flux data are collected either by satellites or from higher or lower altitudes to estimate the plume flux as a whole. Another question is whether high-altitude eruptions, as measured by TOMS in 2001-2002, impact the trees at lower elevations. It is possible that the trees are not affected, as the gases can be partly ejected into the mid-troposphere with plume trajectories showing dispersal at 6.5 to 7.5 km altitudes for several kilometres distance from the source (Queißer et al., 2019). While there are satellite-based measurements of SO_2 loading for eruptive columns between 4 km and 13 km spanning decades (Global Volcanism Program, 2024), we do not include these data in figure 9. The plume descends from 2000 to 800 m elevation for wind speeds of 20 to 35 m/s (Salerno et al., 2009) and those low-altitude plume trajectories will be more relevant to our study). We integrated fluxes from COSPEC data (Salerno et al., 2003; Andronico et al., 2005; Giammanco et al., 2013) to approximate the total SO_2 output for the years 2001 to 2004. We calculate total masses of 1270, 1580, 820, and 910 kt SO_2 for each of 2001, 2002, 2003, and 2004, respectively. While the highest annual mass estimate and the maximum single flux observed during these four years occurs in 2002, most of the emissions of the 2002-2003 eruption occurred after the growing season had ended (October

2002 to January 2003). The 2001 peak of 10000 t/d in July was accompanied by prolonged and elevated SO_2 flux throughout most of the growing season (June through September). Adding these annual flux estimates to the OMI data for 2005 to 2015, we find a positive correlation between the raw ring width of ET-03 and the annual SO_2 data for 2001 to 2015 (Pearson's R of 0.6, $p < 0.05$) but a positive correlation below significance level for the $\delta^{13}C$ of this same site. Additionally, applying the same correlations with a lag of one to three years lowers the RWi-SO_2 correlation below significance level. Therefore, we cannot conclude that the degassing activity of Etna can be linked to the trees in our study.

Conclusions

The dominantly biogenic signature of the soil gas as well as the unremarkable ^{14}C tree ring signatures at our chosen sites near the Valle del Bove demonstrates that magmatic CO_2 is likely not influencing the growth of the trees nor the isotopic compositions of the tree rings. Furthermore, the ^{13}C ratios of the tree rings suggest that SO_2 fumigation as a result of degassing of the volcano did not strongly impact the trees at our sites during the study period of 1998 to 2018. While we can speculate that site ET-03 possesses some anomalous ring widths and $\delta^{13}C$ may be weakly correlated with volcanic SO_2 of Mt. Etna, the evidence is ambiguous. We have found that this approach as applied here is not a feasible method of volcano monitoring, yet this study is valuable in providing a means to assess volcanic plume interactions with tree ring geochemistry in a modern context where sufficient gas data are available. This combined isotope-tree ring methodology would be suited to reconstructions of historic eruption chronologies when combined with oral histories and tephra geochemistry, where available.

References cited

Aiuppa, A., Bellomo, S., D'Alessandro, W., Federico, C., Ferm, M., and Valenza, M., 2004, Volcanic plume monitoring at Mount Etna by diffusive (passive) sampling: Journal of Geophysical Research D: Atmospheres, v. 109, p. 1–11, doi:10.1029/2003JD004481.

Aiuppa, A., Giudice, G., Gurrieri, S., Liuzzo, M., Burton, M., Caltabiano, T., McGonigle, A.J.S., Salerno, G., Shinohara, H., and Valenza, M., 2008, Total volatile flux from Mount Etna: Geophysical Research Letters, v. 35, p. 2008GL035871, doi:10.1029/2008GL035871.

Alfaro-Sánchez, R., Camarero, J.J., Querejeta, J.I., Sagra, J., Moya, D., and Rodríguez-Trejo, D.A., 2020, Volcanic activity signals in tree-rings at the treeline of the Popocatépetl, Mexico: Dendrochronologia, v. 59, p. 125663, doi:10.1016/j.dendro.2020.125663.

Allard, P. et al., 1991, Eruptive and diffuse emissions of CO2 from Mount Etna: Letters to Nature, v. 351, p. 387–391.

Allen, A.G., Mather, T.A., McGonigle, A.J.S., Aiuppa, A., Delmelle, P., Davison, B., Bobrowski, N., Oppenheimer, C., Pyle, D.M., and Inguaggiato, S., 2006, Sources, size distribution, and downwind grounding of aerosols from Mount Etna: Journal of Geophysical Research: Atmospheres, v. 111, p. 2005JD006015, doi:10.1029/2005JD006015.

Andronico, D. et al., 2005, A multi-disciplinary study of the 2002?03 Etna eruption: insights into a complex plumbing system: Bulletin of Volcanology, v. 67, p. 314–330, doi:10.1007/s00445-004-0372-8.

Baillie, M.G.L., and Pilcher, J.R., 1973, A Simple Crossdating Program for Tree-Ring Research: Tree-ring Bulletin, v. 33, p. 7–14.

Battipaglia, G., Cherubini, P., Saurer, M., Siegwolf, R.T.W., Strumia, S., and Francesca Cotrufo, M., 2007, Volcanic explosive eruptions of the Vesuvio decrease tree-ring growth but not photosynthetic rates in the surrounding forests: Global Change Biology, v. 13, p. 1122–1137, doi:10.1111/j.1365-2486.2007.01350.x.

Behncke, B., and Neri, M., 2003, The July-August 2001 eruption of Mt. Etna (Sicily): Bulletin of Volcanology, v. 65, p. 461–476, doi:10.1007/s00445-003-0274-1.

Belmecheri, S., and Lavergne, A., 2020, Compiled records of atmospheric CO2 concentrations and stable carbon isotopes to reconstruct climate and derive plant ecophysiological indices from tree rings: Dendrochronologia, v. 63, p. 125748, doi:10.1016/j.dendro.2020.125748.

Bogue, R.R. et al., 2018, Plant responses to volcanically-elevated CO 2 in two Costa Rican forests: Biogeosciences, p. 1–27.

Bunn, A.G., 2008, A dendrochronology program library in R (dplR): Dendrochronologia, v. 26, p. 115–124, doi:10.1016/j.dendro.2008.01.002.

Bunn, A.G., 2010, Statistical and visual crossdating in R using the dplR library: Dendrochronologia, v. 28, p. 251–258, doi:10.1016/j.dendro.2009.12.001.

Bunn, A., M, K., F, B., F, C., P, M., F, Q., and C, Z., 2023, dplR: Dendrochronology Program Library in R:, https://CRAN.R-project.org/package=dplR.

Burton, M.R., Sawyer, G.M., and Granieri, D., 2013, Deep carbon emissions from volcanoes: Reviews in Mineralogy and Geochemistry, v. 75, p. 323–354, doi:10.2138/rmg.2013.75.11.

Calvari, S., Tanner, L.H., Groppelli, G., and Norini, G., 2004, Valle del bove, eastern flank of etna volcano: A comprehensive model for the opening of the depression and implications for future hazards, *in* Geophysical Monograph Series, Blackwell Publishing Ltd, v. 143, p. 65–75, doi:10.1029/143GM05.

Carn, S.A., Fioletov, V.E., McLinden, C.A., Li, C., and Krotkov, N.A., 2017, A decade of global volcanic SO2 emissions measured from space: Scientific Reports, v. 7, p. 44095, doi:10.1038/srep44095.

Carn, S.A., Strow, L.L., De Souza-Machado, S., Edmonds, Y., and Hannon, S., 2005, Quantifying tropospheric volcanic emissions with AIRS: The 2002 eruption of Mt. Etna (Italy): Geophysical Research Letters, v. 32, p. 2004GL021034, doi:10.1029/2004GL021034.

Chester, D.K., Duncan, A.M., Guest, J.E., and Kilburn, C.R.J., 1985, Etna and the Etna region, *in* Mount Etna, Dordrecht, Springer Netherlands, p. 37–64, doi:10.1007/978-94-009-4079-6_2.

Cook, E., Briffa, K., Shiyatov, S., Mazepa, V., and Jones, P.D., 1990, Data Analysis, *in* Cook, E.R. and kairiukstis, L.A. eds., Methods ofDendrochronology, International Institute for Applied Systems Analysis, p. 97–162.

Cook, A.C., Hainsworth, L.J., Sorey, M.L., Evans, W.C., and Southon, J.R., 2001, Radiocarbon studies of plant leaves and tree rings from Mammoth Mountain , CA : a long-term record of magmatic CO 2 release: Chemical Geology, p. 117–131.

D'Arcy, F., Boucher, É., De Moor, J.M., Hélie, J.-F., Piggott, R., and Stix, J., 2019, Carbon and sulfur isotopes in tree rings as a proxy for volcanic degassing: Geology, v. 47, p. 825–828, doi:10.1130/G46323.1.

D'Arrigo, R.D., Jacoby, G., and Frank, D., 2003, Dendroclimatological Evidence for Major Volcanic Events of the Past Two Millennia, *in* Robock, A. and Oppenheimer, C. eds., Volcanism and the Earth's Atmosphere, American Geophysical Union, Gephyisical Monograph Series, v. 139, p. 1–20, 10.1029/GM139.

Eckstein, D., and Bauch, J., 1969, Beitrag zur Rationalisierung eines dendrochronologischen Verfahrens und zur Analyse seiner Aussagesicherhei: Forstwissenschaftliches Centralblatt, v. 88, p. 230–250.

Evans, W.C., Bergfeld, D., McGeehin, J.P., King, J.C., and Heasler, H., 2010, Tree-ring 14C links seismic swarm to CO2 spike at Yellowstone, USA: Geology, v. 38, p. 1075–1078, doi:10.1130/G31345.1.

Farquhar, G.D., Ehleringer, J.R., and Hubick, K.T., 1989, Carbon Isotope Discrimination and Photosynthesis: Annual Review of Plant Physiology and Plant Molecular Biology, v. 40, p. 503–537, doi:10.1146/annurev.pp.40.060189.002443.

Francey, R.J., and Farquhar, G.D., 1982, An explanation of 13C/12C variations in tree rings: Nature, v. 297, p. 28–31, doi:10.1038/297028a0.

Giammanco, S., Neri, M., Salerno, G.G., Caltabiano, T., Burton, M.R., and Longo, V., 2013, Evidence for a recent change in the shallow plumbing system of Mt. Etna (Italy): Gas geochemistry and structural data during 2001–2005: Journal of Volcanology and Geothermal Research, v. 251, p. 90–97, doi:10.1016/j.jvolgeores.2012.06.001.

Global Volcanism Program, 2002, Report on Etna (Italy) (R. Wunderman, Ed.): Bulletin of the Global Volcanism Network, v. 27, doi:10.5479/si.GVP.BGVN200210-211060.

Global Volcanism Program, 2024, Volcanoes of the World (v. 5.1.6; 2 Mar 2024). Distributed by Smithsonian Institution, compiled by Venzke, E.:, doi:https://doi.org/10.5479/si.GVP.VOTW5-2023.5.1.

Graven, H. et al., 2017, Compiled records of carbon isotopes in atmospheric CO2 for historical simulations in CMIP6: Geoscientific Model Development, v. 10, p. 4405–4417, doi:10.5194/gmd-10-4405-2017.

Harris, I., Jones, P.D., Osborn, T.J., and Lister, D.H., 2014, Updated high-resolution grids of monthly climatic observations – the CRU TS3 .10 Dataset: International Journal of Climatology, v. 34, p. 623–642, doi:10.1002/joc.3711.

Holdaway, R.N., Duffy, B., and Kennedy, B., 2018, Evidence for magmatic carbon bias in 14C dating of the Taupo and other major eruptions: Nature Communications, v. 9, p. 4110, doi:10.1038/s41467-018-06357-0.

Hollstein, E., 1980, Mitteleuropäische Eichenchronologie Trier dendrochronologische Forschungen zur Archäologie und Kunstgeschichte: Trierer Grabungen und Forschungen, v. 11.

Houlié, N., Komorowski, J.C., de Michele, M., Kasereka, M., and Ciraba, H., 2006, Early detection of eruptive dykes revealed by normalized difference vegetation index (NDVI) on Mt. Etna and Mt. Nyiragongo: Earth and Planetary Science Letters, v. 246, p. 231–240, doi:10.1016/j.epsl.2006.03.039.

Johnstone, J.A., Roden, J.S., and Dawson, T.E., 2013, Oxygen and carbon stable isotopes in coast redwood tree rings respond to spring and summer climate signals: Journal of Geophysical Research: Biogeosciences, v. 118, p. 1438–1450, doi:10.1002/jgrg.20111.

Keeling, R.F., Piper, S.C., Bollenbacher, A.F., and Walker, S.J., 2009, Atmospheric CO2 values (ppmv) derived from in situ air samples collected at Mauna Loa Hawaii, USA.:, http://cdiac.ornl.gov/ftp/trends/co2/maunaloa.co2.

Koninklijk Nederlands Meteorologisch Instituut Climatic Research Unit (CRU) TS 4.07 dataset:, http://climexp.knmi.nl/ (accessed January 2024).

Levin, I., Hammer, S., Kromer, B., and Meinhardt, F., 2008, Radiocarbon observations in atmospheric CO2: Determining fossil fuel CO2 over Europe using Jungfraujoch observations as background: Science of The Total Environment, v. 391, p. 211–216, doi:10.1016/j.scitotenv.2007.10.019.

Levin, I., and Kromer, B., 2004, The Tropospheric $^{14}CO_2$ Level in Mid-Latitudes of the Northern Hemisphere (1959–2003): Radiocarbon, v. 46, p. 1261–1272, doi:10.1017/S0033822200033130.

Lewicki, J.L., Hilley, G.E., Shelly, D.R., King, J.C., Mcgeehin, J.P., Mangan, M., and Evans, W.C., 2014, Crustal migration of CO2 -rich magmatic fluids recorded by tree-ring

radiocarbon and seismicity at Mammoth Mountain , CA , USA: Earth and Planetary Science Letters, v. 390, p. 52–58, doi:10.1016/j.epsl.2013.12.035.

Liuzzo, M., Gurrieri, S., Giudice, G., and Giuffrida, G., 2013, Ten years of soil CO2 continuous monitoring on Mt. Etna: Exploring the relationship between processes of soil degassing and volcanic activity: Geochemistry, Geophysics, Geosystems, v. 14, p. 2886–2899, doi:10.1002/ggge.20196.

Martin, B., Bytnerowicz, A., and Thorstenson, Y.R., 1988, Effects of air pollutants on the composition of stable carbon isotopes, δ13C, of leaves and wood, and on leaf injury: Plant Physiology, v. 88, p. 218–223, doi:10.1104/pp.88.1.218.

McCarroll, D., and Loader, N.J., 2004, Stable isotopes in tree rings: Quaternary Science Reviews, v. 23, p. 771–801, doi:10.1016/j.quascirev.2003.06.017.

Oppenheimer, C., Scaillet, B., and Martin, R.S., 2011, Sulfur Degassing From Volcanoes: Source Conditions, Surveillance, Plume Chemistry and Earth System Impacts: Reviews in Mineralogy and Geochemistry, v. 73, p. 363–421, doi:10.2138/rmg.2011.73.13.

Pecoraino, G., and Giammanco, S., 2005, Geochemical Characterization and Temporal Changes in Parietal Gas Emissions at Mt. Etna (Italy) During the Period:, 805–841 p.

Queißer, M., Burton, M., Theys, N., Pardini, F., Salerno, G., Caltabiano, T., Varnam, M., Esse, B., and Kazahaya, R., 2019, TROPOMI enables high resolution SO2 flux observations from Mt. Etna, Italy, and beyond: Scientific Reports, v. 9, p. 957, doi:10.1038/s41598-018-37807-w.

R Core Team, 2023, R: A Language and Environment for Statistical Computing.:, https://www.R-project.org/.

Salerno, G.G., Burton, M., Di Grazia, G., Caltabiano, T., and Oppenheimer, C., 2018, Coupling Between Magmatic Degassing and Volcanic Tremor in Basaltic Volcanism: Frontiers in Earth Science, v. 6, p. 157, doi:10.3389/feart.2018.00157.

Salerno, G.G., Burton, M.R., Oppenheimer, C., Caltabiano, T., Randazzo, D., Bruno, N., and Longo, V., 2009, Three-years of SO2 flux measurements of Mt. Etna using an automated UV scanner array: Comparison with conventional traverses and uncertainties in flux retrieval: Journal of Volcanology and Geothermal Research, v. 183, p. 76–83, doi:10.1016/j.jvolgeores.2009.02.013.

Salerno, G., Caltabiano, T., Bruno, N., and Longo, V., 2003, Anomalous SO2 emissions from Mt. Etna between 2001 and 2002-2003 eruptions:

Saurer, M., Siegwolf, R.T.W., and Schweingruber, F.H., 2004, Carbon isotope discrimination indicates improving water-use efficiency of trees in northern Eurasia over the last 100 years: Global Change Biology, v. 10, p. 2109–2120, doi:10.1111/j.1365-2486.2004.00869.x.

Savard, M.M., Bégin, C., and Parent, M., 2002, Are industrial SO2 emissions reducing CO2 uptake by the boreal forest? Geology, v. 30, p. 403–406, doi:10.1130/0091-7613(2002)030<0403:AISERC>2.0.CO;2.

Seiler, R., Hajdas, I., Saurer, M., Houlié, N., D'Arrigo, R., Kirchner, J.W., and Cherubini, P., 2021, Tree-ring stable isotopes and radiocarbon reveal pre- and post-eruption effects of

volcanic processes on trees on Mt. Etna (Sicily, Italy): Ecohydrology, v. 14, p. e2340, doi:10.1002/eco.2340.

Seiler, R., Houlié, N., and Cherubini, P., 2017, Tree-ring width reveals the preparation of the 1974 Mt. Etna eruption: Scientific Reports, v. 7, p. 44019, doi:10.1038/srep44019.

Sharma, S., and Williams, D.G., 2009, Carbon and oxygen isotope analysis of leaf biomass reveals contrasting photosynthetic responses to elevated CO2 near geologic vents in Yellowstone National Park:

Watt, S.F.L., Pyle, D.M., Mather, T.A., Day, J.A., and Aiuppa, A., 2007, The use of tree-rings and foliage as an archive of volcanogenic cation deposition: Environmental Pollution, v. 148, p. 48–61, doi:10.1016/j.envpol.2006.11.007.

Comprehensive Discussion

Main findings

The key findings presented in this thesis advance our knowledge of volcano monitoring and test the limitations of cross-disciplinary techniques. As a whole, the results presented in this thesis have populated our global dataset of carbon isotopic variations in volcanic regions.

The key findings are summarized below:

- Rapid and efficient capture of gases from volcanic plumes is possible by Unoccupied Aerial Systems (UAS) as long as certain factors are considered. Flight safety must be taken into account first and foremost, especially when researchers are in an active volcanic area. Carbon isotopes can be determined from plume gases collected by drone upon returning the samples to a field-based cavity-ring down spectrometer (CRDS) within 12 hours of sampling, and by calculating a mixing model between the atmospheric and volcanic sources of CO_2.
- Aerial sampling of plumes can provide similar estimates of volcanic $\delta^{13}C$ compared to traditional ground-based methods, on the condition that the number of samples and their CO_2 concentrations are sufficiently high as to allow for robust estimations of the volcanic endmember. If the concentration of gas samples is too low, or if their spread is clustered closest to the atmospheric endmember, the estimates may not be significant.
- At Poás volcano, there is a cyclicity to the variations in $\delta^{13}C$ which may be related to the sealing and unsealing of the magmatic carapace. During quiescence, the hydrothermal system is sealed off from the magmatic system, which interacts with CO_2 as it transits from the magmatic source via hydrothermal buffering. During highly active periods, the

hydrothermal system is more open, resulting in more negative $\delta^{13}C$ approaching the expected value of carbon degassed from the regenerative magma supply of Poás.

- At Stromboli volcano, volcanic plume $\delta^{13}C$ was dynamic between 2018 and 2019, reinforcing the notion that classifying the carbon isotopic signature of a volcano with a static value is not accurate nor appropriate. Rather, these values must be monitored over the course of an individual volcano's behavioural cycle, which warrants frequent measurements of plume $\delta^{13}C$.
- Lack of radiocarbon anomalies in tree rings on the flanks of volcanoes can be interpreted as a lack of prolonged exposure of trees during their growth season to volcanic CO_2 from either soil or plume gases. There is no evidence for magmatic CO_2 reaching trees at 1200 and 1700 metres above sea level on the east side of the Valle del Bove of Etna volcano during 1998 to 2003 based upon the absence of radiocarbon anomalies in tree rings.
- Volcanic plume exposure can otherwise impact the growth of local trees indirectly through SO_2 gas exposure, humidity and temperature changes, and soil acidification which can alter the $\delta^{13}C$ of tree rings. Isolating these factors from one another is difficult, and attempts to do so will be aided by increasing the sample size to as many trees as is feasibly possible within the scope of the study.

Limitations

Due to the exploratory nature of all three studies presented in this thesis, there were several limitations which should be addressed so that future work can continue to refine the methods I

present here. I can identify two main themes of limitations which were applicable in all three studies: calibration and statistics.

Carbon isotope calibration is extremely important because the error of any measurements made will depend on the accuracy and reproducibility that the instrument can provide. I measured known standards to calibrate the Picarro G2201-i CRDS, and I also measured background atmospheric air. Compilations of global atmospheric background $\delta^{13}C$ have become more refined in recent years as efforts are made to reduce uncertainties in carbon cycling modeling (Graven et al., 2017). Both the atmospheric endmember for my carbon mixing models of chapters 1 and 2, as well as the air and soil gas in chapter 3, relied on atmospheric $\delta^{13}C$ estimation for my calculations. In chapter 1, I measured local background at Poás to be around 408 pm and -9.8 ‰ in 2019, while in chapter 2 I measured local background at 401 ppm and -8.9 ‰ in 2018 and about 401 ppm and -9.9 ‰ in 2019. In chapter 3, though not at the summit but instead on the forested flanks of Etna volcano, I measured background atmosphere at 398 ppm and -9.4 ‰ in 2019. Yet, a year-long measurement of background $\delta^{13}C$ measurements at a remote location in Australia reported $\delta^{13}C$ from -7.8 ‰ to -8.9 ‰ over the course of dry and wet seasonal cycles (Munksgaard et al., 2023). Respired CO_2 from trees and soil can vary from -22 to -26 ‰ over the course of days and nights (Kodama et al., 2008). My hypothesis is that winds bringing air from forested slopes of the volcanoes can be causing local variations in atmospheric CO_2 that I report in chapters 1 and 2, but I cannot be certain of this without air transport modelling. We cannot ascribe the variations in background to any source of error in particular, including respired CO_2 from our own breath near the sampling apparatus before sample bags were sealed, as well as residual air left in the bags after they had been evacuated. Nevertheless, any error which the background samples are subject to should be present in the sample gas bags as well, which is

why it was important for us to use our own measurements. This limitation could be addressed by coupling ground-based measurements with satellite-based measurements of regional CO_2 concentrations, for example from the OCO-2 satellite, as has been addressed in atmospheric studies using CRDS (Munksgaard et al., 2023). The global atmospheric CO_2 and $\delta^{13}C$ was used in our calculation of the corrected tree ring $\delta^{13}C$ of chapter 3, which would have been improved if a local measure of CO_2 flux from an Eddy covariance tower were used instead.

The strength of my statistical analyses was another limitation spanning all three chapters. Statistical analyses will be stronger with more samples, as this increases the degrees of freedom associated with the confidence level of each analysis. My UAS approach in chapters 1 and 2 limited the number of samples we could obtain each sampling day, as only one to three flights could be performed on a set of drone batteries before they would need to be returned to our base-camp to charge them. Our tree ring approach in chapter 3 was limited by time and cost, as radiocarbon samples are more than ten times the cost of stable carbon analysis and the preparation of each tree ring for either analysis involved sanding, cutting, grinding, extracting, and weighing phases of lab work. If I were to redesign the study, I would obtain more samples to increase the statistical robustness. I would also pool the wood powders from the two trees of each site (06 and 05, 03 and 04) to increase our chances of capturing an anomaly. However, that would require additional lab time to cut, grind, and pool samples, something that is not feasible in the scope of this work.

The choice of statistical analysis was also a limiting factor in my thesis. In chapters 1 and 2, I used a Keeling approach to model mixing between background air and volcanic gas, for which I performed linear regression. This method is the most accessible form of regression, but it is not powerful. This limitation can be addressed in a future study with the use of a Model II regression

in R (R Core Team, 2023), which has been shown to reduce errors when extrapolating for biogeochemical studies which employ the linear regression Keeling approach (Pataki et al., 2003; Soper et al., 2017). In chapter 3, my statistics methods involve a correlation analysis which could be improved by increasing the number of samples and years analysed as well as using local climate data rather than satellite-based indices. For example, the monthly precipitation and temperature data obtained for the study area was only available at 0.5 degree resolution (about 30 to 50 km) which would not account for microclimate variations.

Finally, access to open data would have better facilitated certain aspects of this work. In all three chapters, atmospheric data would have enhanced the quality of the studies. For example in chapter 1, plume dispersion modelling would have constrained the sources of CO_2 mixing over the crater of Poás volcano in the distal flights performed, validating our hypothesis of the respired CO_2 from the adjacent forested slopes mixing with the background. In chapter 2, there was some confusion over the code for the model used, which, while available on Github, was archived in a way that the documentation was difficult to follow. The SO_2 flux data of Etna volcano was not consistently archived in the literature nor in public domain databases, limiting the integration and correlation of flux data in chapter 3. This limitation could be overcome with implementing consistent gas geochemical and atmospheric data archiving, for example following the guidelines on the Earthchem repository.

Topics of further research

This thesis monitors carbon emissions using isotopes to advance our knowledge of precursory signals and expand our applications of isotopic tools. Sources and sinks of CO_2 are interrelated, and we need to develop new approaches which combine biological, atmospheric, and

volcanological disciplines. Taking this one step further, an interesting crossover study could couple plume measurements as performed in chapters 1 and 2 with tree rings studies as performed in chapter 3. For two months of the growing season, we could deploy a continuous soil flux chamber and take weekly drone flights to sample gases at crater and tree sites. The logical next step in applying the methodology we present in chapters 1 and 2 is to expand high-resolution time-series of stable carbon isotopes at active volcanoes around the world. For chapter 3, the question remains of whether combined $\delta^{13}C$ and ^{14}C tree ring analysis could be used to reconstruct plume degassing. While we did not clearly identify the volcanic signal in our results, this could have been a matter of sampling the wrong location at the wrong time. This warrants further research of tree ring geochemistry in other volcanic regions.

In Canada, there is a need to monitor active volcanoes using methods suitable our mountainous volcanic belt in British Columbia and the Yukon (Kelman and Wilson, 2024). All three monitoring studies presented in this thesis could be adapted to suit the needs of a remote volcanic terrain such as that of the Cascade Volcanic Arc. The glacial capped summit of Mount Meager is host to nearly inaccessible fumaroles located in ice caves, whose gases could potentially be safely sampled with the UAS method presented in the first part of this thesis. The ubiquitous pine trees of Mount Garibaldi could be useful archives of past degassing, since future monitoring will require historic data on its past quaternary eruptions. This could include studies based upon the second method this thesis with tree ring geochemistry as in chapter 3. Both these volcanoes were ranked as a high risk for future eruptions (Kelman and Wilson, 2024) and require an assessment of their hazards (i.e. which reconstructing past degassing could help with) as well as future monitoring (which could incorporate UAS gas monitoring).

General Conclusions

This thesis presents unique methods for monitoring volcanoes through their gas geochemistry which aim to push the limits of what science can do. Volcanoes will not only continue to erupt, but their devastation is becoming increasingly more impactful as climate change and our rising global population are forcing more people to live in known hazard risk areas. For example, the 2021 eruption of Mount Nyiragongo and the 2022 eruption of Hunga-Tonga Hunga-Ha'apai volcanoes each cost 6 million CAD in humanitarian relief alone and displaced thousands of people (International Federation of Red Cross, 2021, 2022). This highlights the need to continue research into novel methods of volcano surveillance such as those presented in this thesis.

In chapter 1, I discussed the first test study of my Compact Aerial Receiver-Initiated Gas-Sampling Operation (CARGO) at Poás volcano, Costa Rica. I built and tested two versions of this instrumentation and flew it into the crater on two different UAS systems in 2019. From this sample collection and subsequent analysis of the $\delta^{13}CO_2$, I was able reach my objective of determining best practices and accuracy of this new tool. My colleagues and I reported a difference of 0.33 ‰ for ground-based and aerial-based $\delta^{13}CO_2$ from the volcanic plume captured during the same timeframe. We used these results along with earlier $\delta^{13}CO_2$ from 2017 to 2019 to identify an isotopic anomaly in the phase of heightened activity immediately prior to a period of high phreatic and phreatomagmatic activity. We attribute this variation to an opening of the magmatic carapace, allowing fractionated carbon from the degassed magma source to dominate the $\delta^{13}CO_2$ signal. This confirms my hypothesis that degassing batches of magma and hydrothermal processes each have some degree of control over fluctuations in carbon isotopes in the volcanic system.

In chapter 2, I present a second test study of the methodology presented in chapter 1 by deployment of two new versions of the CARGO at Stromboli volcano, Italy. I built and tested two improved versions of the instrumentation based on feedback gained from the fieldwork of chapter 1, and flew these apparatuses abord two UAS during a field campaign in 2019. We measured the $\delta^{13}CO_2$ of our gas samples and compared these results with that of the $\delta^{13}CO_2$ we had measured in 2018 using a UAS-based grab sample approach without receiver-initiated sampling. We again noticed an anomaly, this time in the UAS-based results of 2019 which indicated the volcanic source was more than 2 ‰ more negative than usual at that time. We postulated that this was due to the unique timing of sampling, which was 2 weeks prior to a paroxysm, and we supported this with a degassing model. This confirmed the second hypothesis of this thesis, which is that variations in $\delta^{13}C$ of volcanic plumes can be linked to precursory activity.

In chapter 3, I explore the feasibility of a tree ring geochemical method as a surveillance method of the volcanic plume at Etna volcano, Italy. My objective was to determine the limits and reach of combining $\delta^{13}C$ and ^{14}C analyses in tree rings to delineate volcanic plume and magmatic soil gas impregnation of trees. The results over the term of the study indicated that to deliver on this objective, I would have needed to push the boundaries of my study area to higher elevations and include more samples. I was able to determine a lack of evidence for volcanic CO_2 reaching my sites during the study period. The labour-intensive process led me to conclude that this technique, still in its infancy, requires additional refinement before it can be added to routine volcano monitoring programs. Nonetheless, the findings my colleagues and I present in chapter 3 can provide context for future studies in different volcanic regions and historical contexts.

References

Aiuppa, A. et al., 2021, Volcanic CO2 tracks the incubation period of basaltic paroxysms: Science Advances, v. 7, doi:10.1126/sciadv.abh0191.

Aiuppa, A., Federico, C., Giudice, G., and Gurrieri, S., 2005, Chemical mapping of a fumarolic field: La Fossa Crater, Vulcano Island (Aeolian Islands, Italy): Geophysical Research Letters, v. 32, p. 2005GL023207, doi:10.1029/2005GL023207.

Aiuppa, A., Moretti, R., Federico, C., Giudice, G., Gurrieri, S., Liuzzo, M., Papale, P., Shinohara, H., and Valenza, M., 2007, Forecasting Etna eruptions by real-time observation of volcanic gas composition: Geology, v. 35, p. 1115–1118, doi:10.1130/G24149A.1.

Alfaro-Sánchez, R., Camarero, J.J., Querejeta, J.I., Sagra, J., Moya, D., and Rodríguez-Trejo, D.A., 2020, Volcanic activity signals in tree-rings at the treeline of the Popocatépetl, Mexico: Dendrochronologia, v. 59, p. 125663, doi:10.1016/j.dendro.2020.125663.

Allard, P. et al., 1991, Eruptive and diffuse emissions of CO2 from Mount Etna: Letters to Nature, v. 351, p. 387–391.

Ancapichún, S. et al., 2021, Radiocarbon bomb-peak signal in tree-rings from the tropical Andes register low latitude atmospheric dynamics in the Southern Hemisphere: Science of The Total Environment, v. 774, p. 145126, doi:10.1016/j.scitotenv.2021.145126.

Arndt, J., Calabrese, S., D'Alessandro, W., and Planer-Friedrich, B., 2017, Using mosses as biomonitors to study trace element emissions and their distribution in six different

volcanic areas: Journal of Volcanology and Geothermal Research, v. 343, p. 220–232, doi:10.1016/j.jvolgeores.2017.07.004.

Aubaud, C., 2022, Carbon stable isotope constraints on CO2 degassing models of ridge, hotspot and arc magmas: Chemical Geology, v. 605, p. 120962, doi:10.1016/j.chemgeo.2022.120962.

Bellomo, S., Aiuppa, A., D'Alessandro, W., and Parello, F., 2007, Environmental impact of magmatic fluorine emission in the Mt. Etna area: Journal of Volcanology and Geothermal Research, v. 165, p. 87–101, doi:10.1016/j.jvolgeores.2007.04.013.

Belmecheri, S., and Lavergne, A., 2020, Compiled records of atmospheric CO2 concentrations and stable carbon isotopes to reconstruct climate and derive plant ecophysiological indices from tree rings: Dendrochronologia, v. 63, p. 125748, doi:10.1016/j.dendro.2020.125748.

Bonanno, G., Lo Giudice, R., and Pavone, P., 2012, Trace element biomonitoring using mosses in urban areas affected by mud volcanoes around Mt. Etna. The case of the Salinelle, Italy: Environmental Monitoring and Assessment, v. 184, p. 5181–5188, doi:10.1007/s10661-011-2332-z.

Brehm, N. et al., 2021, Eleven-year solar cycles over the last millennium revealed by radiocarbon in tree rings: Nature Geoscience, v. 14, p. 10–15, doi:10.1038/s41561-020-00674-0.

Burton, M.R., Sawyer, G.M., and Granieri, D., 2013, Deep carbon emissions from volcanoes: Reviews in Mineralogy and Geochemistry, v. 75, p. 323–354, doi:10.2138/rmg.2013.75.11.

Calabrese, S., Giammanco, S., Pokorny, B., Levanič, T., and Poličnik, H., 2010, Monitoring Volcanic Eruptions using Trace Metals in Tree-Rings : preliminary results from Mt . Etna.:

Chiodini, G., 2009, CO_2 /CH_4 ratio in fumaroles a powerful tool to detect magma degassing episodes at quiescent volcanoes: Geophysical Research Letters, v. 36, p. 2008GL036347, doi:10.1029/2008GL036347.

Cook, A.C., Hainsworth, L.J., Sorey, M.L., Evans, W.C., and Southon, J.R., 2001, Radiocarbon studies of plant leaves and tree rings from Mammoth Mountain , CA : a long-term record of magmatic CO 2 release: Chemical Geology, p. 117–131.

Coplen, T.B., Brand, W.A., Gehre, M., Gröning, M., Meijer, H.A.J., Toman, B., and Verkouteren, R.M., 2006, New Guidelines for δ^{13} C Measurements: Analytical Chemistry, v. 78, p. 2439–2441, doi:10.1021/ac052027c.

Crann, C.A., Murseli, S., St-Jean, G., Zhao, X., Clark, I.D., and Kieser, W.E., 2017, First Status Report on Radiocarbon Sample Preparation Techniques at the A.E. Lalonde AMS Laboratory (Ottawa, Canada): Radiocarbon, v. 59, p. 695–704, doi:10.1017/RDC.2016.55.

D'Alessandro, W., Brusca, L., Kyriakopoulos, K., Rotolo, S., Michas, G., Minio, M., and Papadakis, G., 2006, Diffuse and focused carbon dioxide and methane emissions from the

Sousaki geothermal system, Greece: Geophysical Research Letters, v. 33, p. 2006GL025777, doi:10.1029/2006GL025777.

De Guzman, C., 2023, Thousands Flee a Volcano in the Philippines Fearing a Possible Violent Eruption: Time, https://time.com/6287385/philippines-mayon-volcano-eruption/ (accessed January 2024).

Delmelle, P., Stix, J., Baxter, P.J., Garcia-Alvarez, J., and Barquero, J., 2002, Atmospheric dispersion, environmental effects and potential health hazard associated with the low-altitude gas plume of Masaya volcano, Nicaragua: Bulletin of Volcanology, v. 64, p. 423–434, doi:10.1007/s00445-002-0221-6.

Edwards, B.A., Pfeffer, M.A., Ilyinskaya, E., Kleine-Marshall, B.I., Mandon, C.L., Cotterill, A., Aiuppa, A., Outridge, P.M., and Wang, F., 2024, Exceptionally low mercury concentrations and fluxes from the 2021 and 2022 eruptions of Fagradalsfjall volcano, Iceland: Science of The Total Environment, v. 917, p. 170457, doi:10.1016/j.scitotenv.2024.170457.

Evans, W.C., Bergfeld, D., McGeehin, J.P., King, J.C., and Heasler, H., 2010, Tree-ring 14C links seismic swarm to CO2 spike at Yellowstone, USA: Geology, v. 38, p. 1075–1078, doi:10.1130/G31345.1.

Fischer, T.P., and Lopez, T.M., 2016, First airborne samples of a volcanic plume for δ13C of CO2 determinations: Geophysical Research Letters, v. 43, p. 3272–3279, doi:10.1002/2016GL068499.Received.

Fleisher, A.J., Long, D.A., Liu, Q., Gameson, L., and Hodges, J.T., 2017, Optical Measurement of Radiocarbon below Unity Fraction Modern by Linear Absorption Spectroscopy: The Journal of Physical Chemistry Letters, v. 8, p. 4550–4556, doi:10.1021/acs.jpclett.7b02105.

Fleisher, A.J., Yi, H., Srivastava, A., Polyansky, O.L., Zobov, N.F., and Hodges, J.T., 2021, Absolute 13C/12C isotope amount ratio for Vienna PeeDee Belemnite from infrared absorption spectroscopy: Nature Physics, v. 17, p. 889–893, doi:10.1038/s41567-021-01226-y.

Fritts, H.C., 1928-, 1976, Tree rings and climate: London, Academic Press.

Giggenbach, W.F., 1996, Chemical Composition of Volcanic Gases, *in* Scarpa, R. and Tilling, R.I. eds., Monitoring and Mitigation of Volcano Hazards, Springer Berlin Heidelberg, p. 221–256.

Global Volcanism Program, 2024, Volcanoes of the World (v. 5.1.6; 2 Mar 2024). Distributed by Smithsonian Institution, compiled by Venzke, E.:, doi:https://doi.org/10.5479/si.GVP.VOTW5-2023.5.1.

Graven, H. et al., 2017, Compiled records of carbon isotopes in atmospheric CO₂ for historical simulations in CMIP6: Geoscientific Model Development, v. 10, p. 4405–4417, doi:10.5194/gmd-10-4405-2017.

Grootes, P.M., Farwell, G.W., Schmidt, F.H., Leach, D.D., and Stuiver, M., 1989, Rapid response of tree cellulose radiocarbon content to changes in atmospheric $^{14}CO_2$ concentration: Tellus B, v. 41B, p. 134–148, doi:10.1111/j.1600-0889.1989.tb00131.x.

Guyette, Henderson, and Cutter, 1992, Reconstructing Soil pH from Manganese Concentrations in Tree-Rings: Forest Science, v. 38, p. 727–737.

Hall, G.S., Yamaguchi, D.K., and Rettberg, T.M., 1990, Multielemental analyses of tree rings by inductively coupled plasma mass spectrometry: Journal of Radioanalytical and Nuclear Chemistry Letters, v. 146, p. 255–265, doi:10.1007/BF02164193.

Helo, C., Longpré, M.-A., Shimizu, N., Clague, D.A., and Stix, J., 2011, Explosive eruptions at mid-ocean ridges driven by CO2-rich magmas: Nature Geoscience, v. 4, p. 260–263, doi:10.1038/ngeo1104.

Hernández, M., Vera-Gargallo, B., Calabi-Floody, M., King, G.M., Conrad, R., and Tebbe, C.C., 2020, Reconstructing Genomes of Carbon Monoxide Oxidisers in Volcanic Deposits Including Members of the Class Ktedonobacteria: Microorganisms, v. 8, p. 1880, doi:10.3390/microorganisms8121880.

Hevia, A., Sánchez-Salguero, R., Camarero, J.J., Buras, A., Sangüesa-Barreda, G., Galván, J.D., and Gutiérrez, E., 2018, Towards a better understanding of long-term wood-chemistry variations in old-growth forests: A case study on ancient Pinus uncinata trees from the Pyrenees: Science of The Total Environment, v. 625, p. 220–232, doi:10.1016/j.scitotenv.2017.12.229.

Holloway, J.R., 1976, Fluids in the evolution of granitic magmas: Consequences of finite CO2 solubility: GSA Bulletin, v. 87, p. 1513–1518, doi:10.1130/0016-7606(1976)87<1513:FITEOG>2.0.CO;2.

Ilyinskaya, E. et al., 2018, Globally Significant CO_2 Emissions From Katla, a Subglacial Volcano in Iceland: Geophysical Research Letters, v. 45, doi:10.1029/2018GL079096.

Ilyinskaya, E. et al., 2017, Understanding the environmental impacts of large fissure eruptions: Aerosol and gas emissions from the 2014–2015 Holuhraun eruption (Iceland): Earth and Planetary Science Letters, v. 472, p. 309–322, doi:10.1016/j.epsl.2017.05.025.

International Federation of Red Cross, 2021, Democratic Republic of Congo and Rwanda, Mount Nyiragongo Eruption: Complex MultiHazard Emergency: Revised Emergency Appeal MDRNYIRA21, www. IFRC. org.

International Federation of Red Cross, 2022, Tonga, Asia Pacific, Volcano and Tsunami: Revised Emergency Appeal MDRTO002, www. IFRC. org (accessed March 2024).

James, M. et al., 2020, Volcanological applications of unoccupied aircraft systems (UAS): Developments, strategies, and future challenges: Volcanica, v. 3, p. 67–114, doi:10.30909/vol.03.01.67114.

Johnstone, J.A., Roden, J.S., and Dawson, T.E., 2013, Oxygen and carbon stable isotopes in coast redwood tree rings respond to spring and summer climate signals: Journal of Geophysical Research: Biogeosciences, v. 118, p. 1438–1450, doi:10.1002/jgrg.20111.

Kelman, M.C., and Wilson, A.M., 2024, Assessing the relative threats from Canadian volcanoes: Canadian Journal of Earth Sciences, v. 61, p. 408–430, doi:10.1139/cjes-2023-0074.

Kern, C., Aiuppa, A., and de Moor, J.M., 2022, A golden era for volcanic gas geochemistry? Bulletin of Volcanology, v. 84, doi:10.1007/s00445-022-01556-6.

Kodama, N. et al., 2008, Temporal dynamics of the carbon isotope composition in a Pinus sylvestris stand: from newly assimilated organic carbon to respired carbon dioxide: Oecologia, v. 156, p. 737–750, doi:10.1007/s00442-008-1030-1.

Kouwenberg, L., Wagner, R., Kürschner, W., and Visscher, H., 2005, Atmospheric CO2 fluctuations during the last millennium reconstructed by stomatal frequency analysis of Tsuga heterophylla needles: Geology, v. 33, p. 33–36, doi:10.1130/G20941.1.

LaMarche, V.C., and Hirschboeck, K.K., 1984, Frost rings in trees as records of major volcanic eruptions: Nature, v. 307, p. 121–126.

Lewicki, J.L., Hilley, G.E., Shelly, D.R., King, J.C., Mcgeehin, J.P., Mangan, M., and Evans, W.C., 2014, Crustal migration of CO2 -rich magmatic fluids recorded by tree-ring radiocarbon and seismicity at Mammoth Mountain , CA , USA: Earth and Planetary Science Letters, v. 390, p. 52–58, doi:10.1016/j.epsl.2013.12.035.

Lin, J., Jach, M.E., and Ceulemans, R., 2001, Stomatal density and needle anatomy of Scots pine (*Pinus sylvestris*) are affected by elevated CO $_2$: New Phytologist, v. 150, p. 665–674, doi:10.1046/j.1469-8137.2001.00124.x.

Liu, E.J. et al., 2020, Aerial strategies advance volcanic gas measurements at inaccessible, strongly degassing volcanoes: Science Advances, v. 6, p. eabb9103, doi:10.1126/sciadv.abb9103.

Liu, E.J., Wood, K., Mason, E., Edmonds, M., Aiuppa, A., Giudice, G., Bitetto, M., and Francofonte, V., 2018, Dynamics of Outgassing and Plume Transport Revealed by

Proximal Unmanned Aerial System (UAS) Measurements at Volcán Villarrica , Chile Geochemistry , Geophysics , Geosystems: , p. 730–750, doi:10.1029/2018GC007692.

Lucic, G., Stix, J., Sherwood Lollar, B., Lacrampe-Couloume, G., Muñoz, A., and Carcache, M.I., 2014, The degassing character of a young volcanic center: Cerro Negro, Nicaragua: Bulletin of Volcanology, v. 76, p. 1–23, doi:10.1007/s00445-014-0850-6.

Mandon, C.L., Christenson, B.W., Schipper, C.I., Seward, T.M., and Garaebiti, E., 2018, Metal transport in volcanic plumes : A case study at White Island and Yasur volcanoes: Journal of Volcanology and Geothermal Research, v. 369, p. 155–171, doi:10.1016/j.jvolgeores.2018.11.024.

Mason, E. et al., 2021, Volatile metal emissions from volcanic degassing and lava–seawater interactions at Kīlauea Volcano, Hawai'i: Communications Earth & Environment, v. 2, p. 79, doi:10.1038/s43247-021-00145-3.

Mattey, D.P., Exley, R.A., and Pillinger, C.T., 1989, Isotopic composition of CO2 and dissolved carbon species in basalt glass: Geochimica et Cosmochimica Acta, v. 53, p. 2377–2386, doi:10.1016/0016-7037(89)90359-1.

McCarroll, D., and Loader, N.J., 2004, Stable isotopes in tree rings: Quaternary Science Reviews, v. 23, p. 771–801, doi:10.1016/j.quascirev.2003.06.017.

McCormick Kilbride, B. et al., 2023, Temporal Variability in Gas Emissions at Bagana Volcano Revealed by Aerial , Ground , and Satellite Observations: Geochemistry, Geophysics, Geosystems, v. 24, p. 1–24, doi:10.1029/2022GC010786.

de Moor, J.M. et al., 2016, Turmoil at Turrialba Volcano (Costa Rica): Degassing and eruptive processes inferred from high-frequency gas monitoring: Journal of Geophysical Research: Solid Earth, v. 121, p. 5761–5775, doi:10.1002/2016JB013150.

Moune, S. et al., 2022, Gas Monitoring of Volcanic-Hydrothermal Plumes in a Tropical Environment: The Case of La Soufrière de Guadeloupe Unrest Volcano (Lesser Antilles): Frontiers in Earth Science, v. 10, p. 795760, doi:10.3389/feart.2022.795760.

Munksgaard, N.C., Lee, I., Napier, T., Zwart, C., Cernusak, L.A., and Bird, M.I., 2023, One year of spectroscopic high-frequency measurements of atmospheric CO_2, CH_4, H_2O and $\Delta^{13}C\text{-}CO_2$ at an Australian Savanna site: Geoscience Data Journal, v. 10, p. 461–470, doi:10.1002/gdj3.180.

Pataki, D.E., Ehleringer, J.R., Flanagan, L.B., Yakir, D., Bowling, D.R., Still, C.J., Buchmann, N., Kaplan, J.O., and Berry, J.A., 2003, The application and interpretation of Keeling plots in terrestrial carbon cycle research: Global Biogeochemical Cycles, v. 17, p. 2001GB001850, doi:10.1029/2001GB001850.

Pearson, C.L., Dale, D.S., Brewer, P.W., Kuniholm, P.I., Lipton, J., and Manning, S.W., 2009, Dendrochemical analysis of a tree-ring growth anomaly associated with the Late Bronze Age eruption of Thera: Journal of Archaeological Science, v. 36, p. 1206–1214, doi:10.1016/j.jas.2009.01.009.

Pearson, C., Manning, S.W., Coleman, M., and Jarvis, K., 2005, Can tree-ring chemistry reveal absolute dates for past volcanic eruptions? Journal of Archaeological Science, v. 32, p. 1265–1274, doi:10.1016/j.jas.2005.03.007.

Perez Catán, S., Bubach, D., Messuti, M.I., Arribére, M.A., and Ribeiro Guevara, S., 2020, Mercury in a geothermal and volcanic area in Patagonia, southern South America: Atmospheric Pollution Research, v. 11, p. 566–573, doi:10.1016/j.apr.2019.12.005.

Poland, M., Elske de Zeeuw-van Dalfsen, Emma Nicholson, Koki Aizawa, and Kyle Anderson, 2025, Recent Advances in Volcano Monitoring, *in* Costanza Bonadonna, Luca Caricchi, Amanda Clarke, Paul Cole, Jan Lindsay, Jake Lowenstern, Richard Robertson, and Mylene Villegas eds., Encyclopedia of Volcanoes, Academic Press.

R Core Team, 2023, R: A Language and Environment for Statistical Computing.:, https://www.R-project.org/.

Rissanen, K., Hölttä, T., Bäck, J., Rigling, A., Wermelinger, B., and Gessler, A., 2021, Drought effects on carbon allocation to resin defences and on resin dynamics in old-grown Scots pine: Environmental and Experimental Botany, v. 185, p. 104410, doi:10.1016/j.envexpbot.2021.104410.

Rizzo, A.L., Jost, H.J., Caracausi, A., Paonita, A., Liotta, M., and Martelli, M., 2014, Real-time measurements of the concentration and isotope composition of atmospheric and volcanic CO2 at Mount Etna (Italy): Geophysical Research Letters, v. 41, p. 2382–2389, doi:10.1002/2014GL059722.Received.

Rodríguez Martín, J.A., Nanos, N., Miranda, J.C., Carbonell, G., and Gil, L., 2013, Volcanic mercury in Pinus canariensis: Naturwissenschaften, v. 100, p. 739–747, doi:10.1007/s00114-013-1070-1.

Salas-Navarro, J., Stix, J., and De Moor, J.M., 2022, A new Multi-GAS system for continuous monitoring of CO2/ CH4 ratios at active volcanoes: Journal of Volcanology and Geothermal Research, v. 426, p. 107533, doi:10.1016/j.jvolgeores.2022.107533.

Saurer, M., Cherubini, P., Bonani, G., and Siegwolf, R., 2003, Tracing carbon uptake from a natural CO2 spring into tree rings: an isotope approach: Tree Physiology, v. 23, p. 997–1004, doi:10.1093/treephys/23.14.997.

Saurer, M., Sahlstedt, E., Rinne-Garmston, K.T., Lehmann, M.M., Oettli, M., Gessler, A., and Treydte, K., 2023, Progress in high-resolution isotope-ratio analysis of tree rings using laser ablation (D. Epron, Ed.): Tree Physiology, v. 43, p. 694–705, doi:10.1093/treephys/tpac141.

Saurer, M., Siegwolf, R.T.W., and Schweingruber, F.H., 2004, Carbon isotope discrimination indicates improving water-use efficiency of trees in northern Eurasia over the last 100 years: Global Change Biology, v. 10, p. 2109–2120, doi:10.1111/j.1365-2486.2004.00869.x.

Seiler, R., Hajdas, I., Saurer, M., Houlié, N., D'Arrigo, R., Kirchner, J.W., and Cherubini, P., 2021, Tree-ring stable isotopes and radiocarbon reveal pre- and post-eruption effects of volcanic processes on trees on Mt. Etna (Sicily, Italy): Ecohydrology, v. 14, p. e2340, doi:10.1002/eco.2340.

Sheppard, P.R., Ort, M.H., Anderson, K.C., Elson, M.D., Vázquez-selem, L., Clemens, A.W., Little, N.C., and Speakman, R.J., 2008, Multiple Dendrochronological Signals Indicate

the Eruption of ParíCutin Volcano, Michoacán, Mexico: Tree-Ring Research, v. 64, p. 97–108, doi:10.3959/2008-3.1.

Sheppard, P.R., Weaver, R., Pringle, P.T., and Kent, A.J.R., 2010, Dendrochemical Evidence of the 1781 Eruption of Mount Hood, Oregon, *in* Stoffel, M., Bollschweiler, M., Butler, D.R., and Luckman, B.H. eds., Tree Rings and Natural Hazards, Dordrecht, Springer Netherlands, Advances in Global Change Research, v. 41, p. 465–467, doi:10.1007/978-90-481-8736-2_43.

Shinohara, H., 2005, A new technique to estimate volcanic gas composition: plume measurements with a portable multi-sensor system: Journal of Volcanology and Geothermal Research, v. 143, p. 319–333, doi:10.1016/j.jvolgeores.2004.12.004.

Shinohara, H., 2008, EXCESS DEGASSING FROM VOLCANOES AND ITS ROLE ON ERUPTIVE AND INTRUSIVE ACTIVITY: , p. 1–31, doi:10.1029/2007RG000244.1.INTRODUCTION.

Shinohara, H., Aiuppa, A., Giudice, G., Gurrieri, S., and Liuzzo, M., 2008, Variation of H2O/CO2 and CO2/SO2 ratios of volcanic gases discharged by continuous degassing of Mount Etna volcano, Italy: Journal of Geophysical Research: Solid Earth, v. 113, p. 1–11, doi:10.1029/2007JB005185.

Sigurdsson, H., 2015, Introduction, *in* The Encyclopedia of Volcanoes, Elsevier, p. 1–12, doi:10.1016/B978-0-12-385938-9.02001-0.

Skomarkova, M.V., Vaganov, E.A., Mund, M., Knohl, A., Linke, P., Boerner, A., and Schulze, E.-D., 2006, Inter-annual and seasonal variability of radial growth, wood density and

carbon isotope ratios in tree rings of beech (Fagus sylvatica) growing in Germany and Italy: Trees, v. 20, p. 571–586, doi:10.1007/s00468-006-0072-4.

Soper, F.M., McCalley, C.K., Sparks, K., and Sparks, J.P., 2017, Soil carbon dioxide emissions from the Mojave desert: Isotopic evidence for a carbonate source: Geophysical Research Letters, v. 44, p. 245–251, doi:10.1002/2016GL071198.

Stix, J., D'Arcy, F., and Salas-Navarro, J., 2024, Volcano gas monitoring, *in* Anbar, A. and Weis, D. eds., Treatise of Geochemistry, Elsevier Science.

Stix, J., De Moor, J.M., Rüdiger, J., Alan, A., Corrales, E., D'Arcy, F., Diaz, J.A., and Liotta, M., 2018, Using Drones and Miniaturized Instrumentation to Study Degassing at Turrialba and Masaya Volcanoes , Central America: Journal of Geophysical Research: Solid Earth, p. 1–20, doi:10.1029/2018JB015655.

Teran-Hinojosa, E., Sobral, H., Hernández-Mendoza, I., Márquez-Herrera, C., and González-Hernández, G., 2019, Laser-induced breakdown spectroscopy characterization of tree rings from the Popocatépetl volcano area, Mexico: Spectrochimica Acta Part B: Atomic Spectroscopy, v. 161, p. 105713, doi:10.1016/j.sab.2019.105713.

Tortini, R., van Manen, S.M., Parkes, B.R.B., and Carn, S.A., 2017, The impact of persistent volcanic degassing on vegetation: A case study at Turrialba volcano, Costa Rica: International Journal of Applied Earth Observation and Geoinformation, v. 59, p. 92–103, doi:10.1016/j.jag.2017.03.002.

Treydte, K.S., Frank, D.C., Saurer, M., Helle, G., Schleser, G.H., and Esper, J., 2009, Impact of climate and CO2 on a millennium-long tree-ring carbon isotope record: Geochimica et Cosmochimica Acta, v. 73, p. 4635–4647, doi:10.1016/j.gca.2009.05.057.

Troll, V.R., Hilton, D.R., Jolis, E.M., Chadwick, J.P., Blythe, L.S., Deegan, F.M., Schwarzkopf, L.M., and Zimmer, M., 2012, Crustal CO2 liberation during the 2006 eruption and earthquake events at Merapi volcano , Indonesia: Geophysical Research Letters, v. 39, p. 1–6, doi:10.1029/2012GL051307.

Urey, H.C., Lowenstam, H.A., Epstein, S., and McKinney, C.R., 1951, Measurement of paleotemperatures and temperatures of the upper cretaceous of england, denmark, and the southeastern united states: Bulletin of the Geological Society of America, v. 62, p. 399–416.

Van Gardingen, P.R., Grace, J., Harkness, D.D., Miglietta, F., and Raschi, A., 1995, Carbon dioxide emissions at an Italian mineral spring: measurements of average CO2 concentration and air temperature: Agricultural and Forest Meteorology, v. 73, p. 17–27, doi:10.1016/0168-1923(94)02176-K.

Vásquez, M., Lara, W., Del Valle, J.I., and Sierra, C.A., 2022, Reconstructing past fossil-fuel CO_2 concentrations using tree rings and radiocarbon in the urban area of Medellín, Colombia: Environmental Research Letters, v. 17, p. 055008, doi:10.1088/1748-9326/ac63d4.

Venturi, S., Tassi, F., Bicocchi, G., Cabassi, J., Capecchiacci, F., Capasso, G., Vaselli, O., Ricci, A., and Grassa, F., 2017, Fractionation processes affecting the stable carbon isotope

signature of thermal waters from hydrothermal / volcanic systems : The examples of Campi Flegrei and Vulcano Island (southern Italy): Journal of Volcanology and Geothermal Research, v. 345, p. 46–57, doi:10.1016/j.jvolgeores.2017.08.001.

Wagner, R.J., Kaye, M.W., Abrams, M.D., Hanson, P.J., and Martin, M., 2012, Tree-Ring Growth and Wood Chemistry Response to Manipulated Precipitation Variation for Two Temperate Quercus Species: Tree-Ring Research, v. 68, p. 17–29, doi:10.3959/2010-6.1.

Watmough, S.A., 1997, An evaluation of the use of dendrochemical analyses in environmental monitoring: Environmental Reviews, v. 5, p. 181–201, doi:10.1139/er-5-3-4-181.

Watt, S.F.L., Pyle, D.M., Mather, T.A., Day, J.A., and Aiuppa, A., 2007, The use of tree-rings and foliage as an archive of volcanogenic cation deposition: Environmental Pollution, v. 148, p. 48–61, doi:10.1016/j.envpol.2006.11.007.

Weigt, R.B., Bräunlich, S., Zimmermann, L., Saurer, M., Grams, T.E.E., Dietrich, H.-P., Siegwolf, R.T.W., and Nikolova, P.S., 2015, Comparison of δ18O and δ13C values between tree-ring whole wood and cellulose in five species growing under two different site conditions: Rapid Communications in Mass Spectrometry, v. 29, p. 2233–2244, doi:10.1002/rcm.7388.

Werner, C. et al., 2019, Carbon Dioxide Emissions from Subaerial Volcanic Regions: Two Decades in Review, *in* Orcutt, B., Daniel, I., and Dasgupta, R. eds., Deep Carbon: Past to Present, Cambridge, Cambridge University Press, p. 188–236, doi:10.1017/9781108677950.

Wilson, L., and Head, J.W., 1981, Ascent and Eruption of Basaltic Magma on the Earth and Moon: Journal of Geophysical Research, v. 86, p. 2971–3001.

Appendix A: Supplementary data for chapter 1

Figure A1: Calibration of actual versus measured stable carbon isotopic ratios with three in-house standards, April 2019

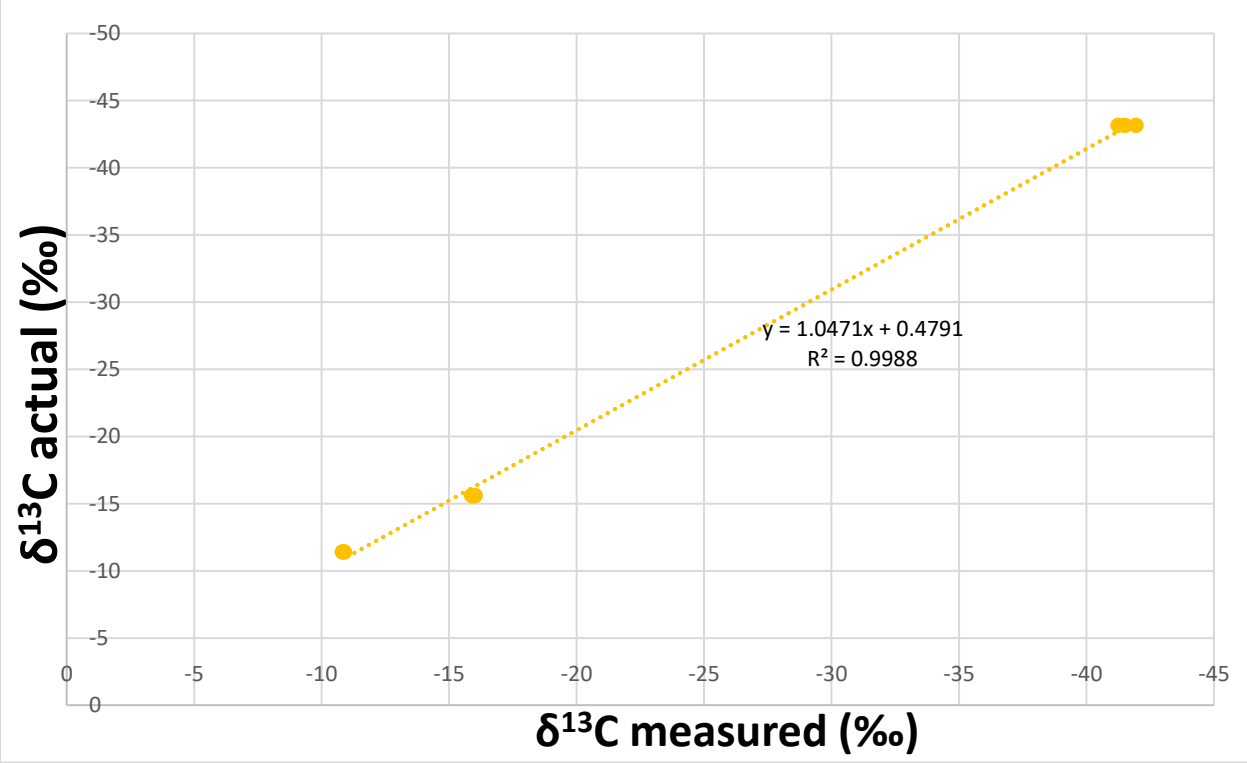

Table A1: All April-May 2019 raw data as measured with the Picarro G2202-i mass analyzer

Analysis date	Site	Analysis	Start_time	End_time	CO2ppm	d13c	d13c_stdev	Undiluted_CO2 ppm	Accepted Value	1/CO2	d13c corrected
25/4/2019		**OVSI-5G**	**14:57**	**15:04**	**750.6**	**-9.96**	**0.61**		**-9.37**		**-9.95**
25/4/2019		Flight #1-1			466.9	-9.96	0.93			0.0021418	-9.95
25/4/2019		Flight #1-2			459.4	-9.95	0.83			0.0021768	-9.94
25/4/2019		Flight #1-3			491.2	-10.44	0.8			0.0020358	-10.45
25/4/2019		**OVSI-4G**	**15:57**	**16:02**	**713.4**	**-4.07**	**0.57**		**-3.6**		**-3.78**
25/4/2019		Flight #1-4			489.1	-10.87	0.78			0.0020446	-10.90
25/4/2019		Flight #2-1			424.1	-10.42	0.91			0.0023579	-10.43
25/4/2019		Flight #2-2			425.9	-10.73	1.03			0.002348	-10.76
25/4/2019		Flight #2-3			426.2	-10.39	0.85			0.0023463	-10.40
25/4/2019		Flight #2-4			407.7	-10.08	0.96			0.0024528	-10.08
25/4/2019		**OVSI-4G**	**17:00**	**17:04**	**628.1**	**-3.97**	**0.59**		**-3.6**		**-3.68**
25/4/2019		Flight #3-1			450.4	-10.79	0.83			0.0022202	-10.82
25/4/2019		Flight #3-2			436.2	-9.74	0.83			0.0022925	-9.72
25/4/2019		Flight #3-3			437.2	-9.77	0.86			0.0022873	-9.75
25/4/2019		Flight #3-4			455.6	-10.92	0.81			0.0021949	-10.96
25/4/2019		Flight #4-1			442.1	-11.38	1.02			0.0022619	-11.44
25/4/2019		Flight #4-2			417	-10.02	0.82			0.0023981	-10.01
25/4/2019		Flight #4-3			423.7	-10.42	0.78			0.0023602	-10.43
25/4/2019		Flight #4-4			422.5	-10.69	0.91			0.0023669	-10.71
25/4/2019		**OVSI-4G**	**18:37**	**18:41**	**851.6**	**-3.66**	**0.52**		**-3.6**		**-3.35**
26/4/2019		**OVSI-4G**	**14:22**	**14:27**	**910.5**	**-3.86**	**0.45**		**-3.6**		**-3.56**
26/4/2019	Boca A	1	14:34	14:40	963.5	-6.55	0.53			0.0010379	-6.38
26/4/2019	Boca A	2	14:46	14:50	1070	-6.07	0.38			0.0009346	-5.88

26/4/2019	Boca A	3	14:58	15:02	1044	-6.24	0.47			0.0009579	-6.05
26/4/2019	Boca A	4	15:07	15:11	973.8	-6.39	0.44			0.0010269	-6.21
26/4/2019	Boca A	5	15:17	15:20	1303	-5.5	0.48			0.0007675	-5.28
26/4/2019		**Std 3**	**15:32**	**15:38**	**730.2**	**-10.79**	**0.58**		**-11.4**		**-10.82**
26/4/2019	Boca A	6	15:47	15:50	1036	-6.71	0.39			0.0009653	-6.55
26/4/2019	Monitoring fumarole	7	15:58	16:04	571.3	-11.85	0.67				-11.93
26/4/2019		**Std 3**	**16:31**	**16:36**	**797.7**	**-10.76**	**0.54**		**-11.4**		**-10.79**
26/4/2019	Monitoring fumarole	8 (20 mils)	17:00	17:04	1300	-3.91	0.37	52000		1.923E-05	-3.62
26/4/2019	Monitoring fumarole	9 (20 mils)	17:25	17:28	1198	-4.35	0.35	47920		2.087E-05	-4.08
26/4/2019	Monitoring fumarole	8 (780 mils air, 20 mils gas)	17:48	17:52	1492	-4.07	0.4	59680		1.676E-05	-3.78
26/4/2019	Monitoring fumarole	9 (780 mils air, 20 mils gas)	17:58	18:02	1274	-4.49	0.37	50960		1.962E-05	-4.22
26/4/2019		**Std 3**	**18:11**	**18:15**	**794.7**	**-11.08**	**0.45**		**-11.4**		**-11.12**
30/4/2019		**OVSI-5G**	**16:16**	**16:22**	**1412**	**-10.31**	**0.41**		**-9.37**		**-10.32**
30/4/2019		**OVSI-5G**	**16:28**	**16:34**	**866.6**	**-10.51**	**0.43**		**-9.37**		**-10.53**
30/4/2019	Fumarole field	Flight #1-1	16:41	16:47	521.9	-8.19	0.78			0.0019161	-8.10
30/4/2019	Fumarole field	Flight #1-2	16:55	16:01	476.6	-8.43	0.78			0.0020982	-8.35
30/4/2019	Fumarole field	Flight #1-3	17:06	17:12	483.9	-8.61	0.76			0.0020665	-8.54
30/4/2019	Fumarole field	Flight #1-4	17:18	17:24	504	-8.67	0.73			0.0019841	-8.60

30/4/2019	Fumarole field	Flight #1-5	17:39	17:45	527.6	-8.42	0.61			0.0018954	-8.34
30/4/2019	Fumarole field	Flight #1-6	17:49	17:53	495.6	-9.1	0.84			0.0020178	-9.05
30/4/2019	Fumarole field	Flight #1-7	17:58	18:00:30	505.3	-8.79	0.79			0.001979	-8.72
30/4/2019	Background	Flight #1-8	18:03	18:08	408	-9.8	0.92			0.002451	-9.78
30/4/2019	Background	Flight #1-9	18:15	18:20	406	-9.64	0.91			0.0024631	-9.61
30/4/2019	Background	Flight #1-10	18:28	18:34	406.6	-9.51	0.98			0.0024594	-9.48
30/4/2019	Taken at ground level	Background 1	18:38	18:44	409.3	-10.35	0.95			0.0024432	-10.36
30/4/2019	Taken at ground level	Background 2	18:48	18:54	411.2	-9.95	0.85			0.0024319	-9.94
30/4/2019		**OVSI-5G**	**19:04**	**19:08**	**523**	**-10.89**	**0.72**		**-9.37**		**-10.92**
30/4/2019		**OVSI-5G**			**616**	**-10.73**	**0.68**		**-9.37**		**-10.76**
1/5/2019		**OVSI-5G**	**7:20**	**7:25**	**553.7**	**-10.34**	**0.67**		**-9.37**		**-10.35**
1/5/2019	Bubbling spring	Vial 1	7:31	7:36	666.5	-4.33	0.6	533200		1.875E-06	-4.05
1/5/2019	Bubbling spring	Vial 2	7:48	7:54	1140	-4.13	0.44	912000		1.096E-06	-3.85
1/5/2019	Bubbling spring	Vial 3	8:00	8:06	704.8	-4.39	0.66	563840		1.774E-06	-4.12
1/5/2019	Bubbling spring	Vial 4	8:12	8:18	919.5	-4.33	0.51	735600		1.359E-06	-4.05
1/5/2019	Bubbling spring	Vial 5	8:22	8:28	873.7	-4.4	0.49	698960		1.431E-06	-4.13
1/5/2019	Diffuse degassing	Vial 6	8:32	8:38	755.9	-4.44	0.61	604720		1.654E-06	-4.17
1/5/2019	Diffuse degassing	Vial 7	8:42	8:48	1078	-4.34	0.39	862400		1.16E-06	-4.07
1/5/2019	Diffuse degassing	Vial 8	8:54	9:00	728.9	-4.45	0.65	583120		1.715E-06	-4.18
1/5/2019	Diffuse degassing	Vial 9	9:06	9:12	902.2	-4.47	0.5	721760		1.386E-06	-4.20
1/5/2019	Diffuse degassing	Vial 10	9:20	9:26	1052	-4.67	0.45	841600		1.188E-06	-4.41
1/5/2019		**OVSI-5G**	**9:32**	**9:38**	**464.4**	**-11.07**	**0.94**		**-9.37**		**-11.11**

1/5/2019	Mound between fumarole field and Boca B	Bag 9					0.39				
1/5/2019	Mound between fumarole field and Boca B	Bag 10	10:02	10:08	522.5	-9.45	0.67			0.0019139	-9.42
1/5/2019	Mound between fumarole field and Boca B	Bag 11	10:12	10:18	492.9	-9.91	0.86			0.0020288	-9.90
1/5/2019	Mound between fumarole field and Boca B	Bag 12	10:24	10:30	471.4	-9.97	0.84			0.0021213	-9.96
1/5/2019	Top of huge rock	Bag 5	10:34	10:40	624.5	-10.37	0.69			0.0016013	-10.38
1/5/2019	Top of huge rock	Bag 6	10:46	10:52	814.4	-6.02	0.44			0.0012279	-5.82
1/5/2019	Top of huge rock	Bag 7	10:57	11:03	589.5	-9.69	0.82			0.0016964	-9.67
1/5/2019	Top of huge rock	Bag 8	11:10	11:16	1308	-3.17	0.42			0.0007645	-2.84
1/5/2019	Top of first rock	Bag 1	11:22	11:29	1531	-4.96	0.33			0.0006532	-4.71
1/5/2019	Top of first rock	Bag 2	15:32	15:40	1117	-6.52	0.37			0.0008953	-6.35
1/5/2019		**OVSI-5G**	**15:45**	**15:50**	**1001**	**-10.8**	**0.45**	**-9.37**			**-10.83**
1/5/2019	Top of first rock	Bag 3									0.48

1/5/2019	Top of first rock	Bag 4	16:40	16:43	4206	-3.67	0.26			0.0002378	-3.36
1/5/2019	Top of first rock	Bag 4	16:50	16:56	2643	-3.54	0.28	5286		0.0001892	-3.23
1/5/2019	Boca B	Bag 13	17:08	17:12	1523	-5.94	0.29			0.0006566	-5.74
1/5/2019	Boca B	Bag 14	17:20	17:24	988.5	-7.36	0.36			0.0010116	-7.23
1/5/2019	Boca B	Bag 15	17:32	17:37	817.3	-8.11	0.38			0.0012235	-8.01
1/5/2019		**OVSI-5G**	**17:41**	**17:47**	**1039**	**-10.9**	**0.35**		**-9.37**		**-10.93**

Table A2: Stable carbon isotopic data from this and previous works

Volcano	Date	Sample site	Source	d13C	Sample code
Poás	Feb-99	Parete Sur (south wall)	Vaselli et al.2019	-6.56	
Poás	Feb-00	Dome	Vaselli et al.2019	-6.13	
Poás	Feb-01	Fumarole Este	Vaselli et al.2019	-4.29	
Poás	Apr-04	Fumarole NE	Vaselli et al.2019	-3.06	
Poás	Feb-01	La Nina	Vaselli et al.2019	-2.57	
Poás	Nov-01	La Nina	Vaselli et al.2019	-3.54	
Poás	Apr-02	La Nina	Vaselli et al.2019	-3.12	
Poás	Nov-01	Fumarole Norte	Vaselli et al.2019	-2.90	
Poás	Nov-01	Fumarole Norte	Vaselli et al.2019	-3.70	
Poás	May-02	Fumarole Norte	Vaselli et al.2019	-2.90	
Poás	Apr-03	Fumarole Norte	Vaselli et al.2019	-2.71	
Poás	Jan-01	Official fumarole	Fischer et al. 2015	-5.6	P1
Poás	Jan-01	Official fumarole	Fischer et al. 2015		P2
Poás	Jan-01	Official fumarole	Fischer et al. 2015		P3
Poás	Mar-01	Official fumarole	Fischer et al. 2015		P4
Poás	Mar-01	Official fumarole	Fischer et al. 2015	-6.8	P5
Poás	Mar-01	Official fumarole	Fischer et al. 2015		P6
Poás	Jul-01	Official fumarole	Fischer et al. 2015	-5.8	P7
Poás	Jul-01	Official fumarole	Fischer et al. 2015		P8
Poás	Mar-03	Official fumarole	Fischer et al. 2015	-3.5	PO 03-1

Poás	Mar-03	Official fumarole	Fischer et al. 2015	-3.5	PO 03-2
Poás	Mar-05	Official fumarole	Fischer et al. 2015	-1.3	PO 05-1
Poás	Feb-06	Official fumarole	Fischer et al. 2015	-2.4	Pt 06-1-1
Poás	May-06	Official fumarole	Fischer et al. 2015	-2.2	Pt 06-1-3
Poás	Feb-07	Official fumarole	Fischer et al. 2015	-4.9	P007-1a
Poás	Feb-06	Naranja fumarole	Fischer et al. 2015	-1.8	Pnar-06a
Poás	Feb-07	Naranja fumarole	Fischer et al. 2015	-4.2	P007-3a
Poás	Mar-08	Naranja fumarole	Fischer et al. 2015	-3.8	ICE-2
Poás	Jun-08	Naranja fumarole	Fischer et al. 2015	-2.8	TF10
Poás	Feb-17	Poás Dome Free	UNA57	-4.35	-
Poás	Feb-17	Poás Lake Bubbles	UNA38	-4.00	PL170224
Poás	Feb-17	Poás Dome	UNA37	-4.20	PO170224
Poás	Apr-17	Poás Dome	UNA32	-6.17	UNM?
Poás	Nov-17	Sulfur chimney fumarole	UNA55	-4.49	PO171110-G2
Poás	Nov-17	Sulfur chimney fumarole	UNA60	-4.44	PO171110-G1
Poás	Jan-18	Bubbling pool, funnel	UNA6	-4.75	PO180123-BP1
Poás	Jan-18	Bubbling pool, funnel	UNA40	-4.68	PO180123-BP2
Poás	Jan-18	Sulfur chimney fumarole	UNA50	-4.70	PO180123-F2
Poás	Jan-18	Sulfur chimney fumarole	UNA56	-4.75	PO180123-F1
Poás	Aug-18	Bubbling pool, funnel	UNA80	-5.14	PO180821
Poás	Jan-19	Sulfur chimney fumarole	UNA67	-4.89	PO190102-G1
Poás	Jan-19	Sulfur chimney fumarole	UNA55	-3.73	PO190102-G2
Poás	Apr-19	Sulfur chimney fumarole	UNA80		PO190409-G1
Poás	Apr-19	Sulfur chimney fumarole	UNA73		PO190409-G2
Poás	Apr-19	Sulfur chimney fumarole	UNA76		PO190426-G1
Poás	Apr-19	Direct average of April 2019	This work	-4.05	
Poás	Apr-19	Bags, vials, Y intercept	This work	-3.64	
Poás	Apr-19	Drone bags, Y intercept	This work	-3.97	
Poás	Apr-19	Boca A	This work	-3.42	
Poás	Apr-19	Boca B	This work	-4.76	
Poás	Apr-19		This work	-3.62	
Poás	Apr-19		This work	-4.08	
Poás	Apr-19		This work	-3.78	
Poás	Apr-19		This work	-4.22	
Poás	Apr-19		This work	-4.05	

Poás	Apr-19	This work	-3.85
Poás	Apr-19	This work	-4.12
Poás	Apr-19	This work	-4.05
Poás	Apr-19	This work	-4.13
Poás	Apr-19	This work	-4.17
Poás	Apr-19	This work	-4.07
Poás	Apr-19	This work	-4.18
Poás	Apr-19	This work	-4.20
Poás	Apr-19	This work	-4.41
Poás			
Poás	Average, April 2019: direct, Boca A, Boca B:	This work	-4.08

Table A3: Statistical results of stable carbon isotopic endmembers from UAS plume samples

Sample subset	$\delta^{13}CO_2$ endmember: intercept of least squares regression (± 95% confidence interval)	Coefficient of determination on least squares regression	$\delta^{13}CO_2$ endmember: Weighted mean (± weighted deviation)	Number of samples (n)
Proximal samples > 50 ppm CO_2 above background (n=7)	-3.97 ± 1.95 ‰	0.81	-2.99 ± 1.62 ‰	7
Proximal samples > 500 ppm CO_2 total (n=4)	-3.88 ± 1.55 ‰	0.93	-3.21 ± 0.86 ‰	4
Distal samples > 50 ppm CO_2 above background (n=4)	-14.6 ± 4.4 ‰	0.67	-13.42 ± 10.75 ‰	4

Appendix B: Supplementary information for chapter 2

Text S1 to S7

Figures S1 to S8

Dataset S1

Dataset S2

Text S1. Sampling techniques and methodology

2018 UAS and non-automated pump

This was the first attempt to capture volcanic gas samples, which was used at Stromboli in 2018. This first approach was a simple combination consisting of a 1.2 L/minute TD-3LS Brailsford® pump powered by a USB battery. The pump and battery were contained in a lightweight plastic container, with tygon tubing leading from the outlet to a 15 cm copper tube filled with copper filings to eliminate H_2S gas from being sampled, in order to reduce interference with subsequent carbon isotopic analysis as described in (Malowany et al., 2015). From the copper tube, short segments of tubing <20 cm were connected in series to two to ten 600 ml gas bags. This payload was placed into a mesh drawstring bag and suspended from a 2 metre long paracord, inspired by similar designs to capture volcanic crater water samples while keeping the UAS above the corrosive gases. This cord was attached with a carabiner to the lower frame of a TurboAce Matrix I quadcopter with a flight time of ~10 minutes. The pump was manually turned on with a switch just before take-off and turned off just after landing.

2019 UAS and CARGO 4.0

Building upon the challenges of the first test in 2018, we decided to build a new custom gas sampling system integrated with telemetry functions for the 2019 sampling campaign at Stromboli. The UAS was maneuvered with one remote controller by the pilot, while the gas sampling unit was controlled by a second person using a secondary remote controller to switch the pump on and off. The Compact Aerial Receiver-initiated Gas-sampling operation (CARGO 4.0) did not include copper tubes in order to limit excess weight for longer flight times. The other main difference is that the pump switch and SO_2 sensor were mapped to channels on a remote controller for the drone, allowing the pilot to use two-way telemetry to read the voltage of the SO_2 sensor and turn the pump on and off for sampling. The payload (700 grams) consisted of a pump (micropump®, model d3k, 2.5 L/minute) connected to an electronic switch (Turnigy 10A/30V) which utilized an empty standard port on the UAS receiver. An SO_2 sensor (Citicell 0-200 ppmv range) was included with a voltage sensor (Futaba SBS-01V) connected to the SBUS2 port of the receiver and one of the inlet tubes of the pump. A portable USB-powered charger supplied power to the pump while a 9 volt battery powered the SO_2 sensor.

The assembly was deployed with two different UAS over the course of the fieldwork; a DJI Matrice 100 on June 17-18 and a DJI Inspire on June 20. The DJI Matrice 100 (UAS #1, figure 1) had a flight time of ~20 minutes and a payload comprising the gas sampling configuration attached on top of the UAS body which was secured with bungee cords, while two to four gas sample bags were attached directly below the drone. The DJI Inspire 1 (UAS #2, figure 1) had a flight time of ~10 minutes with the payload comprising the CARGO 4.0 as a separate unit suspended 1.5 metres below the UAS in a mesh bag.

Fractionation test of the CARGO 4.0

While the first sampling technique in 2018 involved a simple tubing and pump system, the multicomponent assemblies used in 2019 required that the gas pass through an SO_2 sensor before being drawn through the pump and into sample bags (Figure 1c and 1d). We performed a simple test to evaluate possible fractionation from gas flowing through the SO_2 sensor in the 2019 CARGO. We analyzed a gas standard (-15.6 ‰ $\delta^{13}CO_2$) before passing it through the 2019 sampling assembly and collecting the gas for subsequent measurement (supplementary material). The measured value of the standard ranged from -15.77 ± 0.44 ‰ to -15.82 ± 0.38 ‰ $\delta^{13}CO_2$ before passing through the system and from -15.66 ± 0.35 ‰ to -15.83 ± 0.43 ‰ $\delta^{13}CO_2$ after passing through the SO_2 sensor and pump. This is a difference of 0.04 ‰ between the medians of the two sets of samples, indicating that isotopic fractionation due to passage through the SO_2 sensor is negligible or non-existent, as has been shown in other similar systems (Schipper et al., 2017)

Ground-based plume sampling

Ambient plume samples were taken from the crater rim by placing the inlet tube on top of a hiking stick 1 metre above the ground and connected to a mulltiGAS sensor with continuous pumping. When the multiGAS indicated high SO_2 readings, a 600ml sample bag was connected to the outlet tube and filled.

Text S2. Isotopic analysis

The gold standard for $\delta^{13}C$ analysis is Isotope Ratio Mass Spectrometry (IRMS); however, these instruments must be kept in a stable lab environment due to their sensitivity. Rizzo et al. (2014) demonstrated that $\delta^{13}C$ studies of volcanic plumes with laser-based isotope ratio infrared spectrometers (IRIS) are feasible for harsh environments and provide comparable isotopic results to those measured by IRMS. Similarly, Malowany et al. (2017) demonstrated that a Cavity Ring-

Down Spectrometer (CRDS) could be used for near real-time ^{13}C analysis of volcanic plumes. In our study, we used both an IRIS (Delta Ray from Thermo Scientific) and a CRDS (G2201-i from Picarro). We analyzed a subset of samples on each instrument by connecting sample bags to the Picarro instrument until a stable $\delta^{13}C$ signal was achieved, then detaching the bag and immediately measuring the same bag on the Delta Ray instrument. A series of standard gases was used to calibrate the Picarro instrument in 2018, and both the Picarro and Delta Ray in 2019. In 2018, the two instruments were in good agreement, with standard deviations between the same sample bag measured on each instrument never exceeding 0.4 ‰. In 2019, the standard deviations of individual measurements between the two instruments did not exceed 0.7‰, with a maximum difference of 1 ‰ between analysis of the same sample on each instrument.

All samples were analyzed within 12 hours on a Picarro G2201-i CRDS and a Thermo Scientific Delta Ray IRIS at the field station. A copper tube filled with fine copper wire cuttings was used to remove any interference from H_2S, and three in-house standards (-43.15‰, -15.6‰, and -11.4‰) were used to define a calibration curve (supplemental info). A standard was run every 5 to 12 samples at concentrations ranging from 450 to 1050 ppmv CO_2 to monitor instrumental drift. Stable carbon isotopes were calculated using delta notation, where:

$$\delta^{13}C\ (‰) = \left(\frac{\left({}^{13}C/_{12}C\right)_{sample}}{\left({}^{13}C/_{12}C\right)_{standard}} - 1 \right) \cdot 1000 \qquad [1]$$

Carbon isotopic results are reported using the per mil notation which provides values relative to the Vienna Pee Dee Belemnite (VPDB) reference standard. Repeat analysis of 8 standards shows that uncertainties are ~0.3 ‰.

Our data is unique in that we were able to perform the usual calibrations with standards brought into the field in overpressured Wheaton gas bottles, as well as compare our isotopic results across the two portable instruments (Picarro and Delta Ray) in the field. In the following section we explain how we corrected the data.

Text S3. Standards for calibration of isotopic data

The 2018 Picarro data were calibrated with 18 individual standard measurements (Figure S1). The standards were measured at the beginning of the field campaign on May 12, as well as each day before and after samples were analyzed. The standards used were -15.6 per mil, -43.15 per mil, and -11.4 per mil. The Delta Ray analyses were corrected internally by the system which uses an intake of two reference gases from gas cylinders. The difference between the corrected Picarro and Delta Ray data was less than 0.5 per mil with a standard deviation of 0.16 per mil.

The 2019 data, being a larger dataset than that of 2018 as well as having standards analyzed on both the Picarro and Delta Ray instruments, underwent an extensive calibration (Figure S2). The Picarro data were calibrated with 15 individual standard measurements. The standards were measured at the beginning of the field campaign on June 17 as well as each day before and after samples were analyzed. In addition to an internal calibration, the Delta Ray underwent a

calibration with 6 standards. For both Delta Ray and Picarro, the standards used were -15.6 per mil and -43.15 per mil, while the Picarro also used three additional standards for manual calibration of -11.4 per mil, -3.88 per mil, -39.98 per mil, and -0.63 per mil. The difference between the corrected Picarro and Delta ray values was less than 1.0 per mil with a standard deviation of 0.35 per mil.

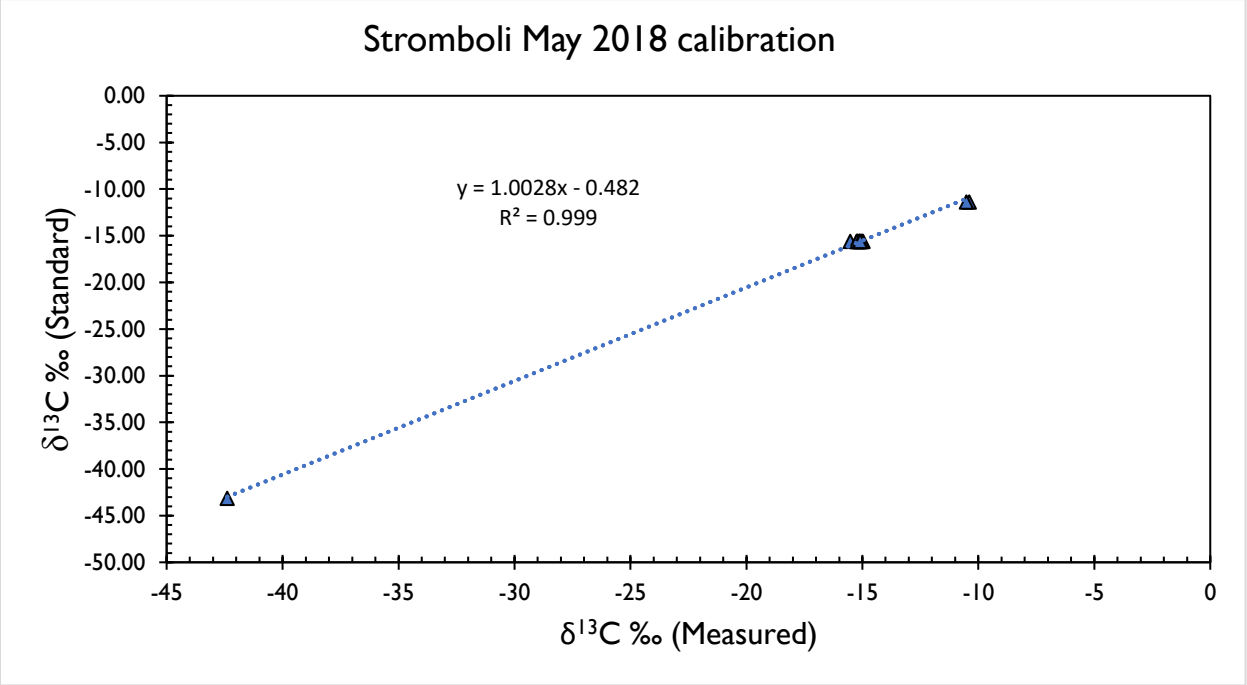

Figure S1. Calibration of 2018 standards measured on the Picarro instrument versus known standard values. The line of best fit is used to correct all Picarro data from the 2018 field campaign. The correction brought the carbon isotopic value 0.75 per mil lighter, on average.

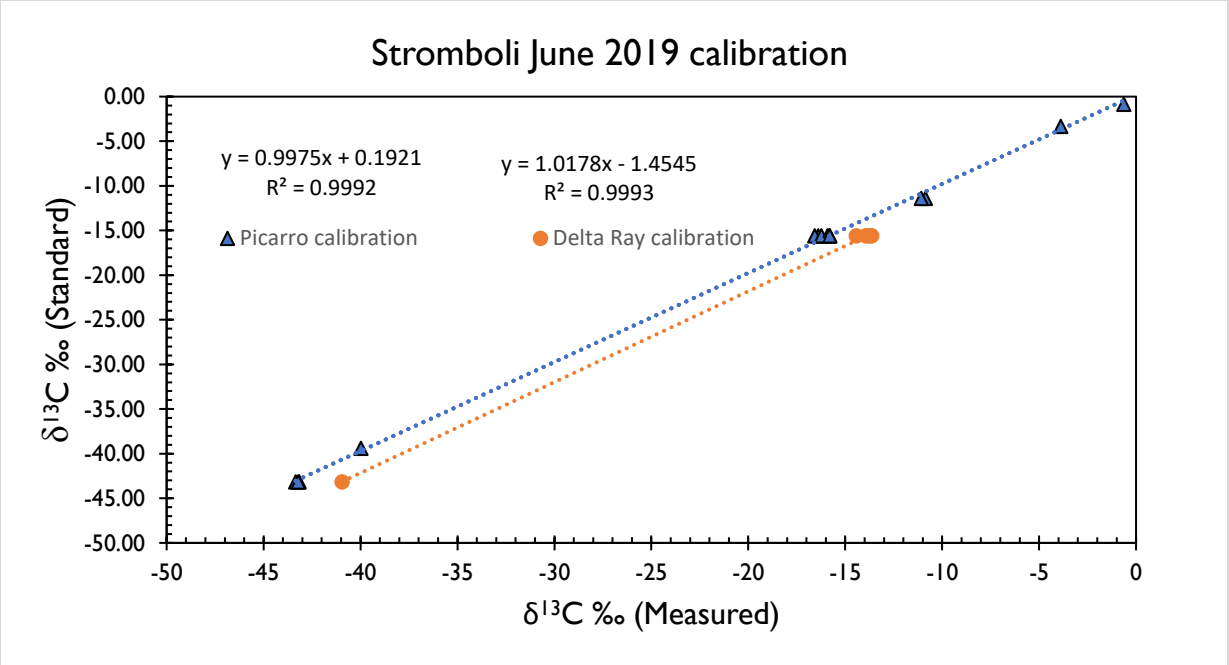

Figure S2: Calibration of 2019 standards measured on the Picarro and Delta Ray instruments versus known standard values. The orange line of best fit is used to correct all Delta Ray data and the blue line of best fit is used to correct all Picarro data from the 2018 field campaign. The correction brought the carbon isotopic value 0.2 per mil heavier for Picarro and 1.6 per mil lighter for Delta Ray, on average.

Text S4. Calibration for concentration

We also performed a test to determine if a correction for the CO_2 concentration between the two instruments was necessary. After plotting concentration for matching analyses from both instruments against each other (Figures S3, S4), we applied a correction to the Picarro dataset based on the Delta Ray concentrations. While the 2018 concentrations of equivalent samples on each instrument was a 20ppm difference on average, the correction brought the difference down to less than 4ppm. However, as we had a smaller subset of samples on the Delta Ray, this led to a coefficient of regression less than 0.5. The 2019 concentrations of equivalent samples on each instrument was a 13ppm difference on average, and the correction brought the difference down to 1ppm. Finally, when the Picarro values which were corrected for concentration were plotted

together with the Delta Ray data, each dataset deviated from the other in that the intercepts were different by 4 per mil or more (Figure S5). Since we could not ascertain which instrument has more accurate concentrations, we decided to omit the correction for concentration to avoid over-processing the data. In future work, we would perform a calibration with standards of known concentration in the same way that the isotopic values were calibrated.

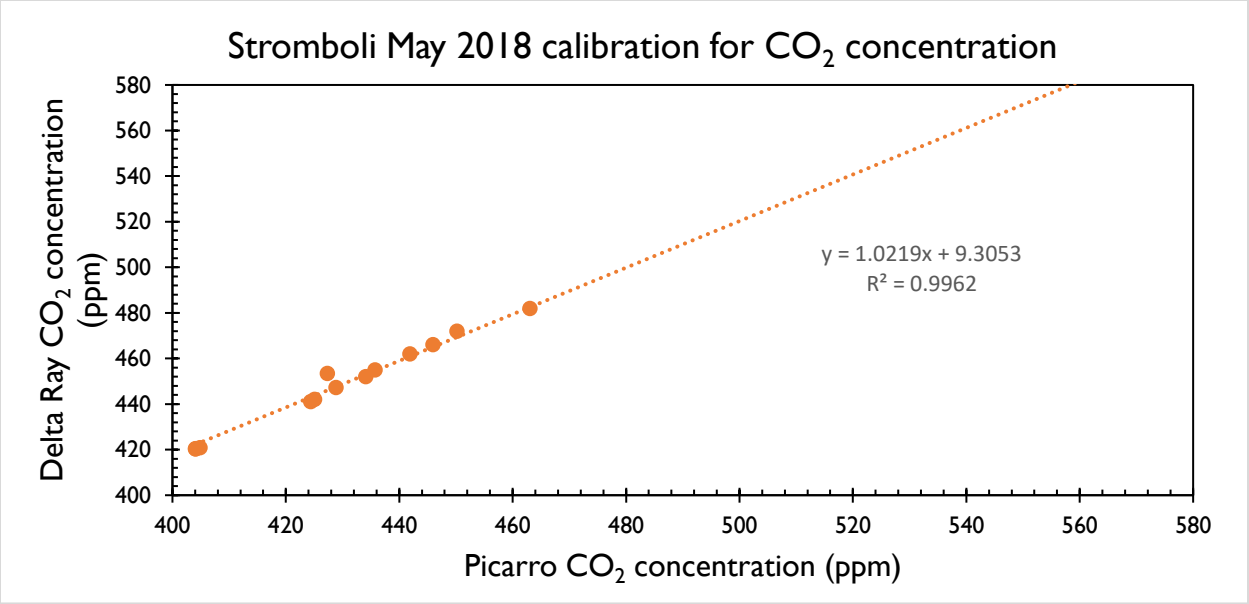

Figure S3: The Picarro versus Delta Ray concentration data for the 2018 field campaign.

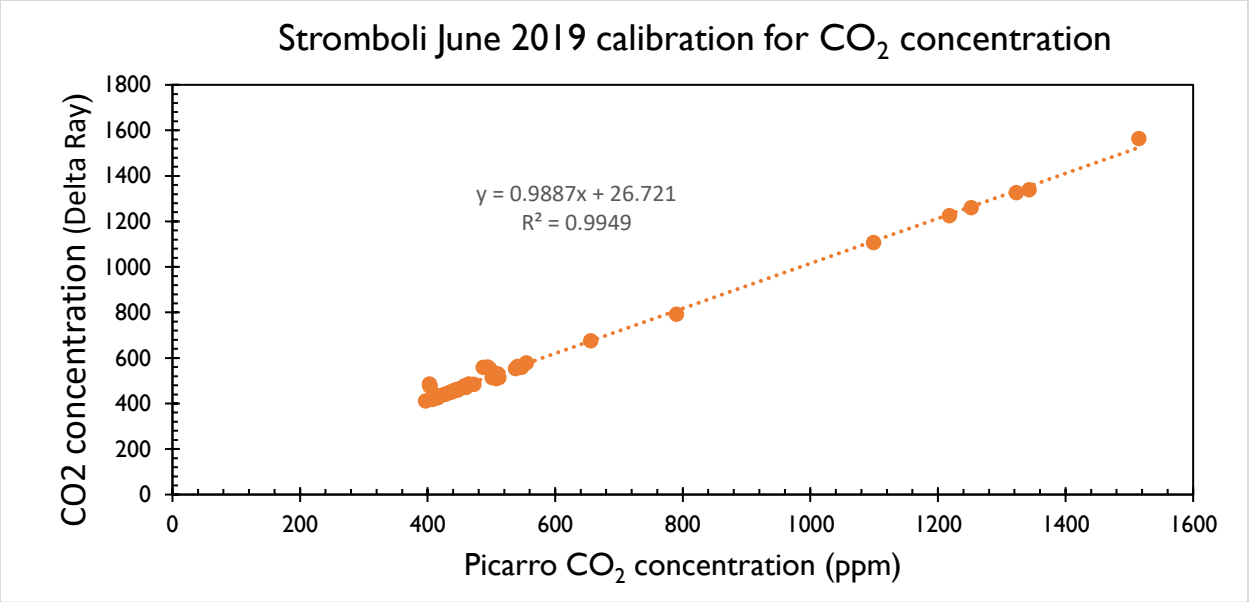

Figure S4: The Picarro versus Delta Ray concentration data for the 2019 field campaign.

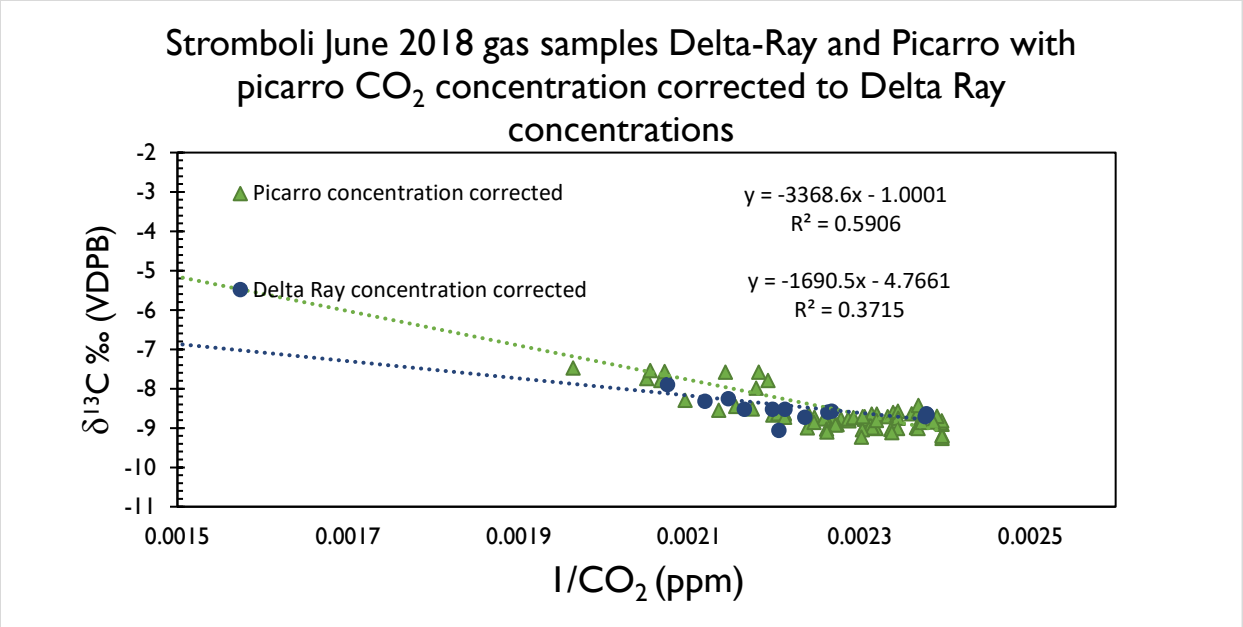

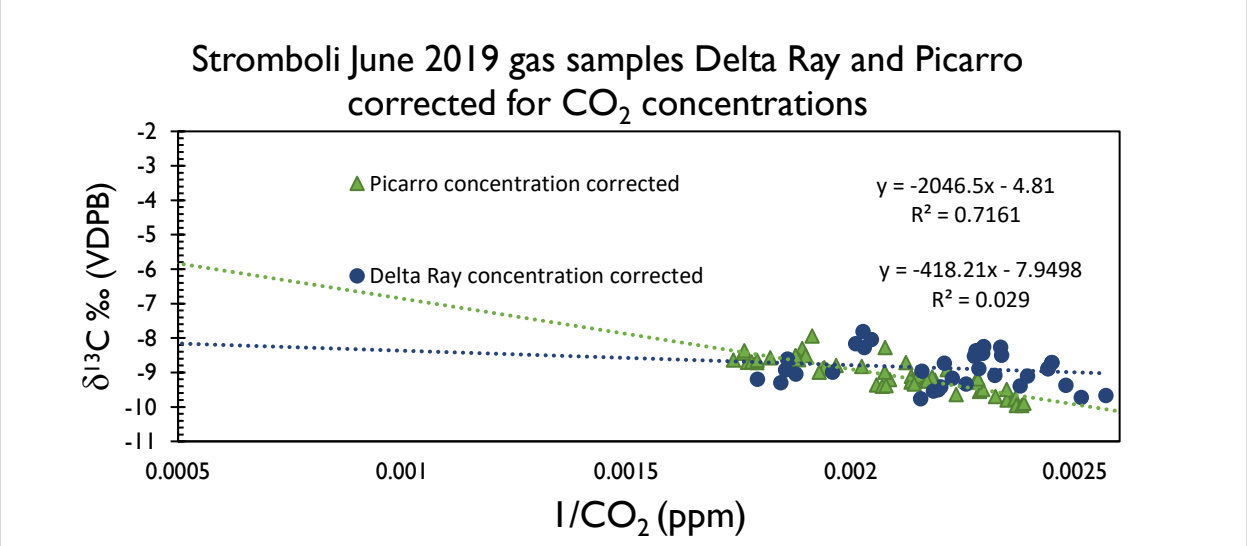

Figure S5: The Picarro and Delta Ray corrected concentration data for the 2018 (top) and 2019 (bottom) field campaigns.

Text S5. Cross calibration of regression analysis between Delta Ray and Picarro

In order to assess whether the difference between 2018 and 2019 data is significant, i.e. whether it represents a true volcanic variation in signature rather than being an artifact of the data processing, we were able to perform many tests to cross-calibrate the data between the two instruments to check the accuracy of each dataset. After calibration, differences between the two samples sets remained, which we discuss below.

The discrepancy between 2018 Delta Ray and Picarro data is likely due to the limited number of samples for a single day of measurements for the Delta Ray. This reduces the accuracy of the dataset, as can be seen by the low coefficient of regression for delta ray in figure S6 (R^2=0.37). It is possible that there were spatial and/or temporal variations at play as well. Unlike 2019, in 2018 we flew from two different take-off points to capture the samples and these flights were vent-specific. On 15 May, we flew from the pizzo targeting the C vent, which coalesces into a bulk plume at around 100 m height where plumes from several vents in the central and south crater merge. On 16 and 17 May, we flew from the helipad targeting the NE vent. While the Picarro collected samples on 15 to 17 May, the Delta Ray collected data only on 16 May. The lower intercept of the Delta Ray data (-4.8‰) is consistent with the 16 May Picarro data (Figure S7), which has a much lower intercept (-3.8‰) compared to the full Picarro dataset (-0.36‰). Furthermore, the combined Picarro and Delta Ray data for 2018 (Figure S6) shows a lower intercept (-2.0‰) than the Picarro data alone (-0.36‰), since the 16 May data are weighted towards lighter values from the additional Delta Ray samples.

The overall intercept for 2019 with Picarro data is -5.0 ‰ and a high R^2 value of 0.7, while the Delta Ray intercept is -7.8 ‰ with a R^2 of 0.03 (Figure S8). The combined data yield an intercept of -5.9 ‰ (R2= 0.3). Again, the 2019 differences between Delta Ray and Picarro are likely due to fewer analyses performed by the Delta Ray as well as a larger spread of data in the Delta Ray results.

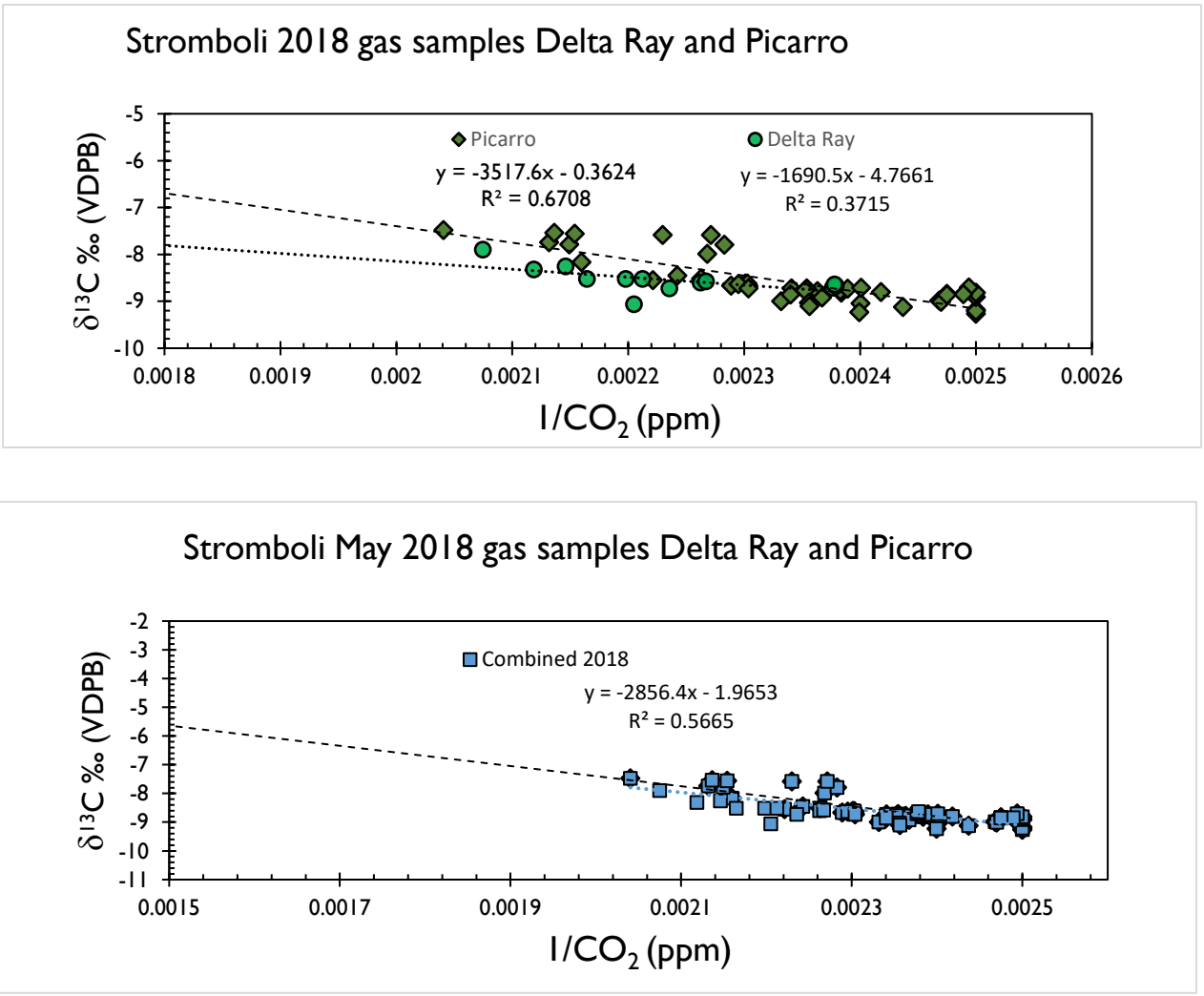

Figure S6: The Picarro and Delta Ray data for 2018 showing the datasets from both instruments plotted separately (top) and combined (bottom).

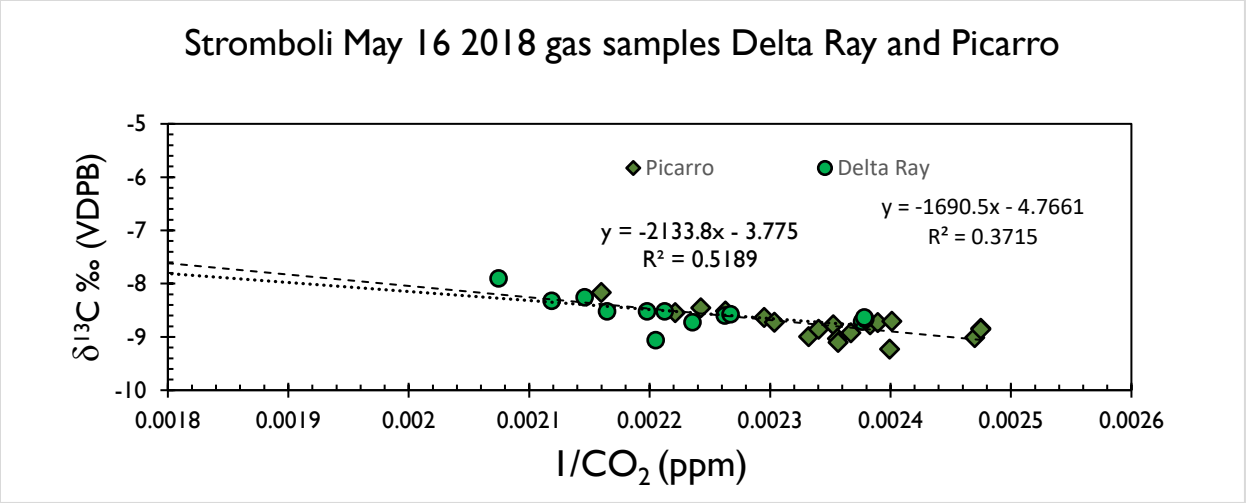

Figure S7: The Picarro and Delta Ray data for May 16 2018 showing the datasets from both instruments plotted separately. These include background, UAS flights, and ground-based plume samples.

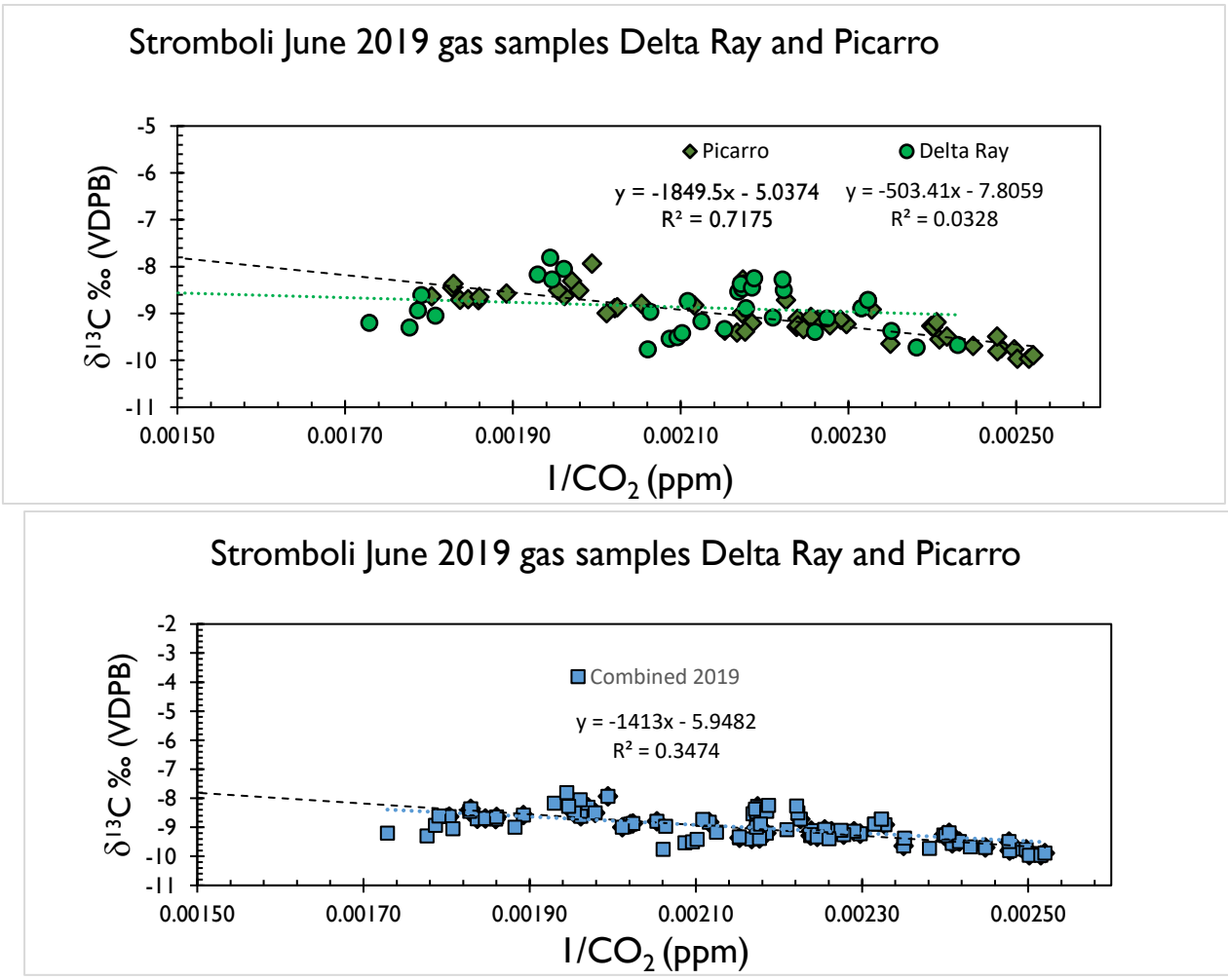

Figure S8: The Picarro and Delta Ray data for 2019 showing the datasets from both instruments plotted separately (top) and combined (bottom).

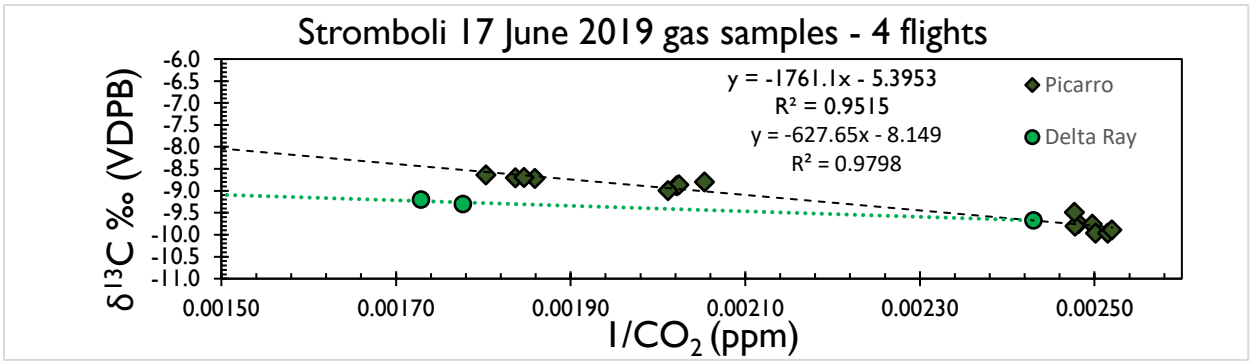

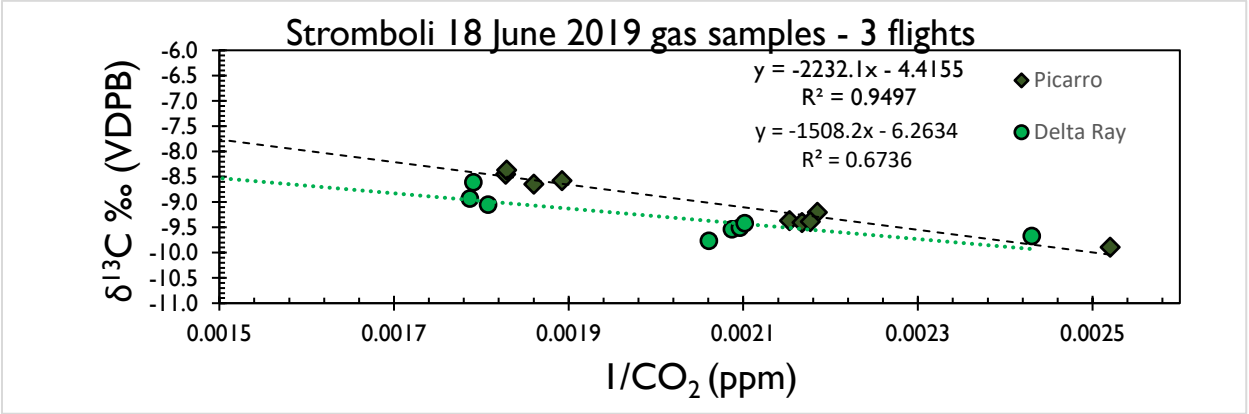

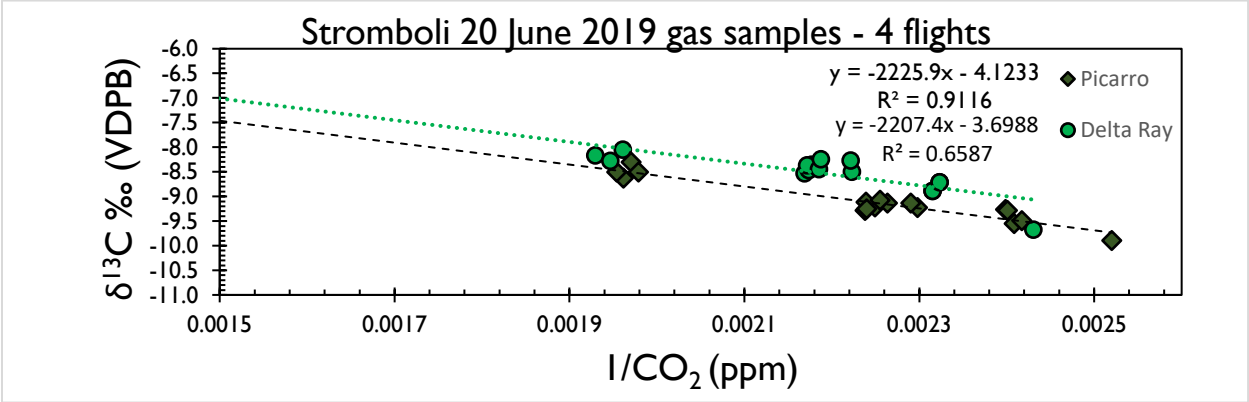

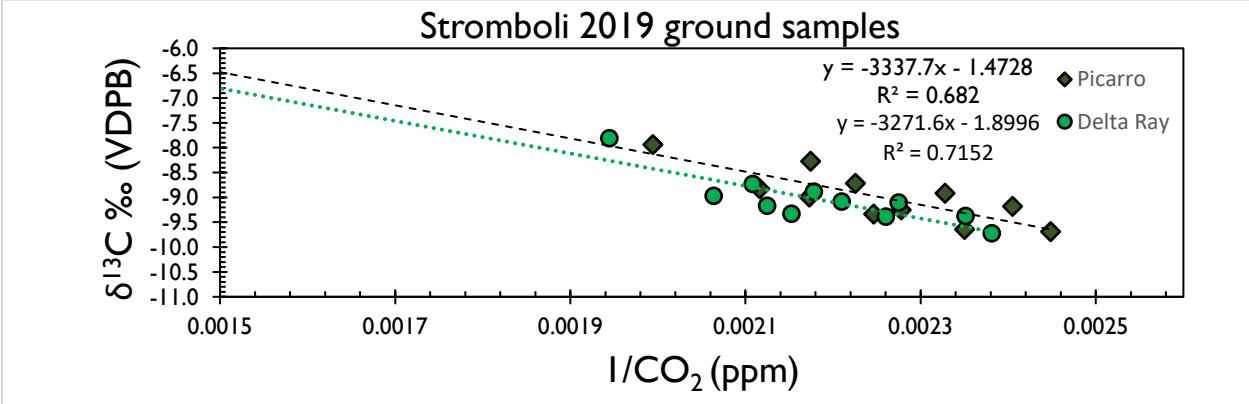

Figure S9*:* Picarro and Delta Ray data for 2019 UAS flights and ground samples.

Text S6. Comparison of Picarro and Delta Ray results for individual days in 2019

In 2019, Picarro data spans June 17, 18, and 20, while the Delta Ray data has just three datapoints from June 17 with most data from June 18 and 20. In 2019, we always flew from the pizzo and targeted the plume emanating from the central and south craters. One factor to consider here is that the plume emanations varied from one day to the next, so we plotted the individual days of data for the 2019 campaign (Figure S9). Of the four individual plots, the intercept on the 17 June is the most negative and the only plot where Delta Ray data comprises just three data points. This may explain the more negative (-8.1 ‰) intercept of the Delta Ray compared to the Picarro (-5.4‰) which has 13 data points. Interestingly, the ground samples for 2019 are much less negative than the UAS data, indicating that the ground samples may have a component of diffuse soil gas from the shallow hydrothermal system that the UAS samples directly above the plumes do not. It is notable that for all individual days of UAS flights, the data regress very well with R^2 values above 0.9 for Picarro and 0.6 for Delta Ray. It is unclear why the R^2 is so low for delta ray for the entire 2019 campaign, except that due to the large correction required to calibrate the data, the resulting values became scattered, leading to greater residuals when a linear regression was performed. Even though the combined dataset for Picarro and Delta Ray has significantly different intercepts in 2018 (-1.97 ‰) and 2019 (-5.95 %), we used the Picarro data because of the greater number of samples which were analyzed by the Picarro instrument compared to the Delta Ray. The intercomparison between the two instruments was used to examine small differences and to verify the overall consistency of our data.

Text S7. Modelling

We use a model which calculates the fraction of CO_2 remaining in the melt as a magma body rises and degasses, with starting parameters of 1000MPa, 2 wt % CO_2, NNO=0 (oxidation state). This is based on the Chosetto model of Moretti and Papale, 2004. We couple the output of this model with the closed and open degassing equations to determine the carbon isotopic signature of the melt and gas at each step of the model (Gerlach and Taylor, 1990). Heavier carbon is preferentially exsolved from a melt into the gas phase, with the gas-melt fractionation factor ranging from +2 to +4.5)(Javoy et al., 1978; Mattey, 1991). Here, we use a value of +3.5 as is common practice in recent studies (e.g., (Aubaud, 2022 and references therein). Accordingly,

$$\delta^{13}C_{gas} = \delta^{13}CO_{melt} + \Delta^{13}C_{gas-melt} \quad [5]$$

The equation for closed-system degassing we use is:

$$\delta^{13}C_{gas(residual)} = \delta^{13}CO_{melt(primordial)} - (1 - F)\Delta^{13}C_{gas-melt} \quad [6]$$

The equation for open-system degassing is:

$$\delta^{13}C_{pm} = \delta^{13}CO_{res} + 1000(1 - F^{\alpha-1}) \quad [7]$$

Data Set S1. Carbon isotopes from Stromboli volcano summit, 2018-2019

The calibrated data for the 2018 and 2019 CO2 concentrations and carbon isotopes from Stromboli volcano

Stromboli 2018	Picarro			Delta Ray				
Sample	$\delta^{13}C$ CO_2	CO_2 ppm	$1/CO_2$	$\delta^{13}C$ CO_2	CO_2 ppm	$1/CO_2$	Date	Type
background-01	-7.60	414	0.00242				2018-05-12	Background
background-02	-7.80	412	0.00243				2018-05-12	Background
background-03	-8.25	412	0.00243				2018-05-12	Background
Piazzo-04	-6.92	419					2018-05-12	Ground
Piazzo-04	-8.58	419	0.00238				2018-05-12	Ground
Helipad-05	-7.77	416	0.00240				2018-05-12	Ground
Helipad-06	-7.56	429	0.00233				2018-05-12	Ground
Helipad-07	-8.05	421	0.00238				2018-05-12	Ground
Helipad-08	-8.14	418	0.00239				2018-05-12	Ground
Helipad-09	-7.54	434	0.00230				2018-05-12	Ground
Helipad-10	-8.08	422	0.00237				2018-05-12	Ground
Helipad-11	-8.43	410	0.00244				2018-05-12	Ground
Bag-1	-8.71	416	0.00240				2018-05-13	Drone
Bag-2	-8.64	413	0.00242				2018-05-13	Drone
Bag-3	-8.71	411	0.00243				2018-05-13	Drone
Bag-4	-8.65	409	0.00244				2018-05-13	Drone
Bag-5	-8.60	410	0.00244				2018-05-13	Drone
Bag-6	-8.57	409	0.00244				2018-05-13	Drone
Bag-7	-8.63	406	0.00246				2018-05-13	Drone
Bag-8	-8.75	409	0.00245				2018-05-13	Drone
Bag-9	-8.58	405	0.00247				2018-05-13	Drone
Bag-10	-8.42	405					2018-05-13	Drone
Bag-1	-8.64	415	0.00241				2018-05-13	Drone
Bag-2	-8.77	416	0.00240				2018-05-13	Drone
Bag-3	-9.02	414	0.00242				2018-05-13	Drone
Bag-4	-9.04	410	0.00244				2018-05-13	Drone
Bag-5	-9.02	409	0.00244				2018-05-13	Drone
Bag-6	-8.92	415	0.00241				2018-05-13	Drone
Bag-7	-9.00	414	0.00241				2018-05-13	Drone
Bag-8	-8.76	421	0.00237				2018-05-13	Drone
Bag-9	-8.92	422	0.00237				2018-05-13	Drone
Bag-10	-8.65	429	0.00233				2018-05-13	Drone
10:41	-9.26	400	0.00250				2018-05-14	Background
10:48	-9.18	400	0.00250				2018-05-14	Background
11:05	-9.21	400	0.00250				2018-05-14	Background
12:32	-8.91	400	0.00250				2018-05-14	Background

	14:02	-8.88	400	0.00250				2018-05-14	Background
	14:12	-8.81	400	0.00250				2018-05-14	Background
	16:42	-8.70	401	0.00249				2018-05-14	Background
	16:58	-8.85	402	0.00249				2018-05-14	Background
	21:30	-8.98	405	0.00247				2018-05-14	Background
Bag-1-1		-8.67	437	0.00229				2018-05-15	Drone
Bag-1-2		-8.63	434	0.00230				2018-05-15	Drone
Bag-1-3		-8.66	434	0.00230				2018-05-15	Drone
Bag-2-1		-8.62	435	0.00230				2018-05-15	Drone
Bag-2-2		-8.62	434	0.00230				2018-05-15	Drone
Bag-2-3		-8.73	427	0.00234				2018-05-15	Drone
Bag-3-1		-8.78	423	0.00236				2018-05-15	Drone
Bag-3-2		-8.72	425	0.00235				2018-05-15	Drone
Bag-3-3		-8.82	420	0.00238				2018-05-15	Drone
Bag-4-1		-9.12	410	0.00244				2018-05-15	Drone
Bag-4-2		-9.05	417	0.00240				2018-05-15	Drone
Bag-4-3		-8.80	414	0.00242				2018-05-15	Drone
Bag-1-1		-9.23	417	0.00240				2018-05-16	Drone
Bag-1-2		-8.92	422	0.00237				2018-05-16	Drone
Bag-1-3		-8.77	420	0.00238				2018-05-16	Drone
Bag-2-1		-8.73	419	0.00239				2018-05-16	Drone
Bag-2-2		-8.71	417	0.00240				2018-05-16	Drone
	10:27:30	-8.77	425	0.00235	-8.6	442	0.00226	2018-05-16	Ground
	9:41	-7.71	570		-8.0	590		2018-05-16	Ground
	10:03	-8.16	463	0.00216	-7.9	482	0.00207	2018-05-16	Ground
	10:17	-8.51	442	0.00226	-8.5	462	0.00216	2018-05-16	Ground
	10:19	-8.63	436	0.00230	-8.5	455	0.00220	2018-05-16	Ground
	10:30	-8.72	434	0.00230	-8.5	452	0.00221	2018-05-16	Ground
	10:13	-9.03	424	0.00236				2018-05-16	Ground
3-1		-9.10	424	0.00236	-8.6	441	0.00227	2018-05-16	Drone
3-2		-8.99	429	0.00233	-8.7	447	0.00224	2018-05-16	Drone
3-3		-8.85	427	0.00234	-9.1	454	0.00221	2018-05-16	Drone
4-1		-8.55	450	0.00222	-8.3	472	0.00212	2018-05-16	Drone
4-2		-8.45	446	0.00224	-8.3	466	0.00215	2018-05-16	Drone
bg-b-1		-9.01	405	0.00247	-8.7	421	0.00238	2018-05-16	Background
bg-b-2		-8.84	404	0.00247	-8.7	420	0.00238	2018-05-16	Background
bg-b-3		-8.86	404	0.00247	-8.6	421	0.00238	2018-05-16	Background
Bag-1-1		-7.79	465	0.00215				2018-05-17	Drone
Bag-1-2		-7.74	469	0.00213				2018-05-17	Drone
Bag-1-3		-7.48	490	0.00204				2018-05-17	Drone
Bag-2-1		-7.99	441	0.00227				2018-05-17	Drone
Bag-2-2		-7.79	438	0.00228				2018-05-17	Drone
Bag-3-1		-7.54	468	0.00214				2018-05-17	Drone
Bag-3-2		-7.58	440	0.00227				2018-05-17	Drone
Bag-3-3		-7.58	448	0.00223				2018-05-17	Drone

Bag-4-1	-7.56	464	0.00215				2018-05-17	Drone
Bag-4-2	-8.30	459					2018-05-17	Drone
Stromboli 2019	**Picarro**			**Delta Ray**				
Sample	$\delta^{13}C$ CO_2	CO_2 ppm	$1/CO_2$	$\delta^{13}C$ CO_2	CO_2 ppm	$1/CO_2$	Date	Type
Flight 6-17-1a	-9.75	402.9	0.00248				2019-06-17	Drone
Flight 6-17-1b	-9.80	403.6	0.00248				2019-06-17	Drone
Flight 6-17-1c							2019-06-17	Drone
Flight 6-17-1d	-9.49	403.7	0.00248				2019-06-17	Drone
Flight 6-17-2a	-8.89	494.7	0.00202				2019-06-17	Drone
Flight 6-17-2b	-8.87	494	0.00202				2019-06-17	Drone
Flight 6-17-2c	-8.99	497.1	0.00201				2019-06-17	Drone
Flight 6-17-2d	-8.80	487	0.00205				2019-06-17	Drone
Flight 6-17-3a	-8.71	544.4	0.00184				2019-06-17	Drone
Flight 6-17-3b	-8.72	537.9	0.00186				2019-06-17	Drone
Flight 6-17-3c	-8.64	554.6	0.00180	-9.20	578.45	0.00173	2019-06-17	Drone
Flight 6-17-3d	-8.70	541.5	0.00185	-9.30	562.83	0.00178	2019-06-17	Drone
Flight 6-17-4a	-9.76	400.4	0.00250				2019-06-17	Background
Flight 6-17-4b	-9.96	399.8	0.00250				2019-06-17	Background
Flight 6-17-4c	-9.96	397.6	0.00252				2019-06-17	Background
Flight 6-17-4d	-9.89	396.8	0.00252	-9.67	411.46	0.00243	2019-06-17	Background
Flight 6-18-1a	-9.36	464.5	0.00215	-9.76	485.27	0.00206	2019-06-18	Drone
Flight 6-18-1b	-9.40	461.4	0.00217	-9.54	479.19	0.00209	2019-06-18	Drone
Flight 6-18-1c	-9.20	457.7	0.00218	-9.51	477.06	0.00210	2019-06-18	Drone
Flight 6-18-1d	-9.38	459.4	0.00218	-9.42	475.83	0.00210	2019-06-18	Drone
Flight 6-18-2a	-8.58	528.4	0.00189				2019-06-18	Drone
Flight 6-18-2b	-8.45	547.1	0.00183	-8.93	559.63	0.00179	2019-06-18	Drone
Flight 6-18-2c	-8.65	537.6	0.00186	-9.05	553.21	0.00181	2019-06-18	Drone
Flight 6-18-2d	-8.37	546.7	0.00183	-8.61	558.4	0.00179	2019-06-18	Drone
Air							2019-06-18	Background
Flight 6-18-3a	-10.38						2019-06-18	Drone
Flight 6-18-3b	0.19						2019-06-18	Drone
Flight 6-18-3c	0.19						2019-06-18	Drone
Flight 6-18-3d	-9.68						2019-06-18	Drone
Flight 6-20-1a	-9.26	416.9	0.00240	-8.71	430.41	0.00232	2019-06-20	Drone
Flight 6-20-1b	-9.55	415.2	0.00241	-8.89	431.9	0.00232	2019-06-20	Drone
Flight 6-20-1c	-9.49	413.7	0.00242	-8.89	431.9	0.00232	2019-06-20	Drone
Flight 6-20-1d	-9.28	416.5	0.00240	-8.71	430.41	0.00232	2019-06-20	Drone
Flight 6-20-2a	-8.31	507.5	0.00197	-8.05	509.95	0.00196	2019-06-20	Drone
Flight 6-20-2b	-8.63	509.8	0.00196	-9.00	531.24		2019-06-20	Drone
Flight 6-20-2c	-8.51	505.3	0.00198	-8.17	518.23	0.00193	2019-06-20	Drone
Flight 6-20-2d	-8.51	511.8	0.00195	-8.27	513.66	0.00195	2019-06-20	Drone
Flight 6-20-3a	-9.21	444.6	0.00225	-8.53	461.12	0.00217	2019-06-20	Drone
Flight 6-20-3b	-9.28	446.8	0.00224	-8.36	459.39	0.00218	2019-06-20	Drone
Flight 6-20-3c	-9.11	446.6	0.00224	-8.47	460.1	0.00217	2019-06-20	Drone
Flight 6-20-3d	-9.25	446.5	0.00224	-8.37	460.45	0.00217	2019-06-20	Drone

Flight 6-20-4a	-9.22	435.2	0.00230	-8.50	449.85	0.00222	2019-06-20	Drone
Flight 6-20-4b	-9.13	436.6	0.00229	-8.27	450.15	0.00222	2019-06-20	Drone
Flight 6-20-4c	-9.13	441.8	0.00226	-8.44	457.63	0.00219	2019-06-20	Drone
Flight 6-20-4d	-9.07	443.4	0.00226	-8.25	457.12	0.00219	2019-06-20	Drone
Sample 120	-9.64	425.5	0.00235	-9.11	439.6	0.00227	2019-06-20	Ground
Sample 114	-9.33	445.2	0.00225	-8.89	459.15	0.00218	2019-06-20	Ground
Sample 104	-7.94	501.4	0.00199	-7.81	514.23	0.00194	2019-06-20	Ground
Sample 102	-9.25	439	0.00228	-9.08	452.52	0.00221	2019-06-20	Ground
Sample 108	-8.99	460.2	0.00217	-8.73	474.29	0.00211	2019-06-20	Ground
Sample 105	-8.83	472.5	0.00212	-8.97	484.56	0.00206	2019-06-20	Ground
Sample 102	-8.72	449.3	0.00223	-9.33	464.62	0.00215	2019-06-21	Ground
Sample 103	-8.92	429.6	0.00233	-9.39	442.42	0.00226	2019-06-21	Ground
Sample 108	-9.69	408.4	0.00245	-9.72	419.95	0.00238	2019-06-21	Ground
Sample 106	-8.28	459.9	0.00217	-9.17	470.64	0.00212	2019-06-21	Ground
Sample 107	-9.18	415.8	0.00241	-9.37	425.3	0.00235	2019-06-21	Ground
Sample 104	-2.58	1515	0.00066	-4.98	1563.88	0.00064	2019-06-21	Ground
Sample 114	-6.51	655.6	0.00153	-7.74	675.17	0.00148	2019-06-21	Ground

Data Set S2. Calculations of discrete carbon isotopes from Stromboli volcano summit, 2018-2019

The calibrated data and calculations using the weighted means method for the 2018 and 2019 CO2 concentrations and carbon isotopes from Stromboli volcano. The weighted means calculations use only plume samples with volcanic CO2 greater than 50 ppm above background as in Schipper et al. 2017

Date	CO2 ppm, background	d13C CO2, background	volcanic CO2 ppm	d13C volcanic
2018-05-12	401	-8.9		
2018-05-12	401	-8.9		
2018-05-12	401	-8.9		
2018-05-12	401	-8.9	18.17	36.77605
2018-05-12	401	-8.9	18.36	-1.69063
2018-05-12	401	-8.9	14.93	22.51727
2018-05-12	401	-8.9	27.67	11.83299
2018-05-12	401	-8.9	19.58	9.293849
2018-05-12	401	-8.9	17.15	9.551665
2018-05-12	401	-8.9	33.23	8.84992
2018-05-12	401	-8.9	20.88	7.606101
2018-05-12	401	-8.9	8.64	13.1951
2018-05-13	401	-8.9	15.09	-3.76303
2018-05-13	401	-8.9	12.48	-0.43567

2018-05-13	401	-8.9	10.16	-1.40136
2018-05-13	401	-8.9	8.45	2.993507
2018-05-13	401	-8.9	9.05	4.492615
2018-05-13	401	-8.9	8.04	7.668122
2018-05-13	401	-8.9	5.17	11.95871
2018-05-13	401	-8.9	7.93	-1.41283
2018-05-13	401	-8.9	3.79	24.81114
2018-05-13	401	-8.9	3.79	
2018-05-13	401	-8.9	13.6	-1.11169
2018-05-13	401	-8.9	15.13	-5.4582
2018-05-13	401	-8.9	12.59	-12.6937
2018-05-13	401	-8.9	9.46	-14.7808
2018-05-13	401	-8.9	8.05	-14.7681
2018-05-13	401	-8.9	13.8	-9.53842
2018-05-13	401	-8.9	13.4	-11.8513
2018-05-13	401	-8.9	20.28	-6.07135
2018-05-13	401	-8.9	21.09	-9.20469
2018-05-13	401	-8.9	27.56	-5.08321
2018-05-14	401	-8.9		
2018-05-14	401	-8.9		
2018-05-14	401	-8.9		
2018-05-14	401	-8.9		
2018-05-14	401	-8.9		
2018-05-14	401	-8.9		
2018-05-14	401	-8.9		
2018-05-14	401	-8.9		
2018-05-14	401	-8.9		
2018-05-15	401	-8.9	35.93	-6.06147
2018-05-15	401	-8.9	33.2	-5.40144
2018-05-15	401	-8.9	33.3	-5.75111
2018-05-15	401	-8.9	33.59	-5.23141
2018-05-15	401	-8.9	33.29	-5.21398
2018-05-15	401	-8.9	26.21	-6.07587
2018-05-15	401	-8.9	22.16	-6.62524
2018-05-15	401	-8.9	23.78	-5.71545
2018-05-15	401	-8.9	18.52	-7.04188
2018-05-15	401	-8.9	9.32	-18.619
2018-05-15	401	-8.9	15.59	-12.7896
2018-05-15	401	-8.9	12.55	-5.7675
2018-05-16	401	-8.9	15.79	-17.6117
2018-05-16	401	-8.9	21.46	-9.29838
2018-05-16	401	-8.9	18.63	-5.99097
2018-05-16	401	-8.9	17.52	-4.90474

2018-05-16	401	-8.9	15.5	-3.73234
2018-05-16	401	-8.9	24.09	-6.62103
2018-05-16	401	-8.9		-4.88899
2018-05-16	401	-8.9	62.02	-3.39987
2018-05-16	401	-8.9	40.88	-4.72965
2018-05-16	401	-8.9	34.71	-5.56717
2018-05-16	401	-8.9	33.09	-6.60073
2018-05-16	401	-8.9	23.48	-11.2234
2018-05-16	401	-8.9	23.38	-12.5613
2018-05-16	401	-8.9	27.83	-10.355
2018-05-16	401	-8.9	26.32	-8.15423
2018-05-16	401	-8.9	49.18	-5.66204
2018-05-16	401	-8.9	44.93	-4.44389
2018-05-16	401	-8.9		
2018-05-16	401	-8.9		
2018-05-16	401	-8.9		
2018-05-17	401	-8.9	64.27	-0.8521
2018-05-17	401	-8.9	68.11	-0.93241
2018-05-17	401	-8.9	89.05	-1.07185
2018-05-17	401	-8.9	39.89	1.148747
2018-05-17	401	-8.9	37.05	4.172694
2018-05-17	401	-8.9	67.09	0.598152
2018-05-17	401	-8.9	39.27	5.845439
2018-05-17	401	-8.9	47.48	3.551565
2018-05-17	401	-8.9	63.26	0.921551
2018-05-17	401	-8.9	57.79	-4.11778

Date	CO2 ppm, background	d13C CO2, background	volcanic CO2 ppm	d13C volcanic
2019-06-17	401	-9.9	1.9	22.53316
2019-06-17	401	-9.9	2.6	5.174622
2019-06-17		-9.9		
2019-06-17	401	-9.9	2.7	50.83622
2019-06-17	401	-9.9	93.7	-4.54413
2019-06-17	401	-9.9	93	-4.40552
2019-06-17	401	-9.9	96.1	-5.2199
2019-06-17	401	-9.9	86	-3.64725
2019-06-17	401	-9.9	143.4	-5.36743
2019-06-17	401	-9.9	136.9	-5.24809
2019-06-17	401	-9.9	153.6	-5.33712
2019-06-17	401	-9.9	140.5	-5.26009
2019-06-17	401	-9.9	-0.6	-101.321
2019-06-17	401	-9.9	-1.2	10.89792
2019-06-17	401	-9.9	-3.4	-2.59995

2019-06-17	401	-9.9	-4.2	-10.5965
2019-06-18	401	-9.9	63.5	-5.98039
2019-06-18	401	-9.9	60.4	-6.11139
2019-06-18	401	-9.9	56.7	-4.28675
2019-06-18	401	-9.9	58.4	-5.84176
2019-06-18	401	-9.9	127.4	-4.41051
2019-06-18	401	-9.9	146.1	-4.45833
2019-06-18	401	-9.9	136.6	-4.96578
2019-06-18	401	-9.9	145.7	-4.14807
2019-06-18				
2019-06-18				
2019-06-18				
2019-06-18				
2019-06-18				
2019-06-20	401	-9.9	15.9	6.764071
2019-06-20	401	-9.9	14.2	0.228133
2019-06-20	401	-9.9	12.7	3.332277
2019-06-20	401	-9.9	15.5	6.64185
2019-06-20	401	-9.9	106.5	-2.31008
2019-06-20	401	-9.9	108.8	-3.93192
2019-06-20	401	-9.9	104.3	-3.14971
2019-06-20	401	-9.9	110.8	-3.46397
2019-06-20	401	-9.9	43.6	-2.91081
2019-06-20	401	-9.9	45.8	-3.89451
2019-06-20	401	-9.9	45.6	-2.21074
2019-06-20	401	-9.9	45.5	-3.56543
2019-06-20	401	-9.9	34.2	-1.30507
2019-06-20	401	-9.9	35.6	-0.51594
2019-06-20	401	-9.9	40.8	-1.61443
2019-06-20	401	-9.9	42.4	-1.27259
2019-06-20	401	-9.9	24.5	-5.44272
2019-06-20	401	-9.9	44.2	-4.20156
2019-06-20	401	-9.9	100.4	-0.10328
2019-06-20	401	-9.9	38	-2.44259
2019-06-20	401	-9.9	59.2	-2.8667
2019-06-20	401	-9.9	71.5	-2.80081
2019-06-21	401	-9.9	48.3	1.113432
2019-06-21	401	-9.9	28.6	4.888605
2019-06-21	401	-9.9	7.4	1.512685
2019-06-21	401	-9.9	58.9	2.770081
2019-06-21	401	-9.9	14.8	10.19643
2019-06-21	401	-9.9	1114	0.049654
2019-06-21	401	-9.9	254.6	-1.17702

2019-06-21	401	-9.9	6.2	4.336437